NATIONAL ADVISORY COMMITTEE FOR AERONAUTICS

TECHNICAL NOTE 2670

HIGH-SPEED SUBSONIC CHARACTERISTICS OF 16 NACA 6-SERIES AIRFOIL SECTIONS

By Milton D. Van Dyke

Ames Aeronautical Laboratory
Moffett Field, Calif.

Washington
March 1952

1B

NATIONAL ADVISORY COMMITTEE FOR AERONAUTIC

TECHNICAL NOTE 2670

HIGH-SPEED SUBSONIC CHARACTERISTICS OF 16 NACA 6-SERIES AIRFOIL SECTIONS

By Milton D. Van Dyke

SUMMARY

A wind-tunnel investigation has been conducted to determine the high-speed subsonic aerodynamic characteristics of NACA 63-, 64-, 65-, and 66-series airfoil sections having thickness ratios of 6, 8, 10, and 12 percent and an ideal lift coefficient of 0.2 with the uniform-load type (a = 1.0) of mean camber line. Section drag, lift, and pitching-moment coefficients measured at Mach numbers as high as 0.90 are presented for angles of attack from -6° to 10° or 12°.

For each thickness ratio, only a slight impairment of high-speed section drag characteristics results from forward movement of position of minimum base-profile pressure up to 40 percent of the chord. At the same time, however, decrease of lift-curve slope and increase of angle of zero lift, both of which adversely affect longitudinal stability and control, are delayed further beyond the critical Mach number. Hence it is concluded that, for 6-series airfoil sections of a given thickness ratio, those with minimum pressure near 40-percent chord possess optimum over-all aerodynamic characteristics.

Appreciable improvement in the high-speed drag of airfoil sections can be achieved only by decreasing their thickness ratio. Fortunately, the accompanying reduction in range of lift coefficient for good high-speed section characteristics is, for these 6-series airfoils, much less severe than consideration of the theoretically predicted critical Mach number would indicate.

INTRODUCTION

In order to avoid excessive power requirements at subsonic speeds, the airfoil sections for an airplane wing of given plan form must be chosen so that the abrupt rise in drag associated with the formation of shock waves is delayed to the highest possible speed. Airfoil sections of the NACA low-drag type have critical speeds already so near to the optimum value for any given thickness ratio (reference 1) that appreciable

improvement can be achieved only by further reduction in thickness. On the other hand, structural considerations and the desirability of obtaining a high maximum lift coefficient prescribe as thick a wing as is consistent with the attainment of the required high speed. Present practice is to choose wing sections of such thickness that the marked drag increase associated with the formation of shock waves will commence almost immediately upon exceeding the maximum level-flight design speed.

This practice might on first thought appear to be a happy compromise. Unfortunately, however, other adverse effects of compressibility, of a more treacherous nature, often manifest themselves at or slightly above the speed at which the marked drag rise begins. Chief among these are an abrupt increase in angle of zero lift for cambered airfoils and a pronounced reduction in lift-curve slope. Both have a deleterious influence upon the airplane trim and longitudinaly stability and control, as discussed for unswept wings in reference 2.

If the speed at which these adverse effects commence is exceeded by the airplane, as in a dive, the increase of angle of zero lift coupled with a decrease in lift-curve slope alters the trim to promote a further diving tendency. Concurrently, greater stability results from the reduction of lift-curve slope and from adverse changes in wing pitching moment. In extreme cases the increase in stability is so great that recovery from the dive cannot be effected by use of normal elevator control. Loss of the aircraft will follow unless drag at lower altitudes limits the speed sufficiently to re-establish elevator control, or other more powerful means of obtaining longitudinal control are provided. It would accordingly appear desirable to choose for a high-speed airplane an airfoil having, at the design lift coefficient, as high a critical speed as is consistent with structural limitations and, further, having as small adverse effects as far beyond that speed as possible.

In the case of a bomber, the level-flight lift coefficient will vary through a wide range even on a single flight as a result of changes in loading caused by fuel consumption and disposal of bombs. In the case of a fighter aircraft, a similarly wide range of operating lift coefficient will be required to attain satisfactory maneuverability. The ideal airfoil for high-speed aircraft would therefore maintain the desired high-speed characteristics throughout a broad range of lift coefficient. That this ideal may be difficult to achieve is indicated by theory which predicts that, as the critical speed of an airfoil is increased by reducing its thickness, the range of lift coefficient over which favorable high-speed characteristics are realized shrinks rapidly.

Because existing theory cannot be relied upon to predict these conflicting effects accurately, the choice of optimum subsonic airfoils must be guided by experiment. Accordingly, in 1945 and 1947 tests were conducted in the Ames 1- by 3-1/2-foot high-speed wind tunnel to determine the subsonic characteristics of 16 NACA 6-series airfoils having various thickness ratios and positions of minimum pressure. The results

for 12 airfoils were originally published in 1945 in a report of limited circulation by Milton D. Van Dyke and Gordon A. Wibbert which was supplemented in 1947 by data for the 63-series sections published in a report of limited circulation by Richard J. Ilk. These results are combined in the present report, and the discussion is somewhat revised, notably by including an analysis of the data according to the transonic similarity rule.

SYMBOLS

c	airfoil chord length
c_d	section drag coefficient
$c_{d_{cr}}$	section drag coefficient at theoretical critical Mach number
c_l	section lift coefficient
$c_{l_{max}}$	maximum section lift coefficient
$c_{m_{c/4}}$	section pitching-moment coefficient about quarter-chord point
$\frac{dc_l}{d\alpha}$	section lift-curve slope, per degree
D_1, D_2	reduced section drag coefficient functions in transonic similarity rule (See equations (2) and (4).)
L_α	reduced section lift-curve-slope function in transonic similarity rule (See equation (6).)
M	free-stream Mach number
M_{cr}	theoretical critical free-stream Mach number
R	free-stream Reynolds number based on chord
t	airfoil maximum thickness
α_o	section angle of attack, degrees
ξ	transonic similarity parameter $\left[\frac{M^2 - 1}{(t/c)^{2/3}}\right]$
ξ_{cr}	transonic similarity parameter at theoretical critical Mach number $\left[\frac{M_{cr}^2 - 1}{(t/c)^{2/3}}\right]$

APPARATUS AND METHODS

The following 16 NACA low-drag airfoil sections, having uniform-load type (a = 1.0) mean camber line, were tested:

63-206	64-206	65-206	66-206
63-208	64-208	65-208	66-208
63-210	64-210	65-210	66-210
63-212	64-212	65-212	66-212

The models were of 6-inch chord, polished aluminum alloy construction, and completely spanned the 1-foot width of the tunnel test section. End leakage was prevented by a compressed rubber gasket at each end of the airfoil to assure two-dimensional flow. Sketches of the airfoils appear in figure 1, and the ordinates for each section are presented in table I. (The airfoil terminology and method of calculating ordinates are described in reference 3.)

The Ames 1- by 3-1/2-foot high-speed wind tunnel, in which the tests were conducted, is a two-dimensional flow, low-turbulence, single-return-type tunnel. It is powered by two 1000-horsepower electric motors driving oppositely rotating propellers. This power is sufficient in all cases to choke the tunnel.

The airfoil lift and pitching moment were determined by tunnel-wall-reaction measurements, using a method similar to that described for measurement of lift in the appendix to reference 3. Previous tests have demonstrated excellent agreement at all Mach numbers between lift and pitching-moment characteristics as determined from wall-reaction measurements and from integration of simultaneously obtained pressure distributions.

Drag was determined by the wake-survey method using a movable 9-inch-wide rake of 35 total-head tubes. The rake was moved to take necessary additional readings when the wake width was greater than 9 inches at the drag-rake station. It was not possible to evaluate the entire drag at the choking Mach number because the airfoil wake then extended from the floor to the ceiling of the tunnel test section. Drag coefficients were computed by the method of reference 4.

For all tests, the free-stream Mach number ranged from 0.30 to the tunnel choking speed - approximately 0.90 Mach number at low angles of attack. The corresponding variation of Reynolds number was from one to nearly two million for the 6-inch-chord models investigated. (See fig. 2.) Each airfoil was tested at angles of attack varying by increments of 2° from -6° to 10° or 12°,[2] which range was ordinarily

[2]In the case of the NACA 65-206 and 66-212 airfoils, the actual angles were 0.5° greater than these values.

sufficient to determine the stall. Settings for angle of attack are believed to be accurate to within $\pm 0.10^{\circ}$; relative readings for any one airfoil are reliable to within $\pm 0.05^{\circ}$.

TEST RESULTS

Drag, lift, and quarter-chord pitching-moment coefficients at constant angle of attack are plotted for each of the 16 airfoils as functions of free-stream Mach number M in figures 3 to 50. Corresponding cross plots at constant Mach number present, in figures 51 to 98, the variation of section lift coefficient with angle of attack, and of section drag and pitching-moment coefficients with lift coefficient. All data have been corrected for tunnel-wall interference by the method of reference 5.

In figures 3 to 50, the experimental point shown at the highest Mach number for each angle of attack was obtained with the wind tunnel choked. Except for the pitching moment, data obtained at the choking speed can be repeated with good agreement. However, it is shown in reference 5 that the choked condition cannot be corrected to free-air flow since, in fact, no equivalent free-air flow exists. The usual correction procedure has nevertheless been applied to these data, and the results are presented as a matter of interest.

These data are considered to be unreliable not only at the choking speed, but also within some range of Mach number below this limit. Shock waves begin to form on one or both surfaces of an airfoil soon after the critical Mach number of the section is exceeded. At some higher speed they will have extended sufficiently far across the tunnel so that their interaction with the tunnel walls can no longer be neglected. An attempt has been made in figures 3 to 98 to indicate by a dashed line the possible extent of the Mach number range below choking within which the data are at least quantitatively unreliable. This range may logically be presumed to be greater at high angles of attack since one surface of the airfoil then shocks at a Mach number far below the choking Mach number.

DISCUSSION

Drag Coefficient

Subcritical characteristics.- Within the low-drag range of lift coefficients, figures 3 to 18 show that the section drag coefficient at constant angle of attack decreases slightly in most cases until a Mach number of 0.40 is reached; this is probably a consequence of increasing Reynolds number rather than any compressibility effect. From this point on, whether considered at constant angle of attack or, as in figure 99, at constant lift coefficient, the drag coefficient remains essentially unchanged until the predicted critical Mach number of the airfoil is exceeded.

A curious phenomenon appears in figures 3 to 18 for higher angles of attack. After an initial rise with Mach number, the drag coefficient drops to a "trough" immediately preceding the final abrupt rise. This trough appears to be characteristic of NACA 6-series airfoils. It appears also in tests of NACA 65_2-215 (a = 0.5) and 66, 2-215 (a = 0.6) airfoils, but is absent in the case of NACA 0015 and 23015 airfoils and scarcely discernible in the case of the NACA 4415 section. (See reference 6.) The trough becomes more gentle if the variation is considered at constant lift coefficient, as in figure 100(a), rather than at constant angle of attack. The cause of this trough has not been determined. It is interesting to note that a similar variation of drag was reported for circular cylinders in reference 7. Balance measurements of the drag of cylinders of various diameters (representing Reynolds numbers of from 0.06×10^6 to 0.25×10^6 at 0.65 Mach number) showed in each case a trough of the same form. (See fig. 100(b).)

Because the forces to be measured vary over a wide range, results at low Mach numbers are unduly affected by errors in tares and zero readings which are negligible at higher speeds. For this reason, low-speed values of drag should be considered as qualitatively rather than quantitatively correct. For example, the consistent reduction in low-speed drag coefficient expected to accompany rearward movement of the position of minimum base-profile pressure is not evident in figure 99.

Low drag range.- At low speeds, the drag polar curves for these airfoils exhibit a characteristic "bucket" (reference 3). The drag has a low value within the range of lift coefficients for which the minimum pressure points on both surfaces lie well back on the airfoil. Outside this range the drag jumps sharply to a higher value. The present tests do not provide enough points to show this variation accurately. Measurements were made at increments of not less than 0.2 lift coefficient, whereas the extent of the low drag range is at most 0.4 lift coefficient at low speeds. Therefore, only one or two test points are available within the low drag range. Many more points would be required, particularly near the ends of the region, to trace the typical bucket curve. However, despite the fact that the drag curves (figs. 51 to 66) were obtained by fairing through widely separated points, they give, particularly for the thicker sections, a suggestion of the typical bucket shape.

This matter has been investigated in greater detail, as shown in figure 101 for two of the airfoils, the NACA 64-206 and 66-212 sections. Here advantage has been taken of the results of tests of the same airfoils in the Langley two-dimensional wind tunnel (reference 3) to fix the extremities of the low drag range. Small-perturbation theory would predict that at any free-stream Mach number M the values of lift coefficient corresponding to each end of the low drag range are equal to the low-speed values multiplied by $(1 - M^2)^{-1/2}$. Low-speed values from reference 3 have been magnified by this factor, and the polar curves of figure 101 are assumed to be flat within these limits and pass through the single available point. In this manner, for every Mach number up to

the critical it is possible to draw curves passing through each point which are remarkably similar to the low-speed curve. The agreement, shown here for only two airfoils, was found to be equally as good for the others. Hence it seems reasonable to assume that for all 16 airfoils investigated the typical bucket form of the drag curve is preserved until the critical speed of the section is exceeded, and the corresponding range of lift coefficients for low drag increases with free-stream Mach number according to the factor $(1 - M^2)^{-1/2}$. Outside the low drag range the drag coefficient rises more rapidly with change of lift coefficient than is indicated by the test results of reference 3. The difference can probably be attributed to the lower Reynolds number of the present tests.

Once the critical Mach number of the section is exceeded it immediately becomes impossible to fit a curve of the form assumed above. The low drag range vanishes; the polar curve becomes more parabolic in form, and, with further increase in speed, shifts so that the lift coefficient for minimum drag approaches zero.

Critical Mach number.- Abrupt changes in the magnitudes of the forces acting upon an airfoil, and of the drag in particular, are known to occur at speeds somewhat in excess of the critical Mach number M_{cr} defined as the Mach number of the free stream for which, at some point on the surface of the airfoil, a velocity equal to the local velocity of sound is first attained. For a given airfoil section, the critical Mach number is a function only of the lift coefficient, and references 1 and 3 present a method for approximating this relationship on the basis of the known low-speed pressure distribution over the surface of the airfoil.

For NACA low-drag airfoils of moderate thickness, the maximum velocity (or minimum pressure), which determines the critical speed, occurs at a point which jumps between the midportion of the airfoil and the nose with change of angle of attack. The variation of critical Mach number with lift coefficient, consequently, has the characteristic jointed form shown in figure 102. The curves consist, for these cambered airfoils, of three connected segments: a central nearly flat portion encompassing the low drag range, which is associated with the realization of the maximum velocity on the upper surface of the airfoil near the position of maximum thickness; and two steeply inclined lines, which are determined by maximum velocity at the nose on the upper or lower surface.

Comparison of the variation of critical Mach number as determined from pressure-distribution measurements over NACA 65_2-215 ($a = 0.5$) and 66,2-215 ($a = 0.6$) airfoils with that predicted by theory has shown good agreement throughout the flat portion of the curve (reference 6). However, the experimentally determined corners are shifted farther out along the flat portion of the theoretical curve. As a result, the range of lift coefficients for high critical Mach numbers extends to considerably higher values than theory would predict. Beyond the corners the experimental curves fall roughly parallel to those predicted by theory.

The discrepancy is caused principally by the fact that the Kármán-Tsien relationship employed in the theoretical method to obtain high-speed pressure coefficients from incompressible values, while giving excellent agreement with experiment over most of the airfoil surface, overestimates the increase at the nose.

In view of this extension of the high critical-speed range of lift coefficient, the flat portions of the theoretical curves shown in figure 102 have been extended for purposes of comparison in the following discussion. This was done by assuming that the critical Mach number continues to be determined by the velocity occurring near the position of maximum thickness.

Drag beyond critical speed.- The critical Mach number is, in itself, of no interest to the designer of high-speed aircraft. It is useful only insofar as it aids in predicting the sudden changes in forces accompanying the formation of shock waves over an airfoil. Thus the Mach number at which the drag coefficient begins suddenly to depart from its low-speed value, termed the Mach number for drag divergence, is of greater practical interest.

The Mach number for drag divergence has been chosen from the experimental curves (figs. 3 to 18) as that Mach number at which the final rise in drag coefficient begins. For low angles of attack, this point is fairly clearly defined. The drag curve can be approximated by a horizontal line followed by a parabolic rise, and the divergence point is taken to be the beginning of the parabola. At higher angles of attack precise determination of the divergence point is rendered difficult by the presence of the trough discussed previously. In these cases the divergence point is taken to be the bottom of the trough.

The Mach numbers for drag divergence selected in this manner are compared in figure 102 with the critical Mach numbers predicted theoretically. It is seen that the Mach number for drag divergence is very nearly equal to the predicted critical Mach number throughout the range of lift coefficient within which the latter has a high value. The Mach number for drag divergence remains high, however, through a considerably wider range than does the theoretical critical Mach number. This widening of the favorable range of lift coefficient is explained in part by the fact, mentioned previously, that the actual extent of high critical Mach numbers is somewhat greater than theory would indicate. However, this does not constitute a complete explanation, because in the tests of thicker airfoils referred to previously (reference 6) the Mach number for drag divergence was found to remain high through a much wider range of lift coefficient than did even the experimentally determined critical Mach number.

A possible explanation for this extension suggests itself. When, as is the case within the favorable range of lift coefficients, sonic velocity first occurs on the gently curved midportion of the airfoil,

only a slight Mach number gradient exists normal to the surface. A small increase of free-stream Mach number above the critical will produce an extensive region of local supersonic flow, culminating in a shock wave extending far out from the airfoil and involving a correspondingly large drag increase. On the other hand, when sonic velocity is first attained on the sharply curved nose of the airfoil, the local Mach number drops abruptly with distance away from the surface. A much greater increase of free-stream Mach number above the critical may then be required to induce a shock wave extensive enough to produce large losses. Furthermore, when sonic velocity appears first on the midportion of the airfoil rather than at the nose, the boundary layer will be more fully developed at the shock wave. The flow may then be more susceptible to separation in the vicinity of the shock, which will result in rapid increase of drag.

It will be noted that the Mach numbers for drag divergence follow, for some distance in each direction, the extended theoretical critical Mach numbers calculated by neglecting the velocity peak at the nose of the airfoil and assuming that the velocity near midchord is always the greatest to be found anywhere on the airfoil.

Insufficient points are available to determine, with any accuracy, the exact amount by which this favorable range of lift coefficients extends beyond that for high critical Mach numbers. In fairing the curves of figure 102, however, the assumption has been made that the variation of Mach number for drag divergence is of the same jointed form as that of critical Mach number. This assumption may be unwarranted; its justification lies in the fact that curves of this form can be drawn to pass through every point. Whether or not this hypothesis is admitted, it is evident that the range of lift coefficients for good high-speed drag characteristics is twice as wide as the theoretical range of high critical speeds for 12-percent-thick airfoils and three times as wide for the 6-percent-thick sections. It should be noted that, even for the thinnest airfoils tested, high Mach numbers for drag divergence are attained over a wide enough range of lift coefficient to insure adequate maneuverability in a fighter airplane at high speeds, and satisfactory performance at diverse loading conditions and altitudes for a high-speed bomber.

The variation of drag coefficient with Mach number at the design lift coefficient of 0.2 is shown for the 16 airfoils in figure 99. Theoretical critical Mach numbers are also indicated (extended values from fig. 102 are shown for the NACA 65-206 and 66-206 sections). It is seen that at design lift the supercritical drag rise is practically unaffected by position of minimum pressure. The critical Mach number increases so slightly with rearward movement of minimum pressure that significant improvement of high-speed drag characteristics can be achieved only by reducing the airfoil thickness ratio.

Finally, the nature of the increase in drag coefficient beyond the theoretical critical Mach number may be considered. Figure 99 suggests

that the form of the rise may be almost identical, at least near the design lift coefficient, for airfoils of widely varying thickness ratios, as well as different positions of minimum pressure. Attempts based on both theory and experiment have in the past been made to obtain some form of universal drag curve applicable beyond the critical speed. The increment in drag coefficient above that observed at the theoretical critical Mach number is shown in figure 103 for all but one of the airfoils near zero angle of attack as a function of the corresponding increment in Mach number. (Values for the NACA 65-206 airfoil are not shown because no experimental points were obtained within the favorable range of predicted critical Mach number.) The points are seen to define a single curve; all scatter lies within the range of experimental uncertainty, and no consistent variation from the mean appears with change of either thickness or minimum-pressure position. Plotting the same points on logarithmic coordinates shows a slope of 2; accordingly a parabola, given by

$$c_d - c_{d_{cr}} = 2.36 (M - M_{cr})^2 \qquad (1)$$

has been fitted in figure 103. This correlation is not confined to zero angle of attack, because for the NACA 66-212 section the angle was 0.5°. It seems likely that equation (1) will predict the supercritical drag characteristics of these airfoils throughout the theoretical range of lift coefficients for high critical Mach numbers. Outside this range, however, the agreement is found to be mediocre.

The question arises whether this empirical correlation is in accord with the transonic similarity rule (reference 8). Unfortunately, the similarity rule is not strictly applicable here. Each group of airfoils having the same minimum-pressure position would constitute a family of "similar" shapes were it not for the fact that their camber is fixed, rather than proportional to thickness. However, it seems reasonable to apply the rule as an approximation in the following way.

If the airfoils were truly similar, their drag coefficients would be related by

$$c_d = (t/c)^{5/3} D_1(\xi) \qquad (2)$$

where t/c is the thickness ratio, and D_1 is some function of the transonic similarity parameter

$$\xi = \frac{M^2 - 1}{(t/c)^{2/3}} \qquad (3)$$

This rule does not apply even approximately to the present airfoils because camber strongly affects the critical Mach number. Except for the skin friction, which lies outside the scope of the similarity theory, the drag must rise from zero at the critical Mach number. Hence the

similarity rule may be written in another form as

$$c_d - c_{d_{cr}} = (t/c)^{5/3} D_2 (\xi - \xi_{cr}) \quad (4)$$

where ξ_{cr}, the value of the similarity parameter at the theoretical critical Mach number, is, within the accuracy of the transonic similarity theory, a constant for truly similar shapes. In this form it seems reasonable to apply the rule to the present airfoils, because the fact that ξ_{cr} is not constant is accounted for. Thus the dissimilarity due to camber is counterbalanced.[2]

Using the similarity rule in this way, the data of figure 103 can be fitted by taking the function D_2 to be twice the square of its argument.[3] This gives

$$c_d - c_{d_{cr}} = 2(t/c)^{5/3} (\xi - \xi_{cr})^2 = 2(t/c)^{1/3} (M^2 - M_{cr}^2)^2 \quad (5)$$

For all 16 airfoils, this expression differs from that of equation (1) by less than 3 percent. Hence there is no need to replot the data; figure 103 may be regarded alternatively as a correlation according to one form of the transonic similarity rule.

Lift Coefficient

Angle of zero lift.- For incompressible flow, thin-airfoil theory permits calculation of the angle of zero lift, which is determined largely by the camber line, as discussed in reference 3. Assuming the theoretical value of the lift-curve slope, 2π per radian, the angle of zero lift for airfoils having a design lift coefficient of 0.2 and an $a = 1.0$ mean camber line is calculated to be -1.82°. The experimental values are, with one exception, slightly less negative than this at low Mach numbers, in agreement with the results of reference 3. (See fig. 104.) The anomalous behavior of the NACA 65-206 airfoil may result from apparent poor model construction near the trailing edge. At low speeds little consistent variation of zero-lift angle, either with thickness or position of minimum pressure, is evident from figure 104.

---

[2]It seems likely that the latter form of the similarity rule will yield better correlation near the critical Mach number even for similar airfoils, because ξ_{cr} is not actually constant but varies markedly with thickness as a result of higher-order effects.

[3]The simplicity of the numerical factor 2 has no significance, because powers of $(\gamma + 1)$ have been neglected in stating the similarity rule, where γ is the adiabatic exponent.

With increase in Mach number, the angle of zero lift is seen to remain sensibly constant, or tend only slightly closer to 0°, up to the extended theoretical value of the critical Mach number taken from figure 102. Approximately 0.075 Mach number above this critical speed, the 12- and 10-percent-thick airfoils exhibit an abrupt increase in angle of zero lift; and the same effect appears to have just commenced at the highest test Mach numbers for the thinner sections. This sudden change in angle of zero lift, together with the decrease in lift-curve slope discussed later, will require large alterations of trim for an airplane in level flight at any wing loading.

Lift at constant angle of attack.- At moderate angles of attack, the increase of lift coefficient with Mach number is in accord with the Prandtl-Glauert factor $(1 - M^2)^{-1/2}$ up to the critical speed of the section. (See figs. 19 to 34.) At greater angles, however, this characteristic curvature no longer appears; the variation is more nearly linear within the Mach number range 0.30 to 0.60, and in many cases the curvature is actually reversed, as it is for the NACA 65-212 section at 6° and -6°. (See fig. 30.) This behavior can possibly be explained as a variation with Reynolds number, which predominates over the compressibility effect at low speeds.

Supercritical characteristics.- At any angle of attack, shortly after the critical Mach number for the section has been exceeded, the losses in lift which accompany shock-wave formation begin to counteract the subcritical rise. An inflection point is reached in the variation of lift coefficient with Mach number for constant angle of attack followed by a peak beyond which the lift falls rapidly. A final abrupt reversal within the last few thousandths of a Mach number before the choking speed often appears in the present tests, and in most other high-speed subsonic wind-tunnel data.

The rapid loss of lift beyond the critical speed, producing as it does a large change in airplane trim and a dangerous increase in stability, must, for airfoils intended for high-speed aircraft, be postponed to as high a Mach number as is practicable at the large lift coefficients required for dive recovery as well as near design lift. Reduction of airfoil thickness, with consequent increase in critical Mach number, serves within the low drag range to raise the speed at which these undesirable effects appear. Consideration of the theoretical variation of critical Mach number with lift coefficient might lead to the conclusion that any improvement inside the low drag range can be achieved only at the expense of greatly impairing the characteristics at other lift coefficients. That this fear is unfounded is demonstrated in figure 102. Mach number for lift divergence, defined as the inflection point in the curves of figures 19 to 34, is shown as a function of lift coefficient, points used in cross plotting again being indicated. It is seen that, in every case, the behavior of Mach number for lift divergence is similar to that of Mach number for drag divergence discussed previously. Instead of falling off rapidly outside a narrow

range of lift coefficient as does the theoretical critical Mach number, it remains high through an even greater range than does the Mach number for drag divergence, running parallel to the extended critical Mach number curve for a considerable distance in each direction. This widening of the favorable range may be caused by the fact, mentioned before, that the boundary layer will be more resistant to separation in the vicinity of a shock wave which appears near the nose than for one occurring first on the midportion of the airfoil.

It is important to observe that the Mach number for lift divergence lies considerably farther above that for drag divergence in the case of 63-, 64-, and 65-series airfoils than it does for the 66-series sections. As a consequence, because supercritical drag rise is essentially the same for all 6-series airfoils of equal thickness, the 66-series airfoils exhibit adverse compressibility effects at lower speeds, and at lower drag coefficients, than do the other sections. In this respect, then, 66-series airfoils are somewhat inferior in high-speed performance to those having minimum pressure farther forward.

Lift-curve slope.- Low-speed lift-curve slopes shown in figure 105 are smaller than those reported in reference 3 for airfoils of the same series, and appreciably less than the theoretical value for thin airfoils (2π per radian). The discrepancy can probably be attributed to differences in Reynolds number. Variation of thickness ratio and minimum pressure position have little effect on the low-speed lift-curve slope; a slight decrease results in every case, however, from rearward movement of minimum pressure. (See fig. 105(b).)

For all 16 airfoils the increase of lift-curve slope with Mach number is well represented at moderate speeds by the factor $(1 - M^2)^{-1/2}$ derived from small perturbation theory. At higher Mach numbers, the rise is somewhat more rapid, reaching a sharp peak beyond the critical speed.[4] This peak is delayed to higher values of Mach number and lift coefficient with decrease of thickness ratio and also with forward movement of the chordwise position of minimum base-profile pressure. This delay is ordinarily desirable. It must be noted, however, that excessively high values of wing lift-curve slope tend to produce airplane instability, as discussed in reference 2. For this reason the present 6-percent-thick sections may be unsuitable for use on unswept-wing aircraft in cases for which the low-speed stability is marginal. Furthermore, great care must be exercised in the choice of a section for the horizontal tail plane when a thin wing section is employed. Serious instability may result if the tail plane is so thick that it experiences a loss of lift-curve slope at a lower Mach number than does the wing.

As discussed previously, the transonic similarity rule is not strictly applicable to these airfoils because of their fixed camber.

[4] For the NACA 65-206 and 66-206 sections, the theoretical critical Mach numbers indicated in figure 105 are the extended values taken from figure 102.

However, according to thin wing theory, lift-curve slope is independent of camber in both subsonic and supersonic flow. It seems reasonable to assume that this is true also in the intermediate transonic range provided that the lift curve is linear. If so, the lift-curve slopes for airfoils having the same thickness distribution but different thickness ratios t/c are related by

$$\frac{dc_l}{d\alpha} = (t/c)^{-1/3} \; L_\alpha(\xi) \qquad (6)$$

where L_α is some function of the transonic similarity parameter ξ (equation 3).

The present lift curves are generally fairly linear up to the design lift coefficient of 0.2 (see figs. 67 to 82). Therefore, the "reduced lift-curve slope," $(t/c)^{1/3}\,(dc_l/d\alpha)$, at design lift has been plotted as a function of the similarity parameter in figure 106. Comparison with figure 105(a) shows that, in general, the correlation of data at high Mach numbers has been significantly improved. Excepting the anomalous results for the 65-208 airfoil, the correlation probably lies within the bounds of experimental error and uncertainty in blockage corrections.

The lift curves themselves (figs. 67 to 82) often show, above the low drag range of lift coefficient, the jog typical of NACA 6-series airfoils, which is analyzed in reference 9. Beyond a Mach number of 0.65 or 0.70 the jog disappears or is obscured by other phenomena. The results of reference 9 indicate that at least for low speeds it will vanish entirely at flight values of Reynolds number, and there is little reason to doubt that it will then disappear at all speeds.

Maximum lift coefficient.- It must at the outset be emphasized that the low-speed values of maximum lift coefficient obtained in these tests are not applicable to flight conditions. Numerous investigations have indicated that scale effect is so great that, at the higher Reynolds numbers of flight, maximum lift coefficients half again as large as those shown in figure 107 may be attained. Other tests of several of the present airfoils at greater values of Reynolds number indicate, as would be anticipated, that the low-speed maximum lift coefficient increases as the minimum pressure is moved forward as far as the 40-percent-chord position. (See reference 3.)

The results of reference 10 indicate that scale effect on maximum lift coefficient vanishes above a Mach number of about 0.55. The present results shown in figure 107 can therefore probably be applied with confidence above 0.60 Mach number. At these higher speeds the maximum lift coefficient is greatest for airfoils having minimum pressure at the 40- or 50-percent-chord position. Thus it is seen that airfoil sections with minimum pressure near 40 percent of the chord, in addition to having almost as good high-speed drag characteristics as sections with minimum pressure farther back, and higher Mach numbers for lift divergence and

for change of angle of zero lift, likewise demonstrate higher maximum lift coefficients at low speeds as reported in reference 3; and, as shown by the present tests, these airfoil sections maintain this superiority up to high Mach numbers.

All 16 airfoils show desirable gradual-stall characteristics up to high Mach numbers (figs. 67 to 82). The nature of the stall seems to be essentially independent of both thickness ratio and position of minimum pressure.

Pitching-Moment Coefficient

The pitching moment of an airfoil, like the angle of zero lift, is determined mainly by the mean camber line. The low-speed value can accordingly be calculated from thin-airfoil theory. For all 16 airfoils considered here, the theoretical value of the quarter-chord pitching-moment coefficient is -0.05. (See reference 3.) Figures 35 to 50 indicate the experimental values to be in most cases smaller than this at low speeds and low angles of attack, and reference 3 reports that such is generally the case for airfoils cambered with the uniform-load type ($a = 1.0$) of mean camber line.

At moderate angles of attack, the variation of pitching-moment coefficient with Mach number up to the critical is represented roughly by the factor $(1 - M^2)^{-1/2}$ from small-perturbation theory. At higher Mach numbers the variation definitely departs from this rule.

It would be desirable at this point to define a moment divergence, analogous to the drag and lift divergences discussed previously, and to consider as before the Mach number at which it occurs. However, consideration of figures 35 to 50 indicates that changes in pitching-moment coefficient are much less pronounced near the critical speed than are changes in either drag or lift coefficient. Consequently, formulation of a criterion for moment divergence has not been attempted.

Figure 108 presents the variation with Mach number of the quarter-chord moment coefficient at the design lift coefficient.[5] The variation is similar for all 16 airfoils, no effects of changing either thickness or minimum-pressure position being discernible.

Because of the strong effect of camber upon pitching moment, no attempt has been made to apply the transonic similarity rule.

---

[5]Again, for the NACA 65-206 and 66-206 airfoils extended values of M_{cr} are shown.

CONCLUSIONS

The most important conclusions to be drawn from tests at high subsonic speeds of 16 NACA 6-series airfoil sections are the following:

1. The "bucket" form of the low drag range of the drag curve appears to persist up to the critical speed of the section, the corresponding range of lift coefficient increasing with Mach number by the factor $(1 - M^2)^{-1/2}$.

2. The Mach number at which a rapid increase in drag coefficient begins is very nearly equal to the critical Mach number predicted by the theory of references 1 or 3 throughout the range of lift coefficient within which the theoretical value is high. Outside this range, all 16 airfoils continue to exhibit good drag and lift characteristics through a considerably wider range of lift coefficient.

3. Near design lift, the increase in section drag coefficient beyond the predicted critical Mach number is nearly identical for all 16 airfoils and can be represented by a parabola. This correlation is in accord with the transonic similarity rule.

4. Within the limits investigated, variation of chordwise position of minimum base-profile pressure has almost no effect on the high-speed drag characteristics of these airfoils. Appreciable improvement can be achieved only by reduction of thickness ratio.

5. The 66-series airfoils tested were found to be decidedly inferior to the other sections as far as maintaining good high-speed lift characteristics beyond the critical speed. Forward movement of the position of minimum pressure to 40-percent of the chord, in addition to raising the maximum lift coefficient at high speed, produces two effects favorable to high-speed stability and control. Abrupt increases in angle of zero lift and decreases in lift-curve slope are both delayed to Mach numbers farther above that at which the drag begins to rise.

Ames Aeronautical Laboratory,
National Advisory Committee for Aeronautics,
Moffett Field, Calif., December 13, 1951.

REFERENCES

1. Heaslet, Max. A.: Critical Mach Numbers of Various Airfoil Sections. NACA ACR 4G18, 1944.

2. Hood, Manley J., and Allen, H. Julian: The Problem of Longitudinal Stability and Control at High Speeds. NACA Rep. 767, 1943.

3. Abbott, Ira H., von Doenhoff, Albert E., and Stivers, Louis S., Jr.: Summary of Airfoil Data. NACA Rep. 824, 1945.

4. Heaslet, Max. A.: Theoretical Investigation of Methods for Computing Drag from Wake Surveys at High Subsonic Speeds. NACA ARR 5C21, 1945.

5. Allen, H. Julian, and Vincenti, Walter G.: Wall Interference in a Two-Dimensional-Flow Wind Tunnel, with Consideration of the Effect of Compressibility. NACA Rep. 782, 1944.

6. Graham, Donald J., Nitzberg, Gerald E., and Olson, Robert N.: A Systematic Investigation of Pressure Distributions at High Speeds over Five Representative NACA Low-Drag and Conventional Airfoil Sections. NACA Rep. 832, 1945.

7. Knowler, A. E., and Pruden, F. W.: On the Drag of Circular Cylinders at High Speeds. R.&M. No. 1933, British A.R.C., 1944.

8. von Kármán, Theodor: The Similarity Law of Transonic Flow. Jour. Math. and Phys., vol. XXVI, no. 3, October 1947, pp. 182-190.

9. von Doenhoff, Albert E., and Tetervin, Neal: Investigation of the Variation of Lift Coefficient with Reynolds Number at a Moderate Angle of Attack on a Low-Drag Airfoil. NACA CB(19), 1942.

10. Spreiter, John R., and Steffen, Paul J.: Effect of Mach and Reynolds Numbers on Maximum Lift Coefficient. NACA TN 1044, 1946.

TABLE I.- AIRFOIL ORDINATES

[Stations and ordinates given in percent of airfoil chord]

NACA 63-206

Upper surface		Lower surface	
Station	Ordinate	Station	Ordinate
0	0	0	0
.458	.551	.542	-.451
.703	.677	.797	-.537
1.197	.876	1.303	-.662
2.438	1.241	2.562	-.869
4.932	1.776	5.068	-1.144
7.429	2.189	7.571	-1.341
9.930	2.526	10.070	-1.492
14.934	3.058	15.066	-1.712
19.941	3.451	20.059	-1.859
24.950	3.736	25.050	-1.946
29.960	3.926	30.040	-1.982
34.970	4.030	35.030	-1.970
39.981	4.042	40.019	-1.900
44.991	3.972	45.009	-1.782
50.000	3.826	50.000	-1.620
55.008	3.612	54.992	-1.422
60.015	3.338	59.985	-1.196
65.020	3.012	64.980	-.952
70.023	2.642	69.977	-.698
75.023	2.237	74.977	-.447
80.022	1.804	79.978	-.212
85.019	1.356	84.981	-.010
90.013	.900	89.987	.134
95.006	.454	94.993	.178
100.000	0	100.000	0

L. E. radius: 0.297
Slope of radius through L. E.: 0.0842

NACA 63-208

Upper surface		Lower surface	
Station	Ordinate	Station	Ordinate
0	0	0	0
.444	.715	.556	-.615
.687	.876	.813	-.736
1.179	1.131	1.321	-.917
2.418	1.592	2.582	-1.220
4.909	2.266	5.091	-1.634
7.406	2.780	7.594	-1.932
9.906	3.201	10.094	-2.167
14.912	3.861	15.088	-2.515
19.922	4.345	20.078	-2.753
24.934	4.690	25.066	-2.900
29.947	4.918	30.053	-2.974
34.961	5.030	35.039	-2.970
39.974	5.027	40.026	-2.885
44.988	4.919	45.012	-2.729
50.000	4.717	50.000	-2.511
55.011	4.429	54.989	-2.239
60.019	4.069	59.981	-1.927
65.026	3.645	64.974	-1.585
70.030	3.170	69.970	-1.226
75.031	2.657	74.969	-.867
80.029	2.115	79.971	-.523
85.025	1.563	84.975	-.217
90.017	1.013	89.983	.021
95.008	.494	94.992	.138
100.000	0	100.000	0

L. E. radius: 0.503
Slope of radius through L. E.: 0.0842

NACA 63-210

Upper surface		Lower surface	
Station	Ordinate	Station	Ordinate
0	0	0	0
.430	.876	.570	-.776
.669	1.107	.831	-.967
1.162	1.379	1.338	-1.165
2.398	1.939	2.602	-1.567
4.886	2.753	5.114	-2.121
7.382	3.372	7.618	-2.524
9.882	3.877	10.118	-2.843
14.890	4.666	15.110	-3.320
19.902	5.240	20.098	-3.648
24.917	5.647	25.083	-3.857
29.933	5.910	30.067	-3.966
34.951	6.030	35.049	-3.970
39.968	6.009	40.032	-3.867
44.985	5.861	45.015	-3.671
50.000	5.599	50.000	-3.393
55.013	5.235	54.987	-3.045
60.024	4.786	59.976	-2.644
65.032	4.264	64.968	-2.205
70.037	3.684	69.963	-1.740
75.038	3.061	74.962	-1.271
80.036	2.414	79.964	-.822
85.030	1.761	84.970	-.415
90.021	1.121	89.979	-.087
95.010	.530	94.990	.102
100.000	0	100.000	0

L. E. radius: 0.770
Slope of radius through L. E.: 0.0842

NACA 63-212

Upper surface		Lower surface	
Station	Ordinate	Station	Ordinate
0	0	0	0
.417	1.032	.583	-.932
.657	1.260	.843	-1.120
1.145	1.622	1.355	-1.408
2.378	2.284	2.622	-1.912
4.863	3.238	5.137	-2.606
7.358	3.963	7.642	-3.115
9.859	4.554	10.141	-3.520
14.868	5.470	15.132	-4.124
19.882	6.137	20.118	-4.545
24.900	6.606	25.100	-4.816
29.920	6.902	30.080	-4.958
34.941	7.030	35.059	-4.970
39.962	6.991	40.038	-4.849
44.982	6.799	45.018	-4.609
50.000	6.473	50.000	-4.267
55.016	6.030	54.984	-3.840
60.029	5.491	59.971	-3.349
65.038	4.870	64.962	-2.810
70.043	4.182	69.957	-2.238
75.045	3.451	74.955	-1.661
80.042	2.698	79.958	-1.106
85.035	1.947	84.965	-.601
90.025	1.224	89.975	-.190
95.012	.566	94.988	.066
100.000	0	100.000	0

L. E. radius: 1.087
Slope of radius through L. E.: 0.0842

TABLE I.- CONTINUED

[Stations and ordinates given in percent of airfoil chord]

NACA 64-206

Upper surface		Lower surface	
Station	Ordinate	Station	Ordinate
0	0	0	0
.459	.542	.541	-.442
.704	.664	.796	-.524
1.198	.859	1.302	-.645
2.440	1.208	2.560	-.836
4.934	1.719	5.066	-1.087
7.432	2.115	7.568	-1.267
9.933	2.444	10.067	-1.410
14.937	2.970	15.063	-1.624
19.943	3.367	20.057	-1.775
24.952	3.667	25.048	-1.877
29.961	3.879	30.039	-1.935
34.971	4.011	35.029	-1.951
39.981	4.066	40.019	-1.924
44.991	4.014	45.009	-1.824
50.000	3.878	50.000	-1.672
55.008	3.670	54.992	-1.480
60.015	3.402	59.985	-1.260
65.020	3.080	64.980	-1.020
70.023	2.712	69.977	-.768
75.025	2.307	74.975	-.517
80.024	1.868	79.976	-.276
85.020	1.410	84.980	-.064
90.015	.940	89.985	.094
95.007	.473	94.993	.159
100.000	0	100.000	0

L. E. radius: 0.256
Slope of radius through L. E.: 0.084

NACA 64-208

Upper surface		Lower surface	
Station	Ordinate	Station	Ordinate
0	0	0	0
.445	.706	.555	-.606
.688	.862	.812	-.722
1.180	1.110	1.320	-.896
2.421	1.549	2.579	-1.177
4.912	2.189	5.088	-1.557
7.410	2.681	7.590	-1.833
9.910	3.089	10.090	-2.055
14.915	3.741	15.085	-2.395
19.924	4.232	20.076	-2.640
24.935	4.598	25.065	-2.808
29.948	4.856	30.052	-2.912
34.961	5.009	35.039	-2.949
39.974	5.063	40.026	-2.921
44.988	4.978	45.012	-2.788
50.000	4.787	50.000	-2.581
55.011	4.506	54.989	-2.316
60.020	4.152	59.980	-2.010
65.027	3.734	64.973	-1.674
70.031	3.263	69.969	-1.319
75.032	2.749	74.968	-.959
80.031	2.200	79.969	-.608
85.027	1.634	84.973	-.288
90.019	1.067	89.981	-.033
95.010	.522	94.990	.110
100.000	0	100.000	0

L. E. radius: 0.470
Slope of radius through L. E.: 0.084

NACA 64-210

Upper surface		Lower surface	
Station	Ordinate	Station	Ordinate
.0	0	0	0
.431	.867	.569	-.767
.673	1.056	.827	-.916
1.163	1.394	1.337	-1.140
2.401	1.884	2.599	-1.512
4.890	2.656	5.110	-2.024
7.387	3.248	7.613	-2.400
9.887	3.737	10.113	-2.703
14.894	4.514	15.106	-3.168
19.905	5.097	20.095	-3.505
24.919	5.533	25.081	-3.743
29.934	5.836	30.066	-3.892
34.951	6.010	35.049	-3.950
39.968	6.059	40.032	-3.917
44.985	5.938	45.015	-3.748
50.000	5.689	50.000	-3.483
55.014	5.333	54.986	-3.143
60.025	4.891	59.975	-2.749
65.033	4.375	64.967	-2.315
70.038	3.799	69.962	-1.855
75.040	3.176	74.960	-1.386
80.038	2.518	79.962	-.926
85.032	1.849	84.968	-.503
90.023	1.188	89.977	-.154
95.012	.564	94.988	.068
100.000	0	100.000	0

L. E. radius: 0.720
Slope of radius through L. E.: 0.084

NACA 64-212

Upper surface		Lower surface	
Station	Ordinate	Station	Ordinate
0	0	0	0
.418	1.025	.582	-.925
.659	1.245	.841	-1.105
1.147	1.593	1.353	-1.379
2.382	2.218	2.618	-1.846
4.868	3.123	5.132	-2.491
7.364	3.815	7.636	-2.967
9.865	4.386	10.135	-3.352
14.872	5.291	15.128	-3.945
19.886	5.968	20.114	-4.376
24.903	6.470	25.097	-4.680
29.921	6.815	30.079	-4.871
34.941	7.008	35.059	-4.948
39.961	7.052	40.039	-4.910
44.982	6.893	45.018	-4.703
50.000	6.583	50.000	-4.377
55.016	6.151	54.984	-3.961
60.029	5.619	59.971	-3.477
65.039	5.004	64.961	-2.944
70.045	4.322	69.955	-2.378
75.047	3.590	74.953	-1.800
80.045	2.825	79.955	-1.233
85.038	2.054	84.962	-.708
90.027	1.303	89.973	-.269
95.013	.604	94.987	.028
100.000	0	100.000	0

L. E. radius: 1.040
Slope of radius through L. E.: 0.084

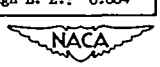

TABLE I.- CONTINUED

[Stations and ordinates given in percent of airfoil chord]

NACA 65-206

Upper surface		Lower surface	
Station	Ordinate	Station	Ordinate
0	0	0	0
.460	.524	.540	-.424
.706	.642	.794	-.502
1.200	.822	1.300	-.608
2.444	1.140	2.556	-.768
4.939	1.625	5.061	-.993
7.437	2.012	7.563	-1.164
9.936	2.340	10.064	-1.306
14.939	2.869	15.061	-1.523
19.945	3.277	20.055	-1.685
24.953	3.592	25.047	-1.802
29.962	3.824	30.038	-1.880
34.971	3.982	35.029	-1.922
39.981	4.069	40.019	-1.927
44.990	4.078	45.010	-1.888
50.000	4.003	50.000	-1.797
55.009	3.836	54.991	-1.646
60.016	3.589	59.984	-1.447
65.022	3.276	64.978	-1.216
70.026	2.907	69.974	-.963
75.028	2.489	74.972	-.699
80.027	2.029	79.973	-.437
85.024	1.538	84.976	-.192
90.018	1.027	89.982	.007
95.009	.511	94.991	.121
100.000	0	100.000	0

L. E. radius: 0.240
Slope of radius through L. E.: 0.084

NACA 65-208

Upper surface		Lower surface	
Station	Ordinate	Station	Ordinate
0	0	0	0
.447	.675	.553	-.575
.691	.824	.809	-.684
1.184	1.050	1.316	-.836
2.426	1.451	2.574	-1.079
4.918	2.059	5.082	-1.427
7.415	2.540	7.585	-1.692
9.915	2.948	10.085	-1.914
14.919	3.603	15.081	-2.257
19.927	4.107	20.073	-2.515
24.937	4.493	25.063	-2.703
29.949	4.777	30.051	-2.833
34.961	4.968	35.039	-2.908
39.974	5.069	40.026	-2.927
44.987	5.069	45.013	-2.879
50.000	4.960	50.000	-2.754
55.012	4.733	54.988	-2.543
60.022	4.408	59.978	-2.266
65.029	4.001	64.971	-1.941
70.034	3.525	69.966	-1.581
75.037	2.991	74.963	-1.201
80.036	2.413	79.964	-.821
85.031	1.804	84.969	-.458
90.023	1.181	89.977	-.147
95.012	.568	94.988	.064
100.000	0	100.000	0

L. E. radius: 0.434
Slope of radius through L. E.: 0.084

NACA 65-210

Upper surface		Lower surface	
Station	Ordinate	Station	Ordinate
0	0	0	0
.435	.819	.565	-.719
.678	.999	.822	-.859
1.169	1.273	1.331	-1.059
2.408	1.757	2.592	-1.385
4.898	2.491	5.102	-1.859
7.394	3.069	7.606	-2.221
9.894	3.555	10.106	-2.521
14.899	4.338	15.101	-2.992
19.909	4.938	20.091	-3.346
24.921	5.397	25.079	-3.607
29.936	5.732	30.064	-3.788
34.951	5.954	35.049	-3.894
39.968	6.067	40.032	-3.925
44.984	6.058	45.016	-3.868
50.000	5.915	50.000	-3.709
55.014	5.625	54.986	-3.435
60.027	5.217	59.973	-3.075
65.036	4.712	64.964	-2.652
70.043	4.128	69.957	-2.184
75.045	3.479	74.955	-1.689
80.044	2.783	79.956	-1.191
85.038	2.057	84.962	-.711
90.028	1.327	89.972	-.293
95.014	.622	94.986	.010
100.000	0	100.000	0

L. E. radius: 0.687
Slope of radius through L. E.: 0.084

NACA 65-212

Upper surface		Lower surface	
Station	Ordinate	Station	Ordinate
0	0	0	0
.423	.970	.577	-.870
.664	1.176	.836	-1.036
1.154	1.491	1.346	-1.277
2.391	2.058	2.609	-1.686
4.878	2.919	5.122	-2.287
7.373	3.593	7.627	-2.745
9.873	4.162	10.127	-3.128
14.879	5.073	15.121	-3.727
19.890	5.770	20.110	-4.178
24.906	6.300	25.094	-4.510
29.923	6.687	30.077	-4.743
34.942	6.942	35.058	-4.882
39.961	7.068	40.039	-4.926
44.981	7.044	45.019	-4.854
50.000	6.860	50.000	-4.654
55.017	6.507	54.983	-4.317
60.032	6.014	59.968	-3.872
65.043	5.411	64.957	-3.351
70.050	4.715	69.950	-2.771
75.053	3.954	74.947	-2.164
80.052	3.140	79.948	-1.548
85.045	2.302	84.955	-.956
90.033	1.463	89.967	-.429
95.017	.672	94.983	-.040
100.000	0	100.000	0

L. E. radius: 1.000
Slope of radius through L. E.: 0.084

TABLE I.- CONCLUDED

[Stations and ordinates given in percent of airfoil chord]

NACA 66-206

Upper surface		Lower surface	
Station	Ordinate	Station	Ordinate
0	0	0	0
.461	.509	.539	-.409
.707	.622	.793	-.482
1.202	.798	1.298	-.584
2.447	1.102	2.553	-.730
4.941	1.572	5.059	-.940
7.439	1.947	7.561	-1.099
9.939	2.268	10.061	-1.234
14.942	2.791	15.058	-1.445
19.947	3.196	20.053	-1.604
24.954	3.513	25.046	-1.723
29.962	3.754	30.038	-1.810
34.971	3.929	35.029	-1.869
39.981	4.042	40.019	-1.900
44.990	4.095	45.010	-1.905
50.000	4.088	50.000	-1.882
55.009	4.020	54.991	-1.830
60.018	3.886	59.982	-1.744
65.026	3.641	64.974	-1.581
70.031	3.288	69.969	-1.344
75.034	2.848	74.966	-1.058
80.034	2.339	79.966	-.747
85.031	1.780	84.969	-.434
90.023	1.182	89.977	-.148
95.012	.578	94.988	.054
100.000	0	100.000	0

L.E. radius: 0.223
Slope of radius through L.E.: 0.084

NACA 66-208

Upper surface		Lower surface	
Station	Ordinate	Station	Ordinate
0	0	0	0
.449	.658	.551	-.558
.693	.803	.807	-.663
1.186	1.024	1.314	-.810
2.429	1.403	2.571	-1.031
4.922	1.987	5.078	-1.355
7.419	2.453	7.581	-1.605
9.918	2.851	10.082	-1.817
14.922	3.498	15.078	-2.152
19.929	3.996	20.071	-2.404
24.939	4.384	25.061	-2.594
29.950	4.681	30.050	-2.737
34.962	4.895	35.038	-2.835
39.974	5.033	40.026	-2.891
44.987	5.095	45.013	-2.905
50.000	5.081	50.000	-2.875
55.012	4.991	54.988	-2.801
60.024	4.811	59.976	-2.669
65.034	4.489	64.966	-2.429
70.041	4.034	69.959	-2.090
75.045	3.469	74.955	-1.679
80.045	2.823	79.955	-1.231
85.040	2.119	84.960	-.773
90.030	1.380	89.970	-.346
95.016	.654	94.984	-.022
100.000	0	100.000	0

L.E. radius: 0.411
Slope of radius through L.E.: 0.084

NACA 66-210

Upper surface		Lower surface	
Station	Ordinate	Station	Ordinate
0	0	0	0
.436	.806	.564	-.706
.679	.980	.821	-.840
1.171	1.245	1.329	-1.031
2.412	1.699	2.588	-1.327
4.902	2.401	5.098	-1.769
7.399	2.958	7.601	-2.110
9.898	3.432	10.102	-2.398
14.903	4.202	15.097	-2.856
19.912	4.796	20.088	-3.204
24.924	5.257	25.076	-3.467
29.937	5.608	30.063	-3.664
34.952	5.862	35.048	-3.802
39.968	6.024	40.032	-3.882
44.984	6.095	45.016	-3.905
50.000	6.074	50.000	-3.868
55.016	5.960	54.984	-3.770
60.030	5.736	59.970	-3.594
65.042	5.332	64.958	-3.272
70.051	4.759	69.949	-2.815
75.056	4.071	74.944	-2.281
80.055	3.289	79.945	-1.697
85.049	2.445	84.951	-1.099
90.037	1.570	89.963	-.536
95.019	.724	94.981	-.092
100.000	0	100.000	0

L.E. radius: 0.662
Slope of radius through L.E.: 0.084

NACA 66-212

Upper surface		Lower surface	
Station	Ordinate	Station	Ordinate
0	0	0	0
.424	.953	.576	-.853
.666	1.154	.834	-1.014
1.156	1.462	1.344	-1.248
2.395	1.991	2.605	-1.619
4.883	2.809	5.117	-2.177
7.379	3.459	7.621	-2.611
9.878	4.011	10.122	-2.977
14.883	4.905	15.117	-3.559
19.894	5.596	20.106	-4.004
24.908	6.132	25.092	-4.342
29.925	6.539	30.075	-4.595
34.943	6.833	35.057	-4.773
39.962	7.018	40.038	-4.876
44.981	7.095	45.019	-4.905
50.000	7.068	50.000	-4.862
55.019	6.931	54.981	-4.741
60.036	6.659	59.964	-4.517
65.051	6.169	64.949	-4.109
70.061	5.487	69.939	-3.543
75.066	4.661	74.934	-2.871
80.065	3.739	79.935	-2.147
85.057	2.755	84.943	-1.409
90.043	1.750	89.957	-.716
95.022	.789	94.978	-.157
100.000	0	100.000	0

L.E. radius: 0.952
Slope of radius through L.E.: 0.084

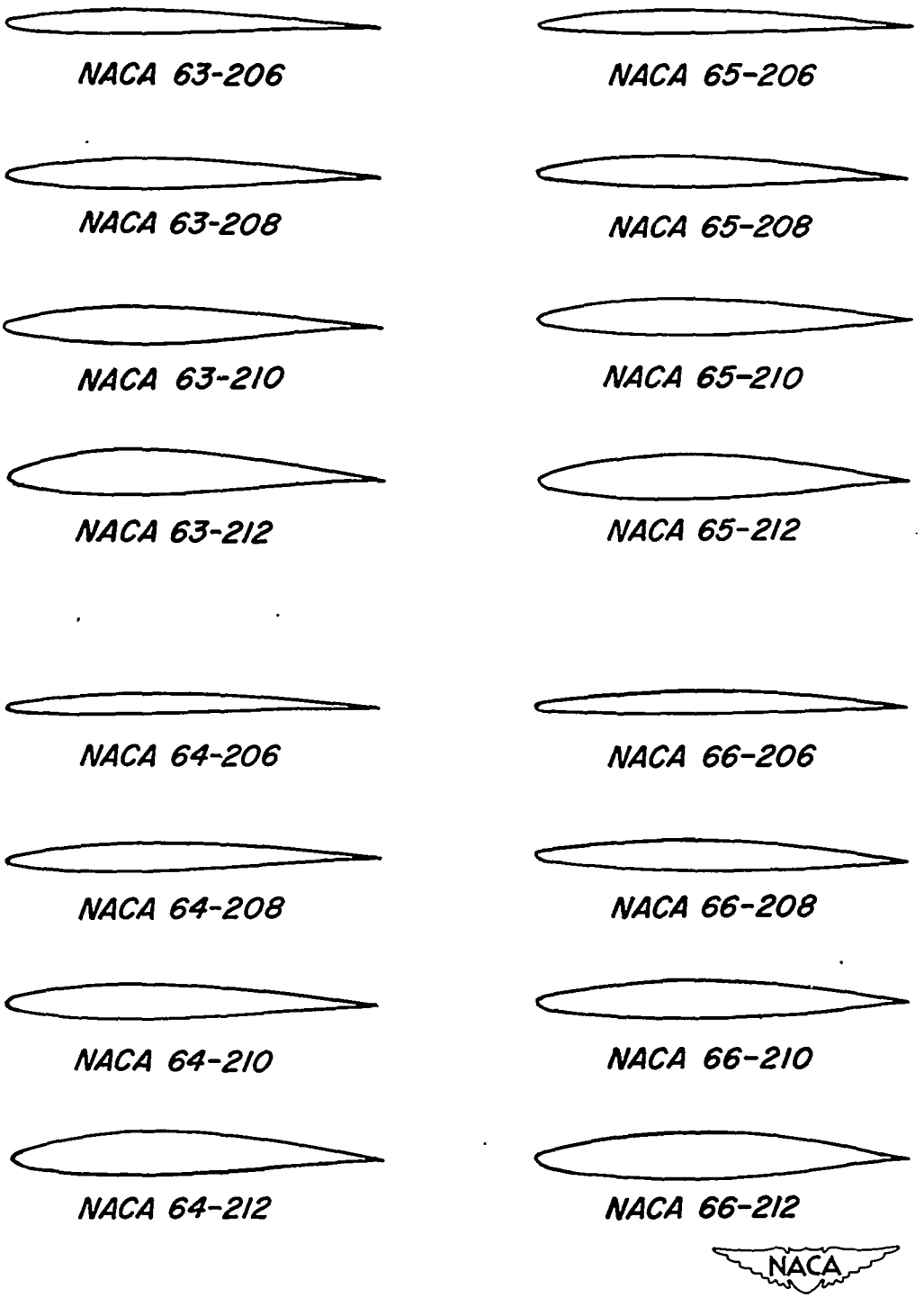

Figure 1.- NACA 6-series airfoil sections having uniform-load type (a=1.0) mean camber line.

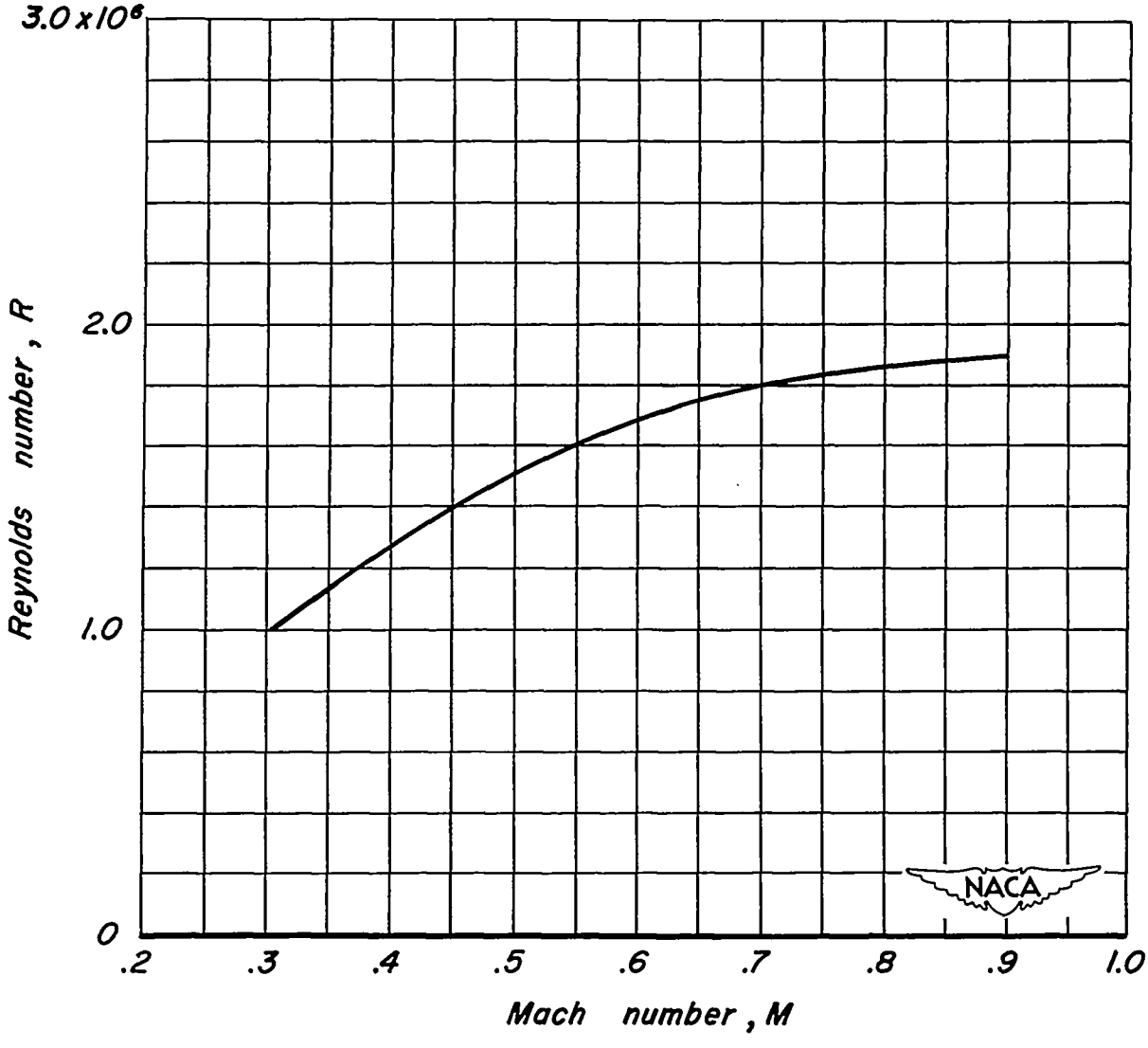

Figure 2.- Variation of Reynolds number with Mach number.

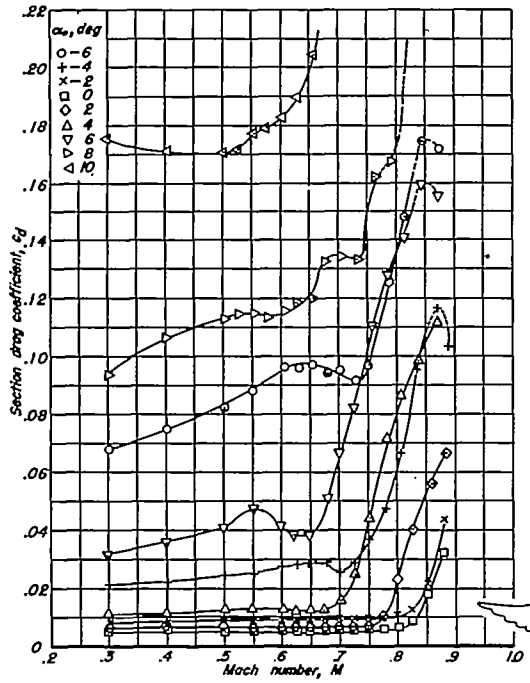

Figure 3.- The variation of section drag coefficient with Mach number for the NACA 63-206 airfoil.

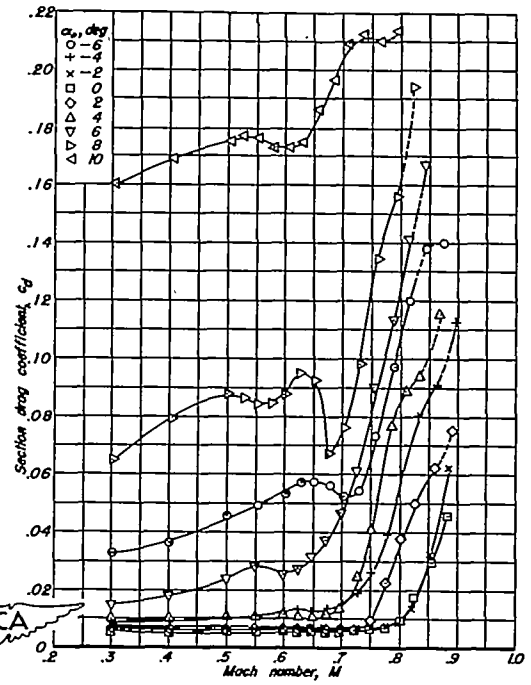

Figure 4.- The variation of section drag coefficient with Mach number for the NACA 63-208 airfoil.

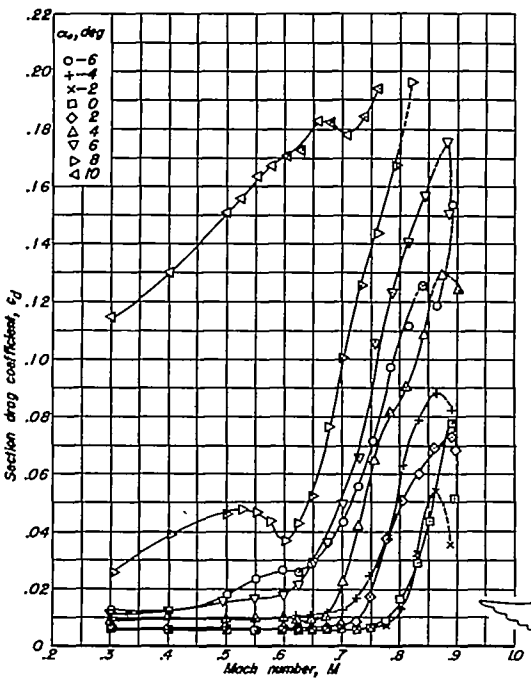

Figure 5.- The variation of section drag coefficient with Mach number for the NACA 63-210 airfoil.

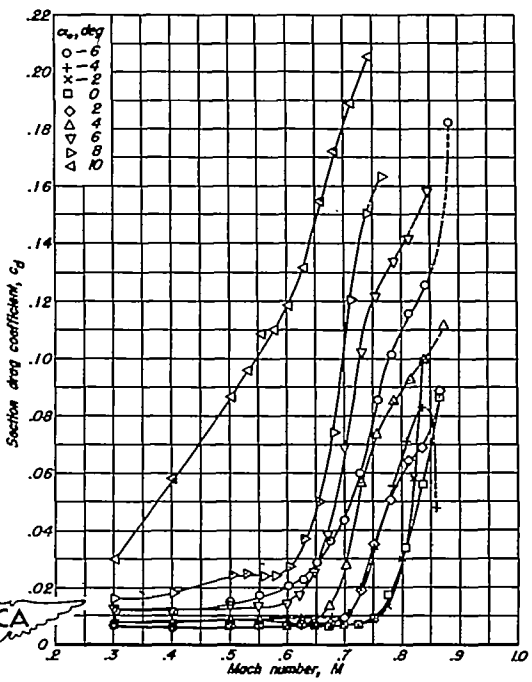

Figure 6.- The variation of section drag coefficient with Mach number for the NACA 63-212 airfoil.

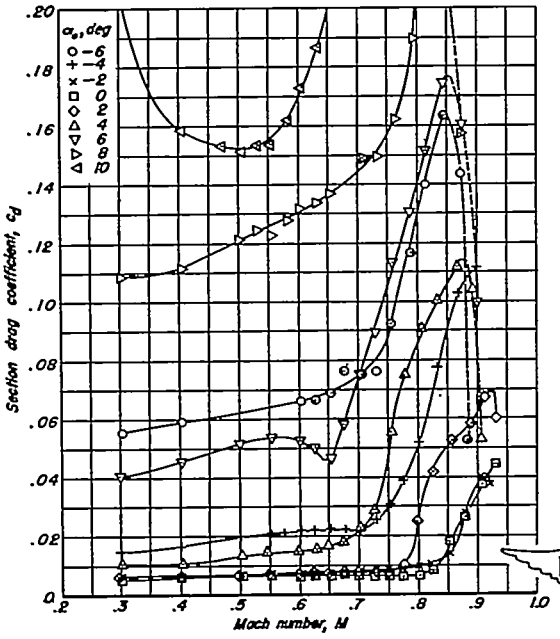

Figure 7.- Variation of section drag coefficient with Mach number for the NACA 64-206 airfoil.

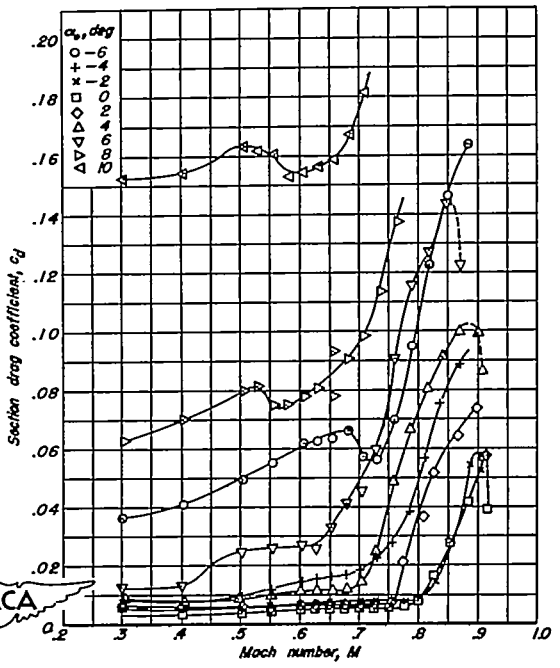

Figure 8.- Variation of section drag coefficient with Mach number for the NACA 64-208 airfoil.

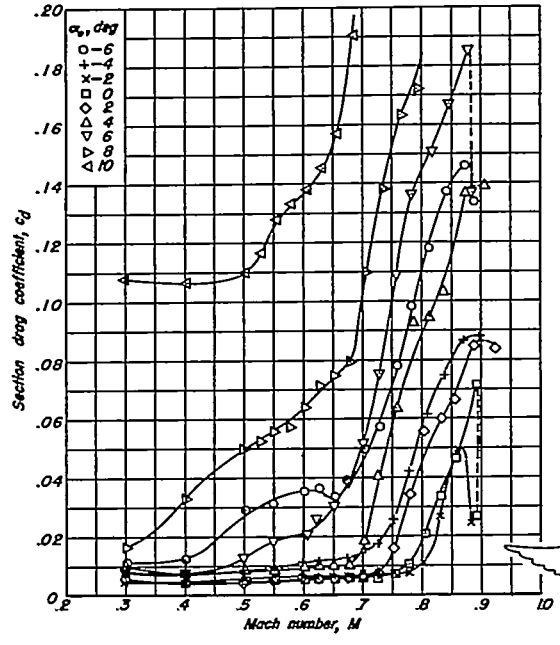

Figure 9.- Variation of section drag coefficient with Mach number for the NACA 64-210 airfoil.

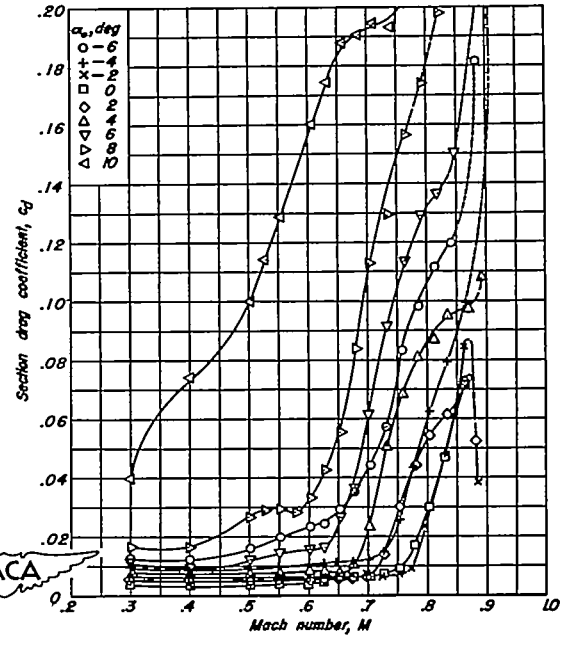

Figure 10.- Variation of section drag coefficient with Mach number for the NACA 64-212 airfoil.

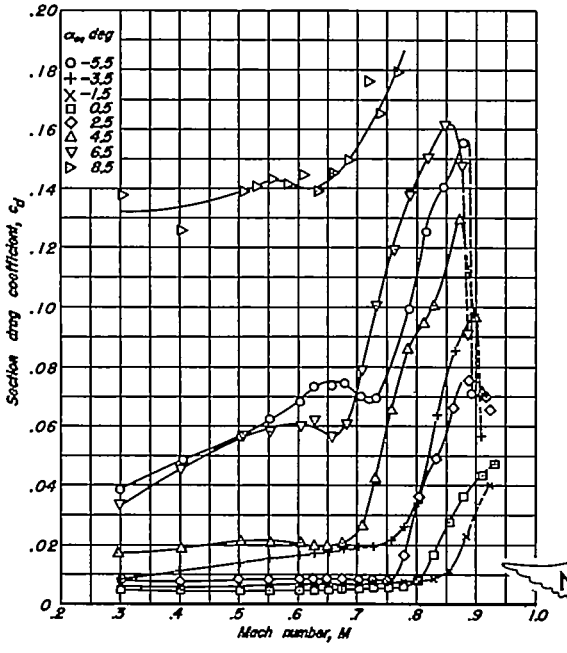

Figure 11.-Variation of section drag coefficient with Mach number for the NACA 65-206 airfoil.

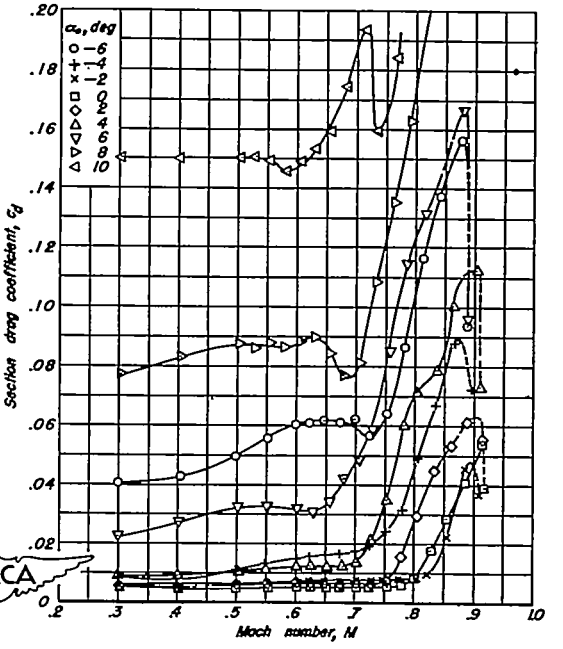

Figure 12.-Variation of section drag coefficient with Mach number for the NACA 65-208 airfoil.

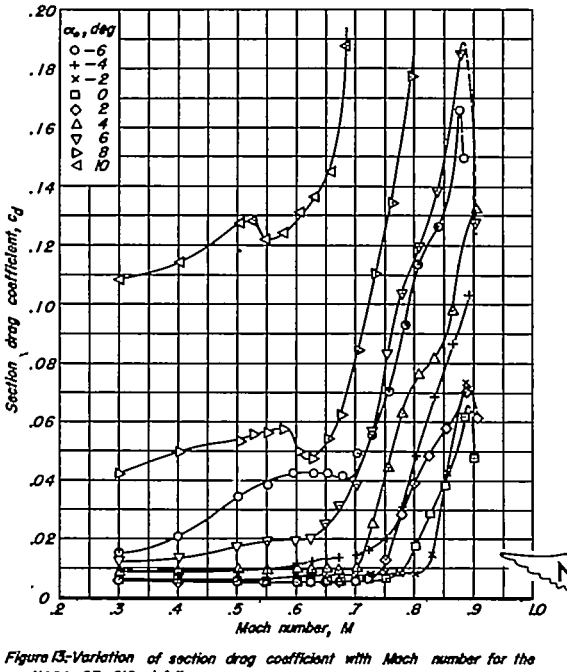

Figure 13.-Variation of section drag coefficient with Mach number for the NACA 65-210 airfoil.

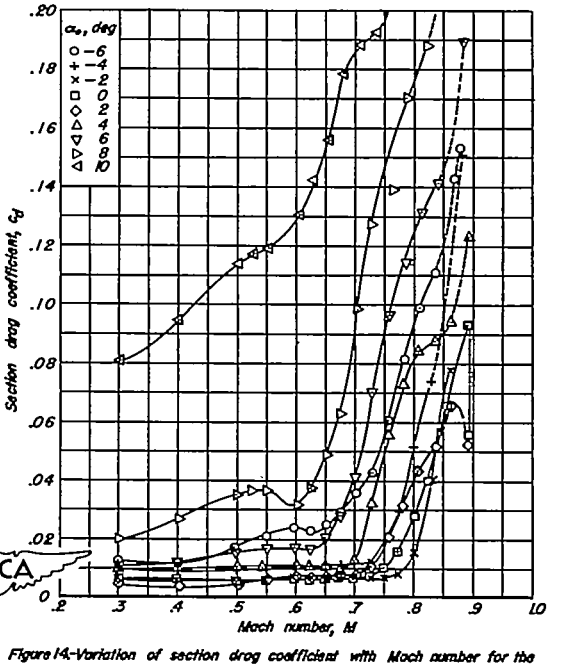

Figure 14.-Variation of section drag coefficient with Mach number for the NACA 65-212 airfoil.

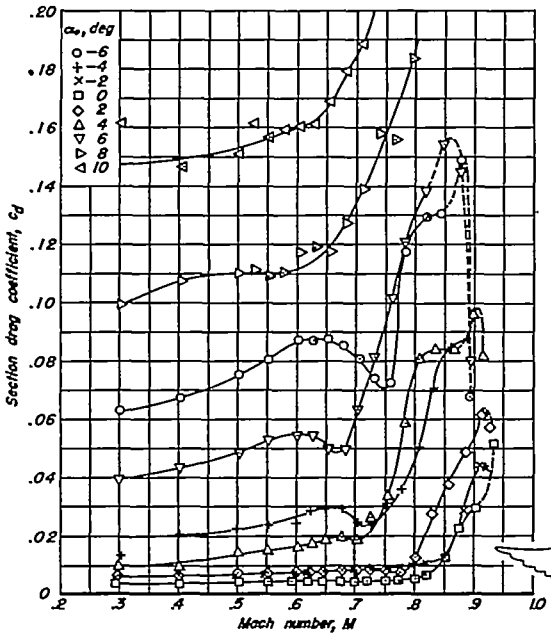

Figure 15.-Variation of section drag coefficient with Mach number for the NACA 66-206 airfoil.

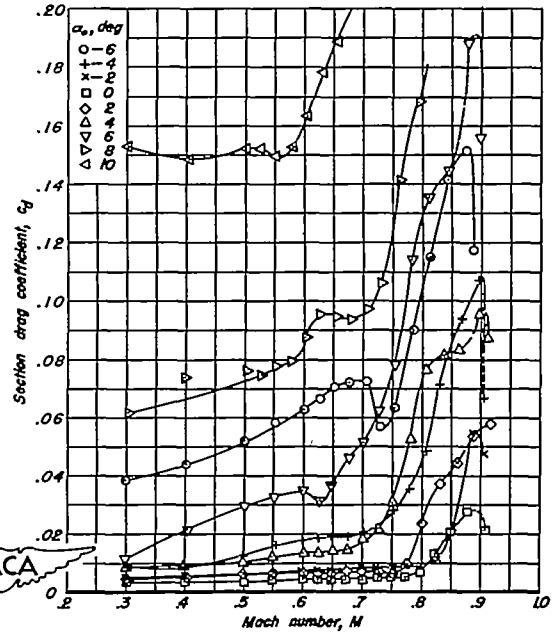

Figure 16.-Variation of section drag coefficient with Mach number for the NACA 66-208 airfoil.

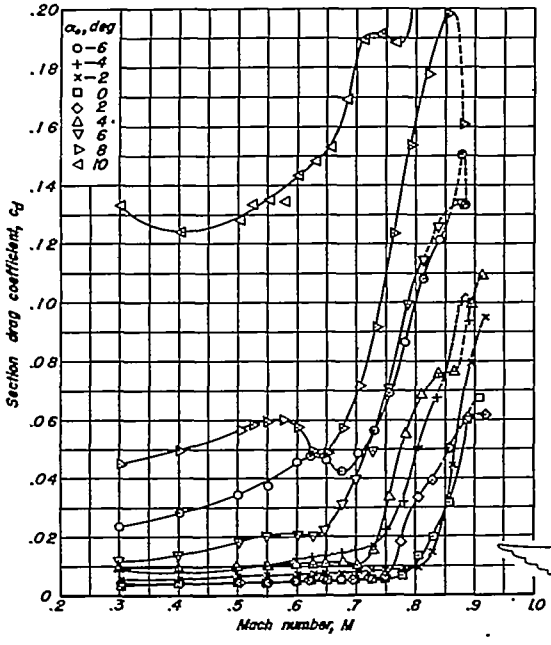

Figure 17.-Variation of section drag coefficient with Mach number for the NACA 66-210 airfoil.

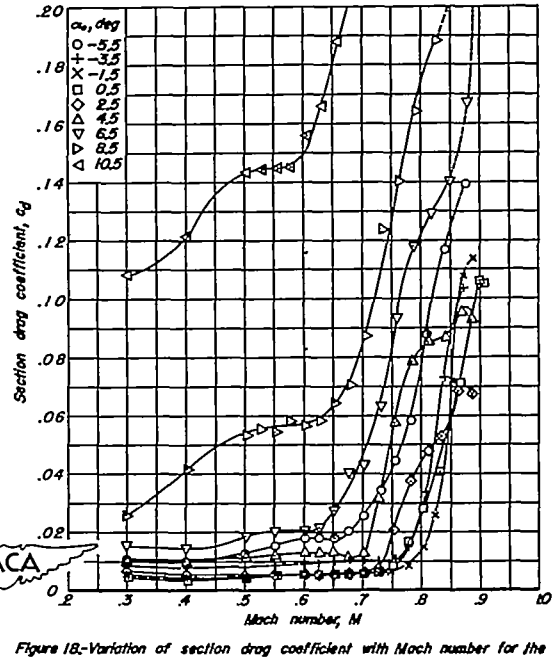

Figure 18.-Variation of section drag coefficient with Mach number for the NACA 66-212 airfoil.

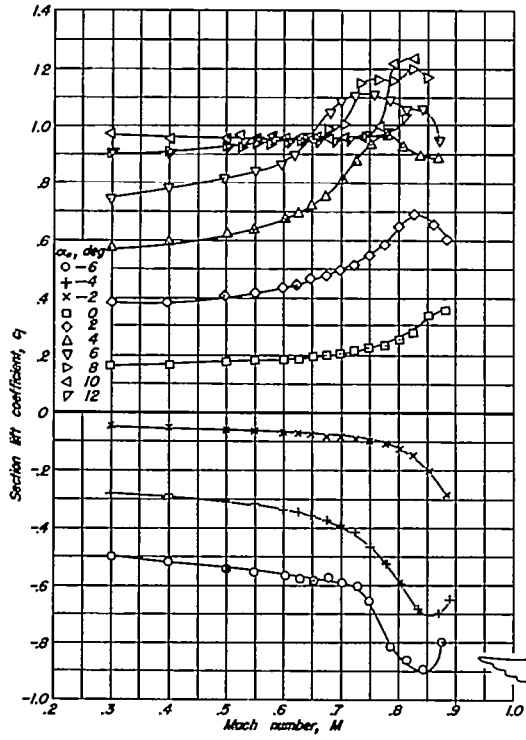

Figure 19.-The variation of section lift coefficient with Mach number for the NACA 63-206 airfoil.

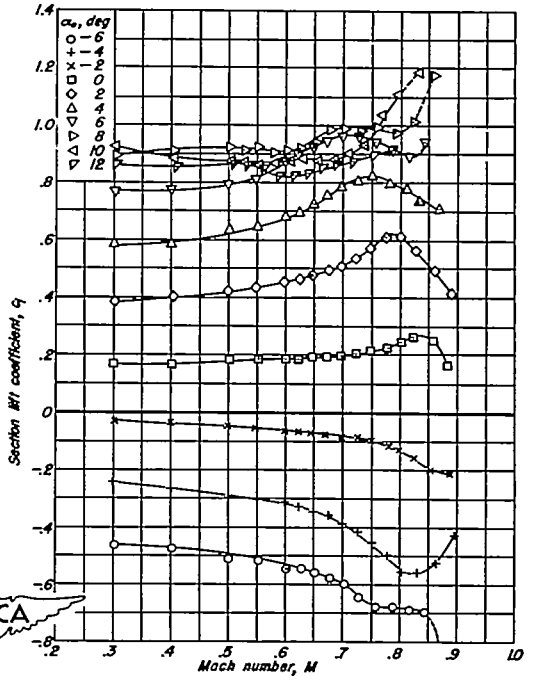

Figure 20.-The variation of section lift coefficient with Mach number for the NACA 63-208 airfoil.

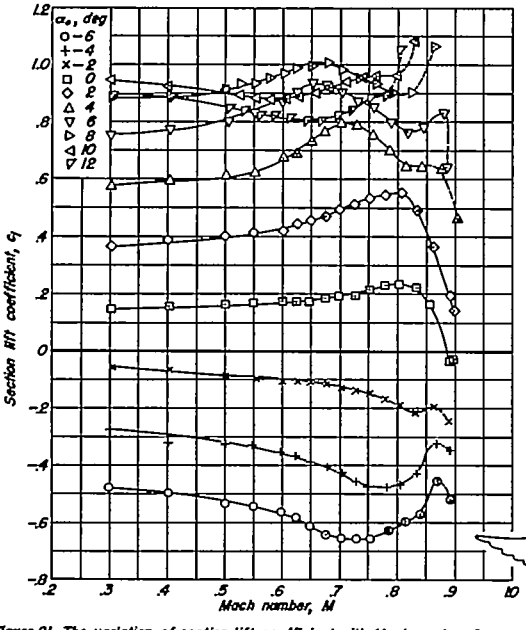

Figure 21.-The variation of section lift coefficient with Mach number for the NACA 63-210 airfoil.

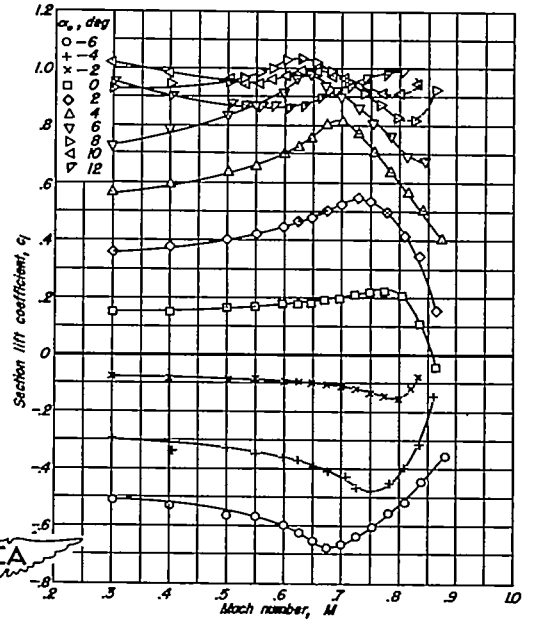

Figure 22.-The variation of section lift coefficient with Mach number for the NACA 63-212 airfoil.

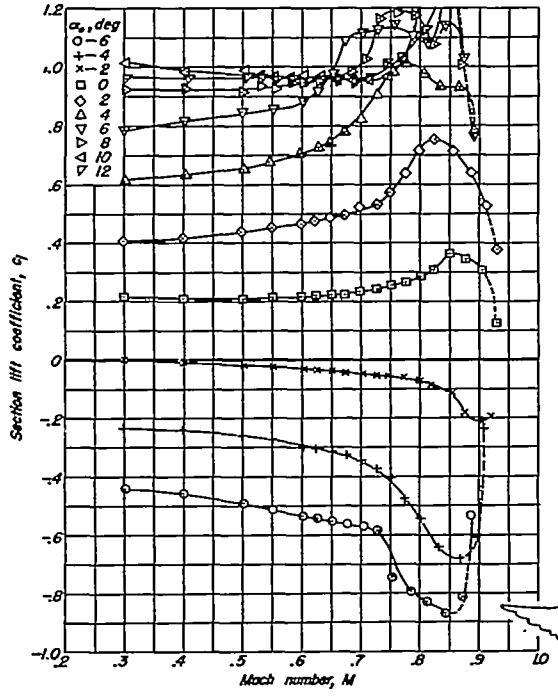

Figure 23.–Variation of section lift coefficient with Mach number for the NACA 64-206 airfoil.

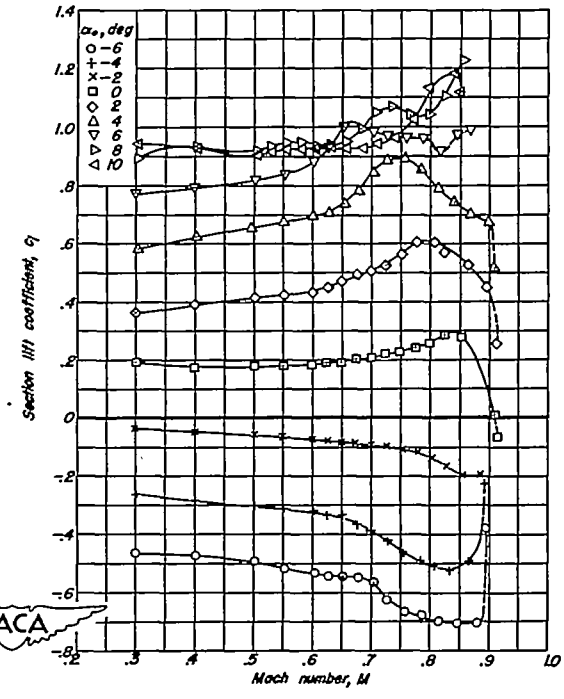

Figure 24.–Variation of section lift coefficient with Mach number for the NACA 64-208 airfoil.

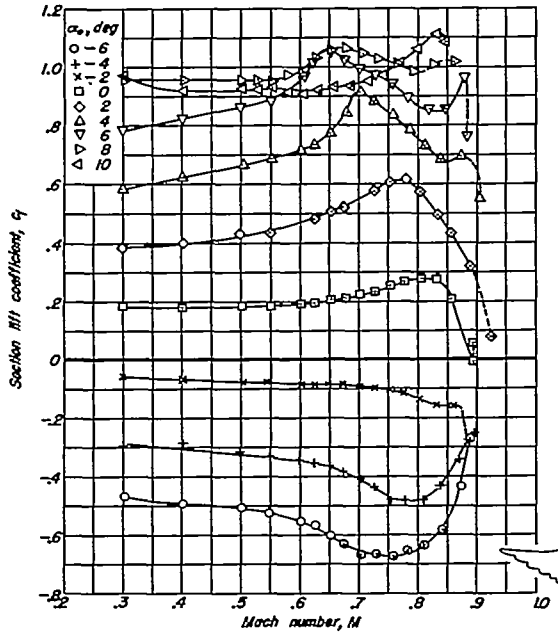

Figure 25.–Variation of section lift coefficient with Mach number for the NACA 64-210 airfoil.

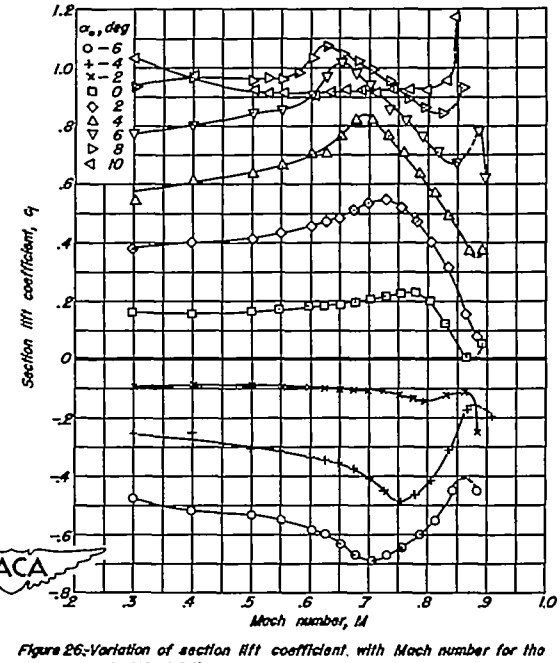

Figure 26.–Variation of section lift coefficient with Mach number for the NACA 64-212 airfoil.

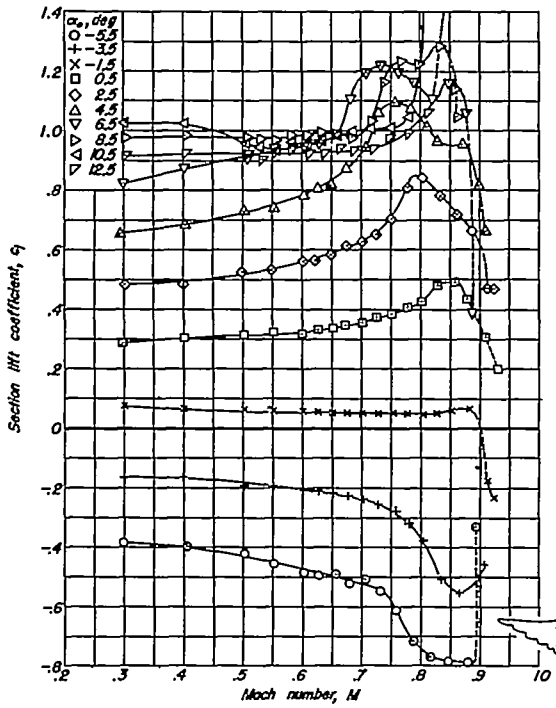

Figure 27.-Variation of section lift coefficient with Mach number for the NACA 65-206 airfoil.

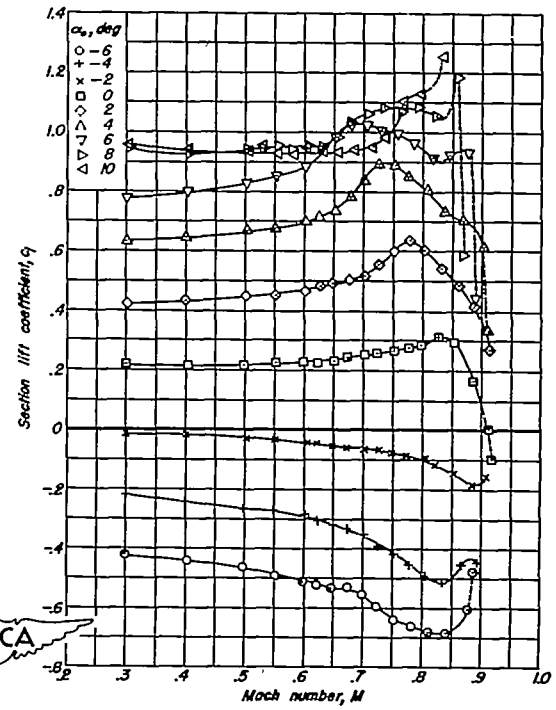

Figure 28.-Variation of section lift coefficient with Mach number for the NACA 65-208 airfoil.

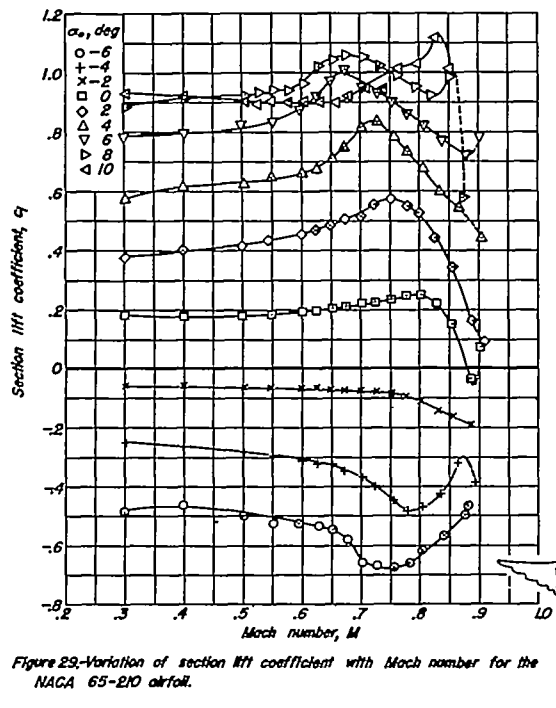

Figure 29.-Variation of section lift coefficient with Mach number for the NACA 65-210 airfoil.

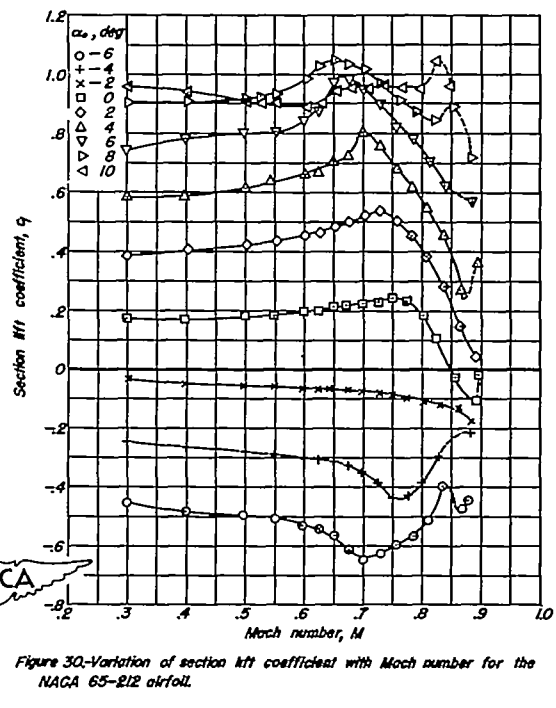

Figure 30.-Variation of section lift coefficient with Mach number for the NACA 65-212 airfoil.

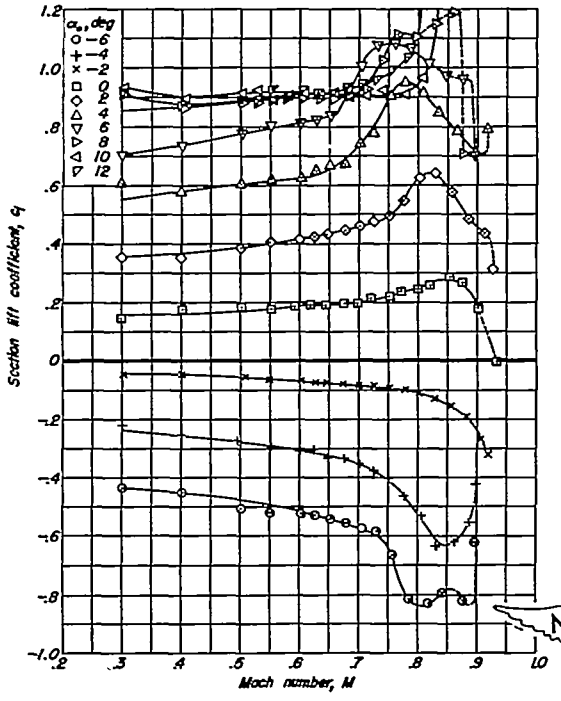

Figure 31.-Variation of section lift coefficient with Mach number for the NACA 66-206 airfoil.

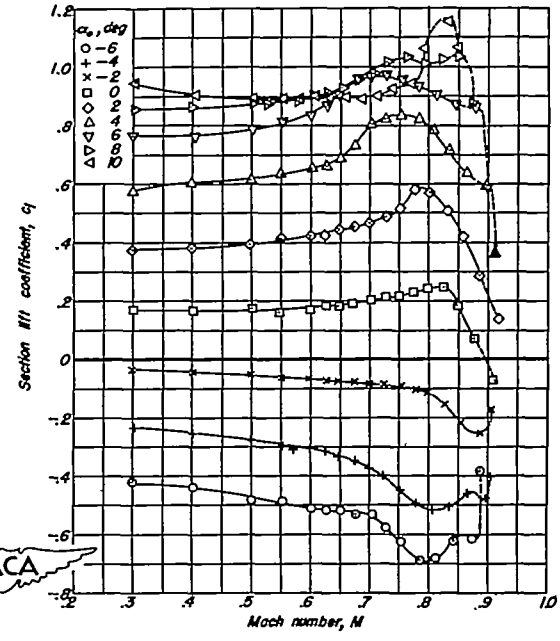

Figure 32.-Variation of section lift coefficient with Mach number for the NACA 66-208 airfoil.

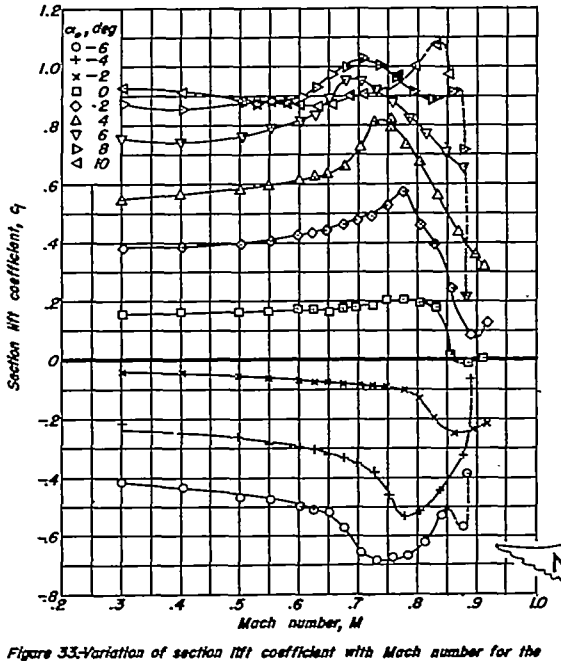

Figure 33.-Variation of section lift coefficient with Mach number for the NACA 66-210 airfoil.

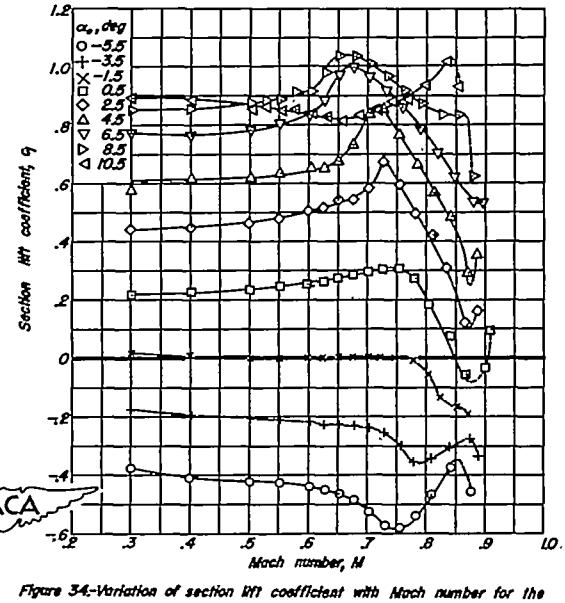

Figure 34.-Variation of section lift coefficient with Mach number for the NACA 66-212 airfoil.

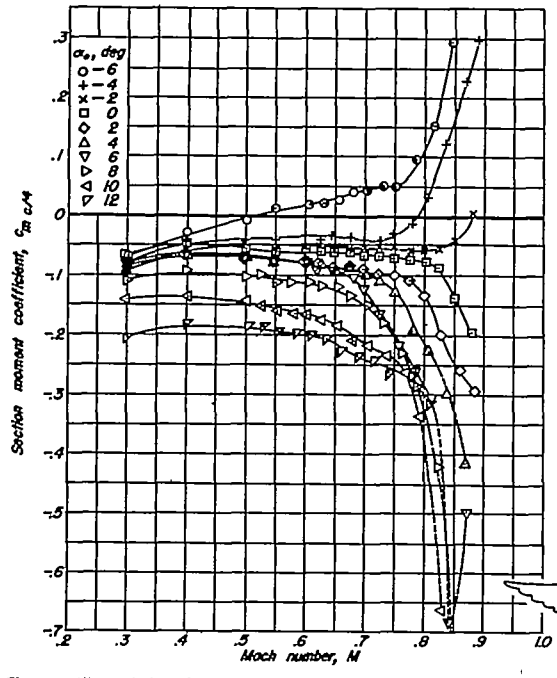

Figure 35.-The variation of section moment coefficient with Mach number for the NACA 63-206 airfoil.

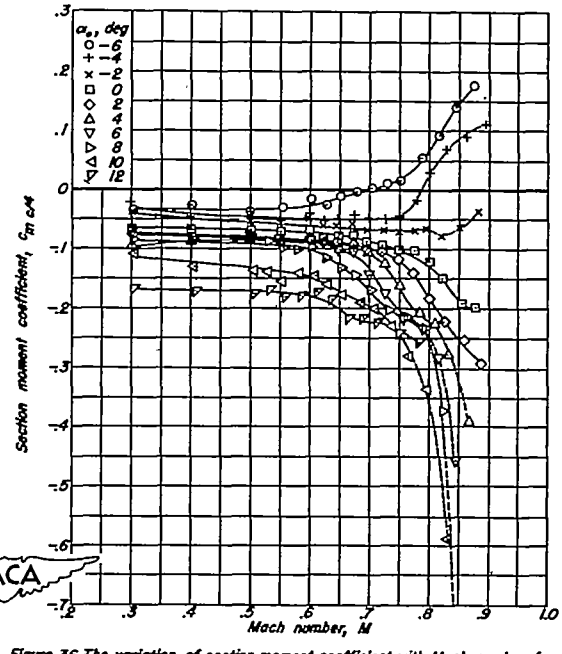

Figure 36.-The variation of section moment coefficient with Mach number for the NACA 63-208 airfoil.

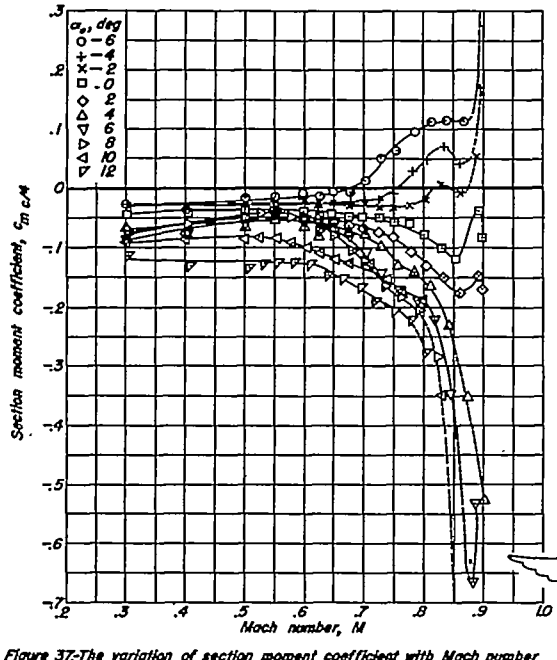

Figure 37.-The variation of section moment coefficient with Mach number for the NACA 63-210 airfoil.

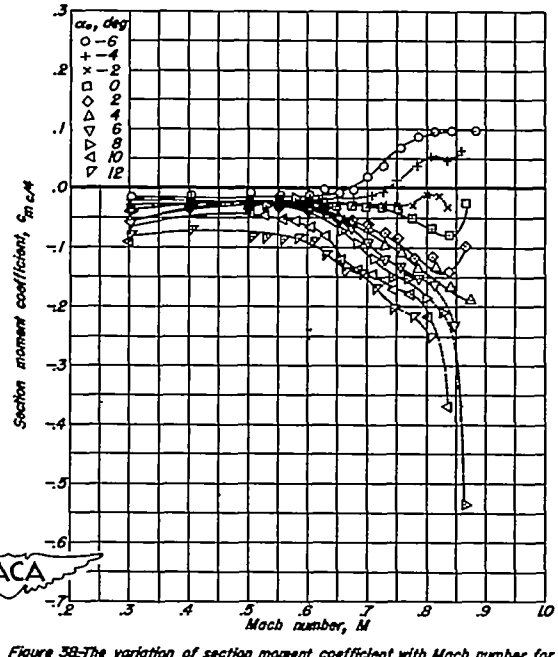

Figure 38.-The variation of section moment coefficient with Mach number for the NACA 63-212 airfoil.

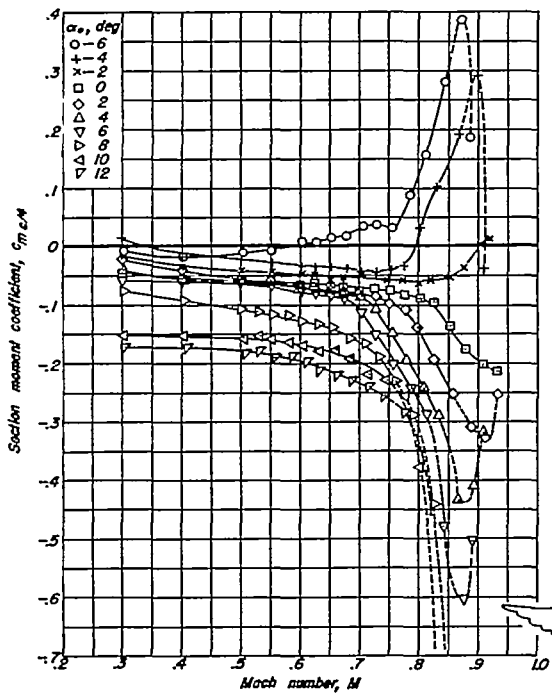

Figure 39.-Variation of section moment coefficient with Mach number for the NACA 64-206 airfoil.

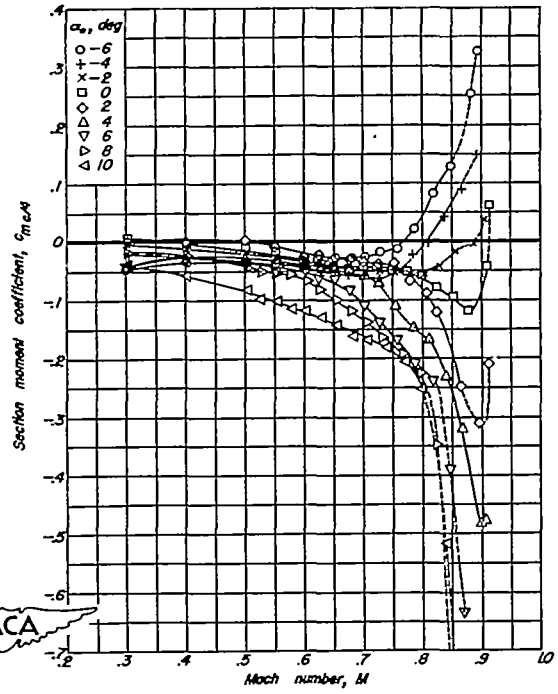

Figure 40.-Variation of section moment coefficient with Mach number for the NACA 64-208 airfoil.

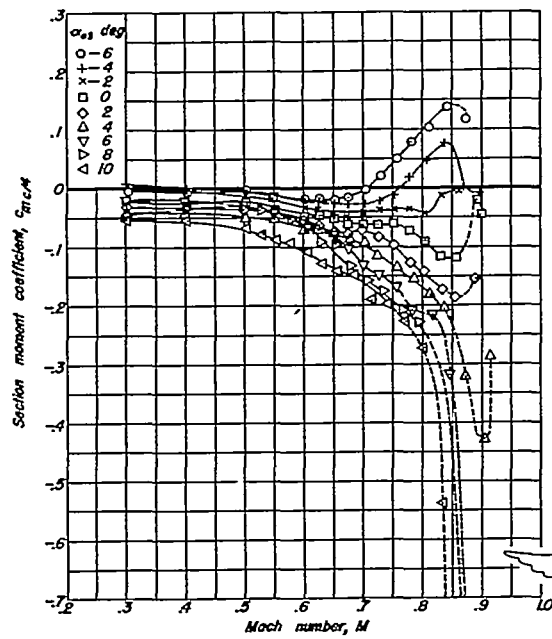

Figure 41.-Variation of section moment coefficient with Mach number for the NACA 64-210 airfoil.

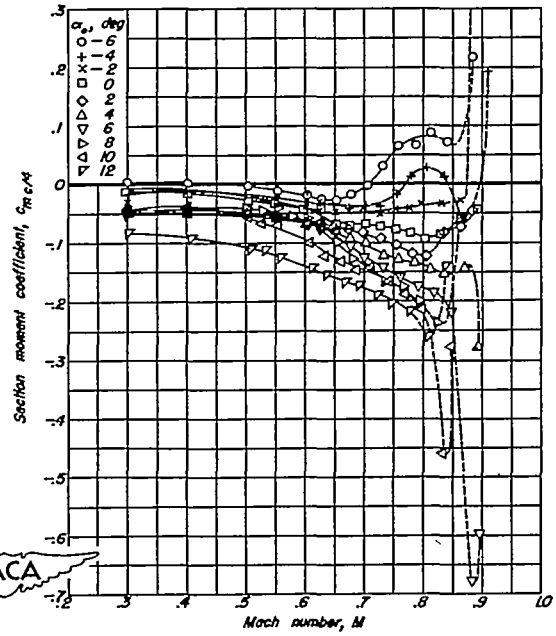

Figure 42.-Variation of section moment coefficient with Mach number for the NACA 64-212 airfoil.

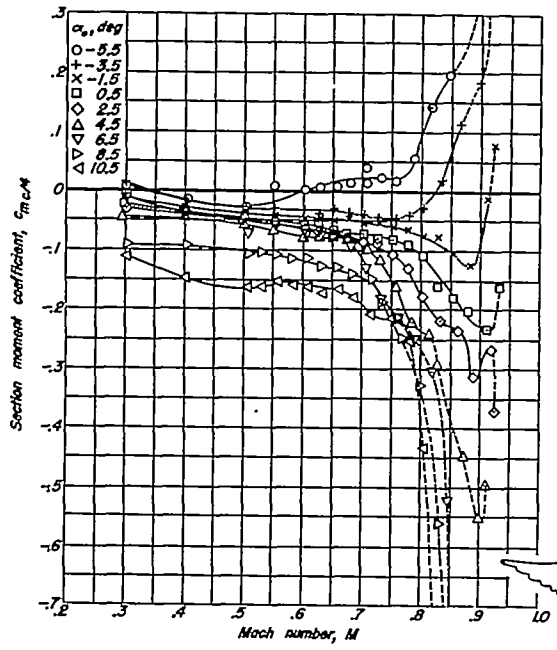

Figure 43.-Variation of section moment coefficient with Mach number for the NACA 65-206 airfoil.

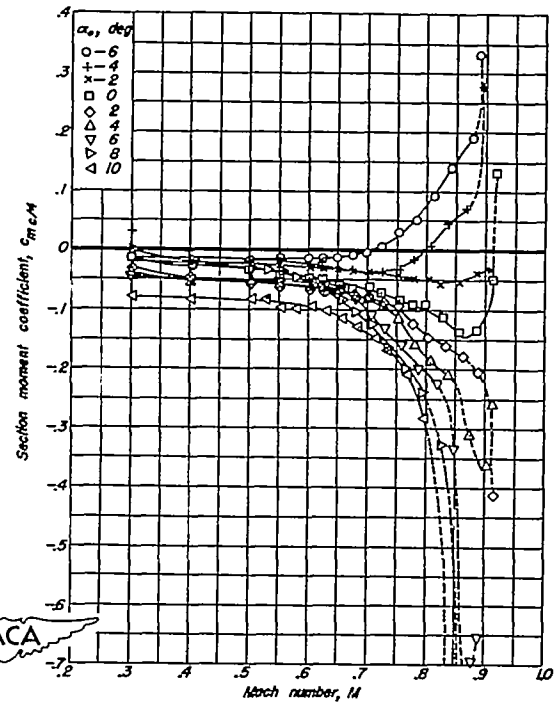

Figure 44.-Variation of section moment coefficient with Mach number for for NACA 65-208 airfoil.

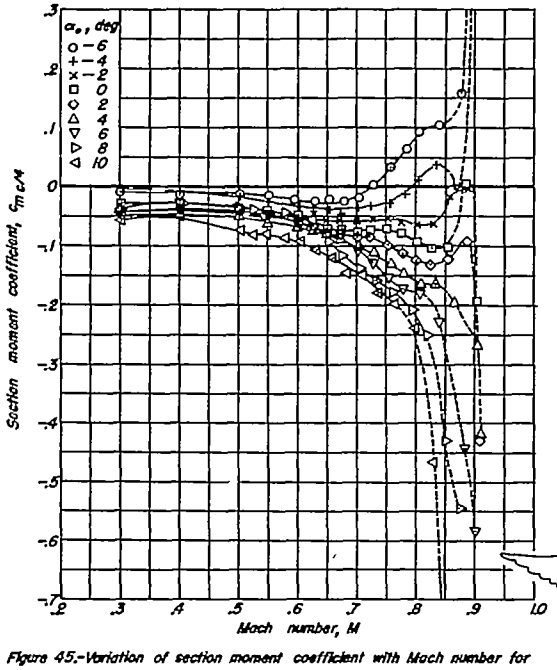

Figure 45.-Variation of section moment coefficient with Mach number for the NACA 65-210 airfoil.

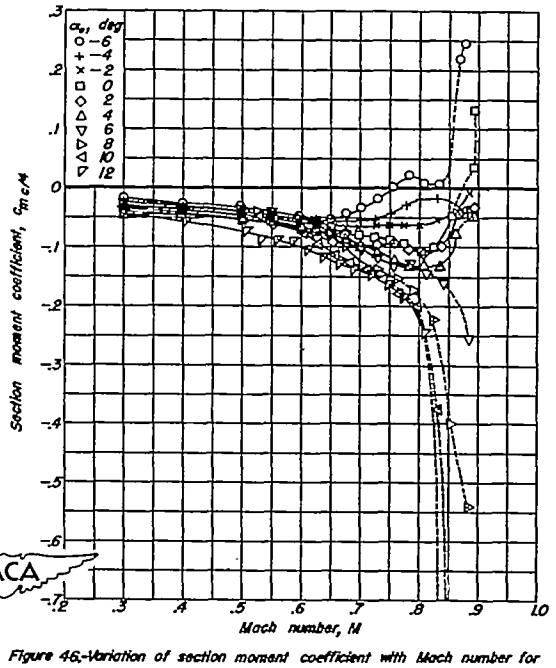

Figure 46.-Variation of section moment coefficient with Mach number for the NACA 65-212 airfoil.

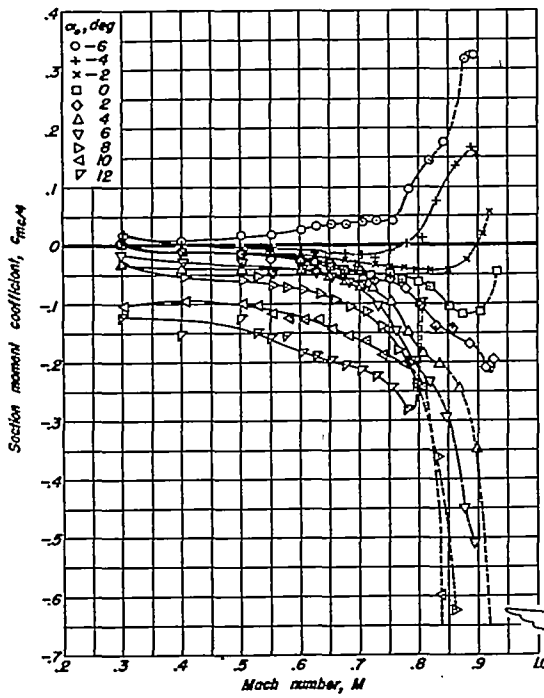

Figure 47.-Variation of section moment coefficient with Mach number for the NACA 66-206 airfoil.

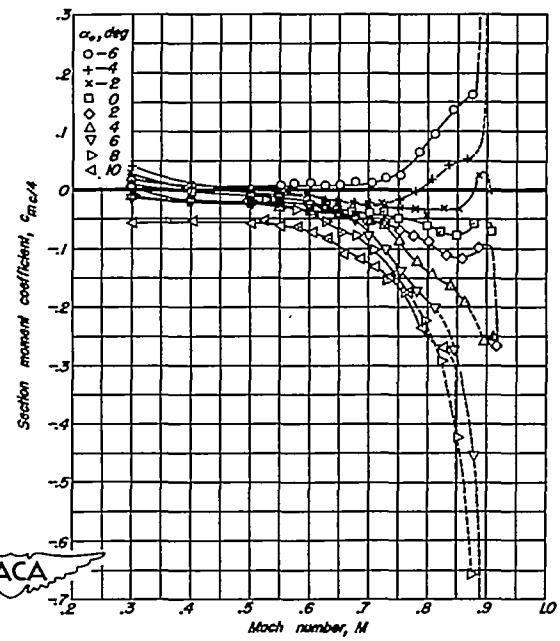

Figure 48.-Variation of section moment coefficient with Mach number for the NACA 66-208 airfoil.

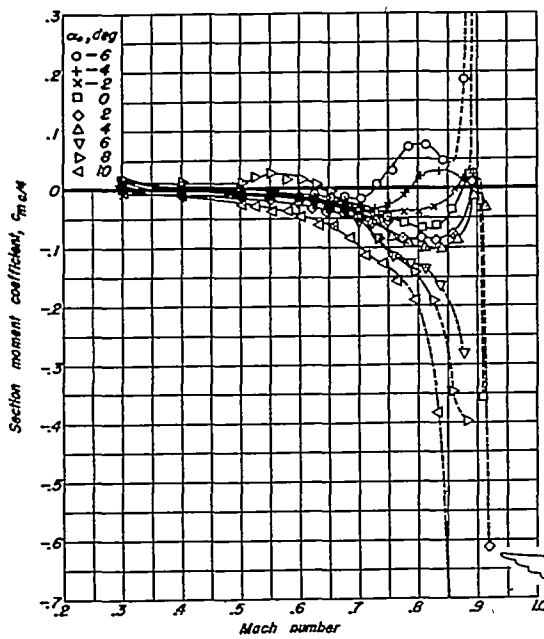

Figure 49.-Variation of section moment coefficient with Mach number for the NACA 66-210 airfoil.

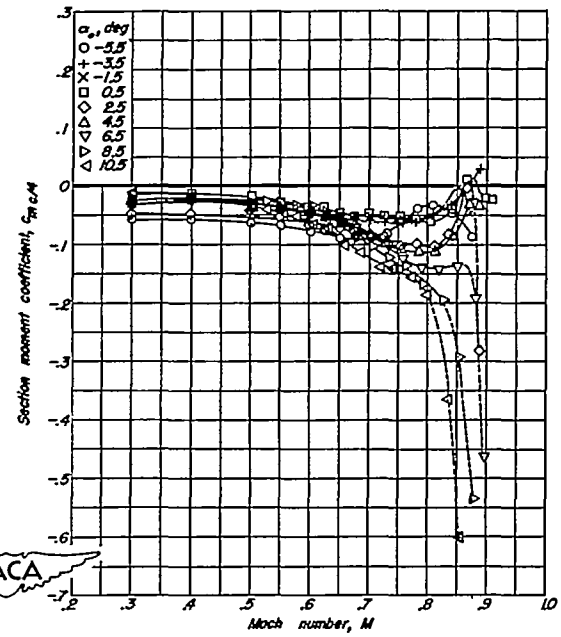

Figure 50.-Variation of section moment coefficient with Mach number for the NACA 66-212 airfoil.

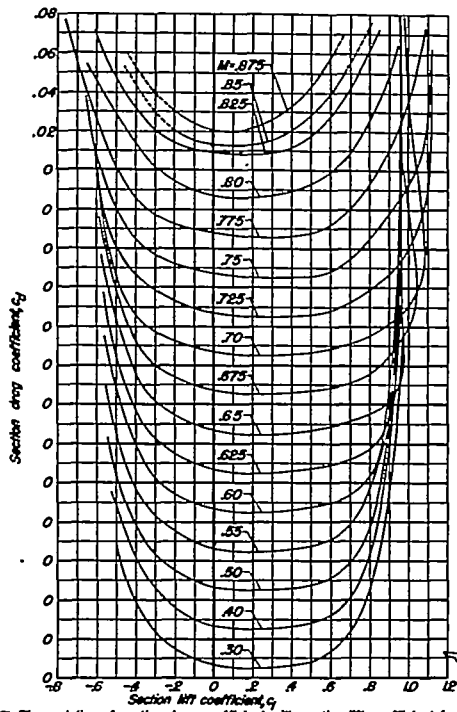

Figure 51.-The variation of section drag coefficient with section lift coefficient for the NACA 63-206 airfoil.

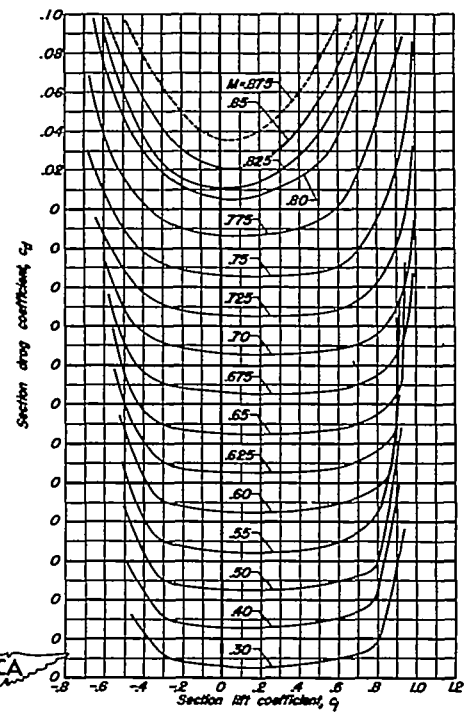

Figure 52.-The variation of section drag coefficient with section lift coefficient for the NACA 63-208 airfoil.

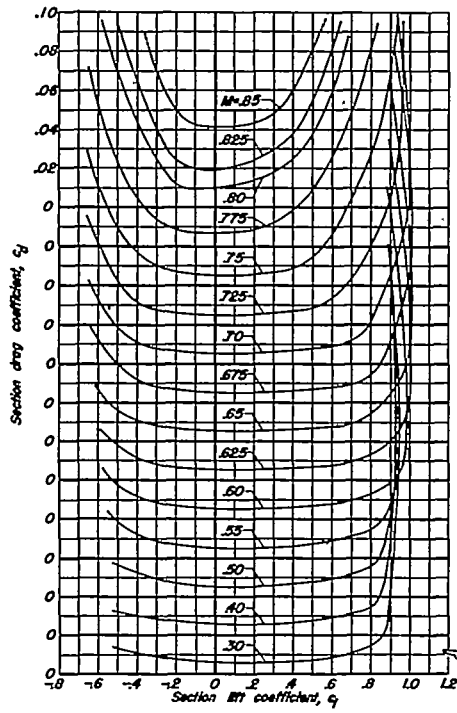

Figure 53.-The variation of section drag coefficient with section lift coefficient for the NACA 63-210 airfoil.

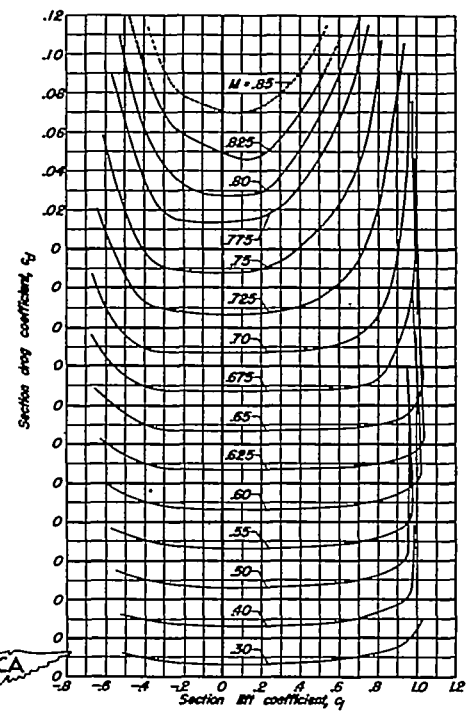

Figure 54.-The variation of section drag coefficient with section lift coefficient for the NACA 63-212 airfoil.

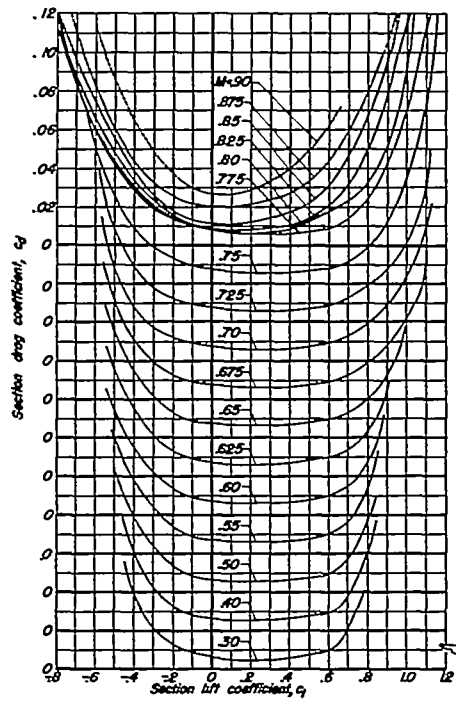

Figure 55.-The variation of section drag coefficient with section lift coefficient for the NACA 64-206 airfoil.

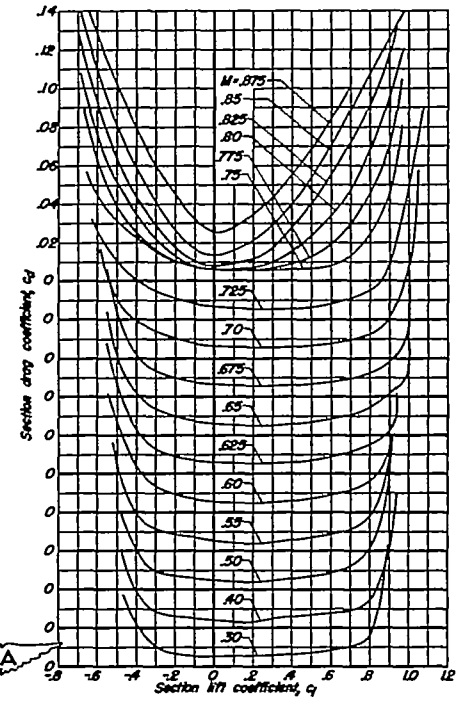

Figure 56.-The variation of section drag coefficient with section lift coefficient for the NACA 64-208 airfoil.

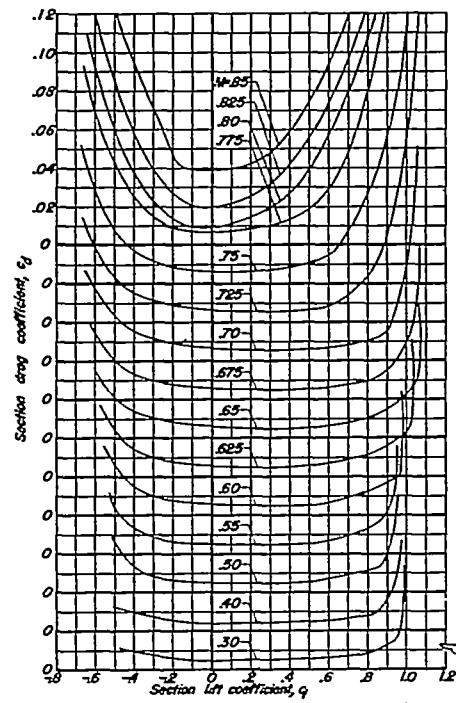

Figure 57.-The variation of section drag coefficient with section lift coefficient for the NACA 64-210 airfoil.

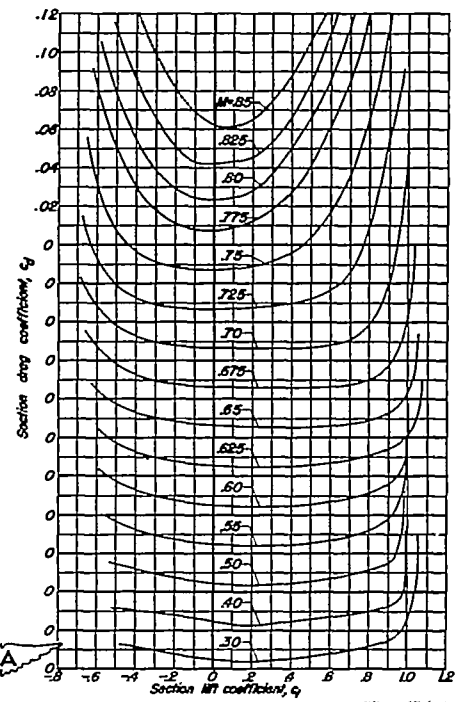

Figure 58.-The variation of section drag coefficient with section lift coefficient for the NACA 64-212 airfoil.

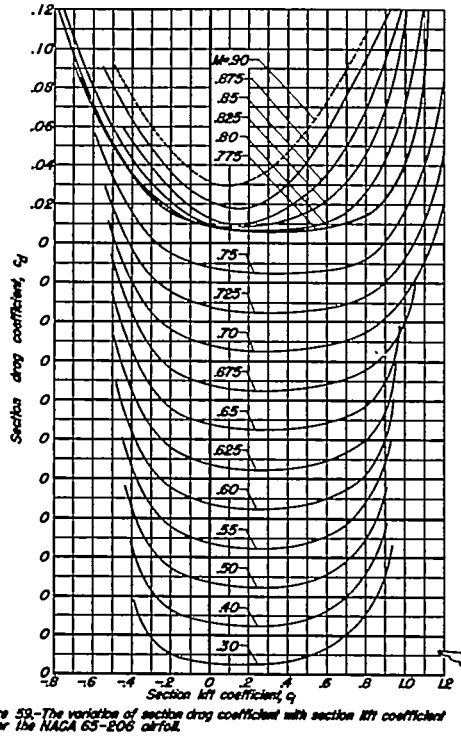

Figure 59.-The variation of section drag coefficient with section lift coefficient for the NACA 65-208 airfoil.

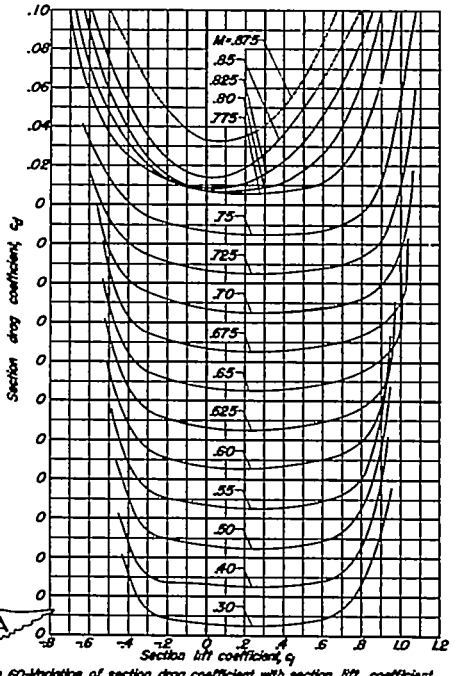

Figure 60.-Variation of section drag coefficient with section lift coefficient for the NACA 65-208 airfoil.

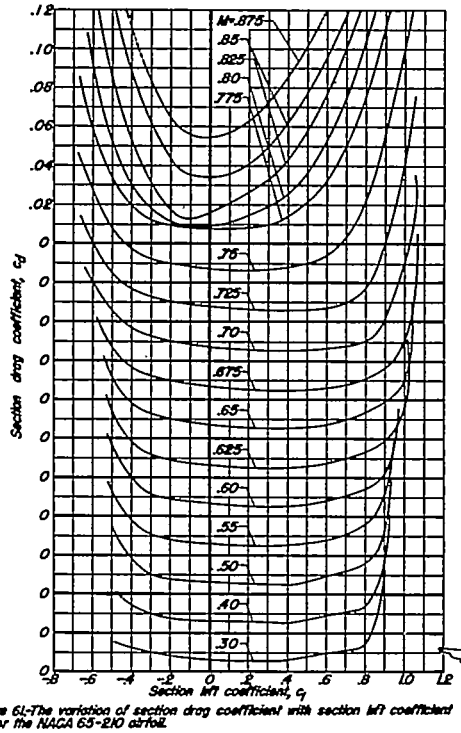

Figure 61.-The variation of section drag coefficient with section lift coefficient for the NACA 65-210 airfoil.

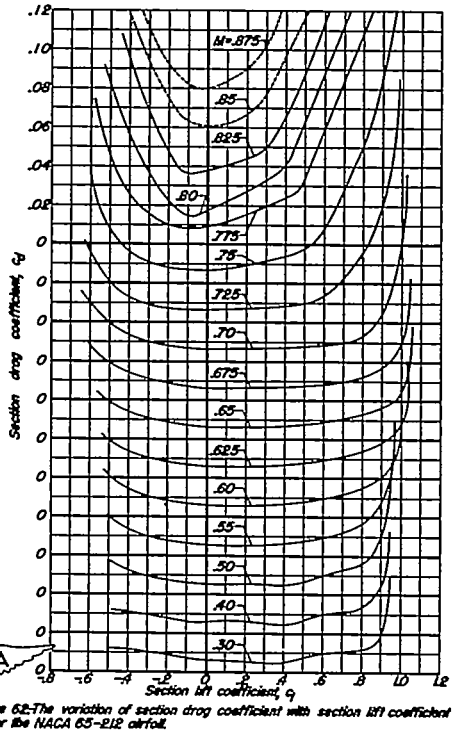

Figure 62.-The variation of section drag coefficient with section lift coefficient for the NACA 65-212 airfoil.

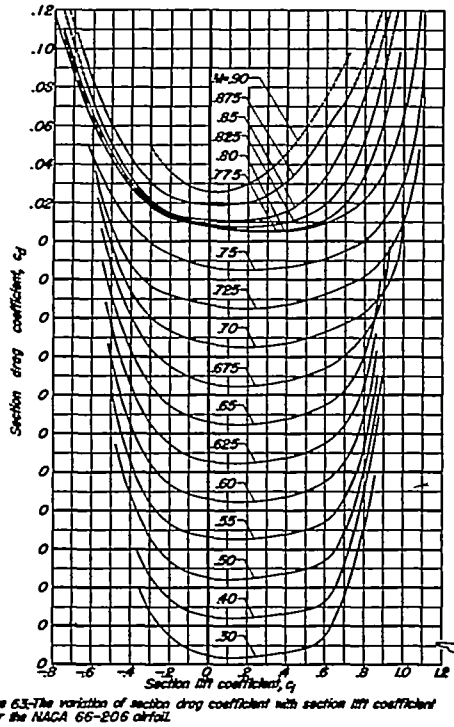

Figure 63.-The variation of section drag coefficient with section lift coefficient for the NACA 66-206 airfoil.

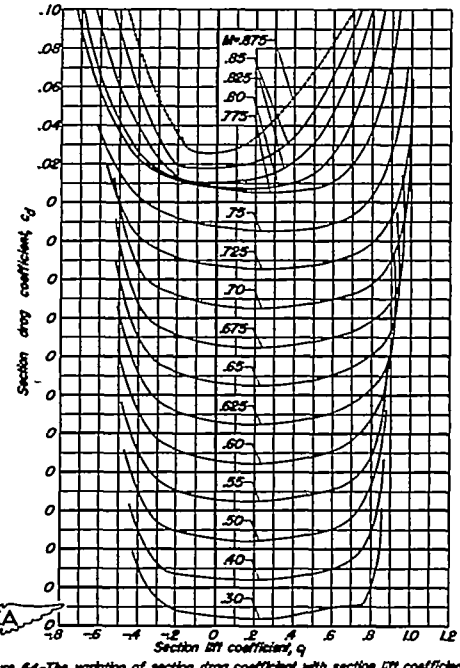

Figure 64.-The variation of section drag coefficient with section lift coefficient for the NACA 66-208 airfoil.

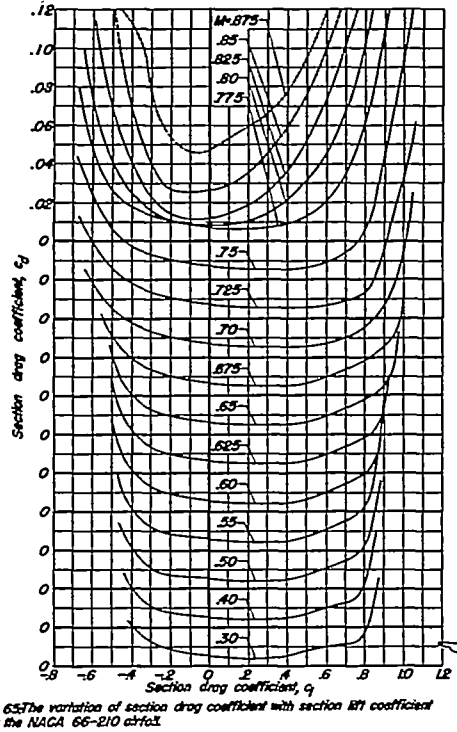

Figure 65.-The variation of section drag coefficient with section lift coefficient for the NACA 66-210 airfoil.

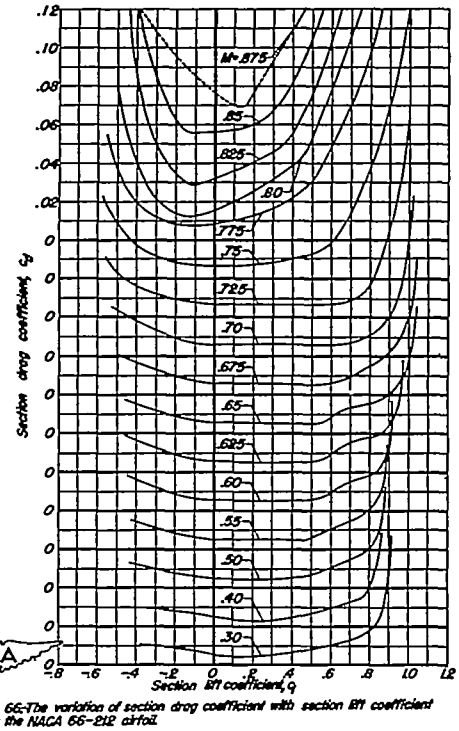

Figure 66.-The variation of section drag coefficient with section lift coefficient for the NACA 66-212 airfoil.

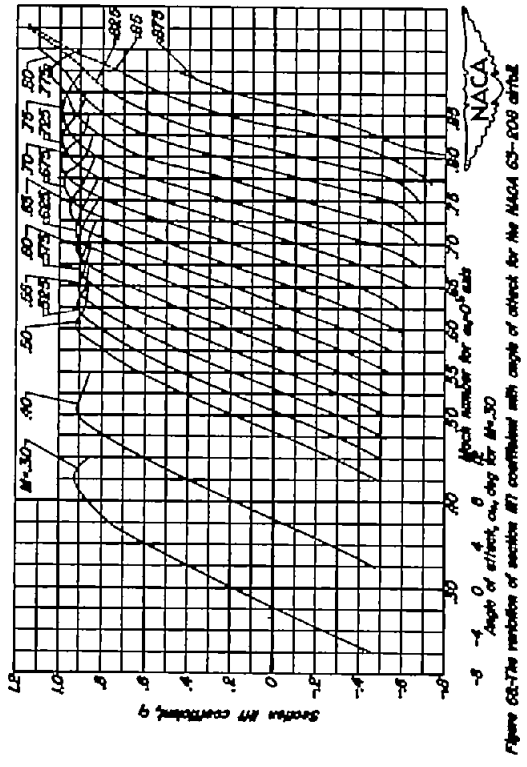

Figure 68.-The variation of section lift coefficient with angle of attack for the NACA 63-608 airfoil.

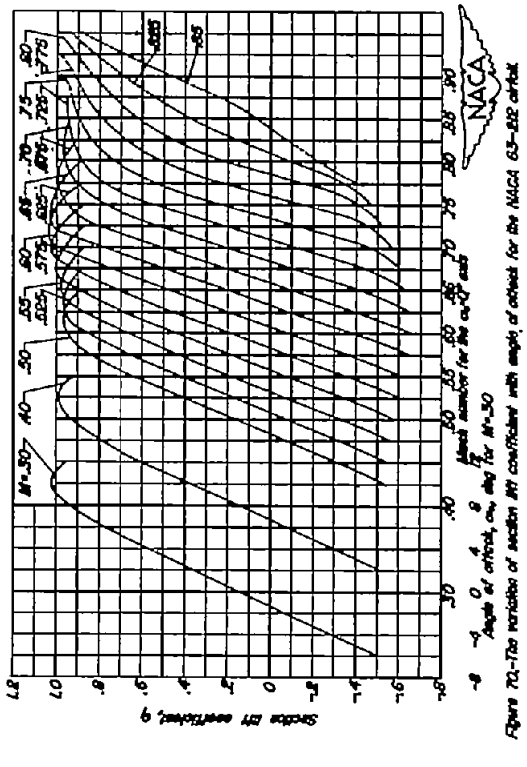

Figure 70.-The variation of section lift coefficient with angle of attack for the NACA 63-612 airfoil.

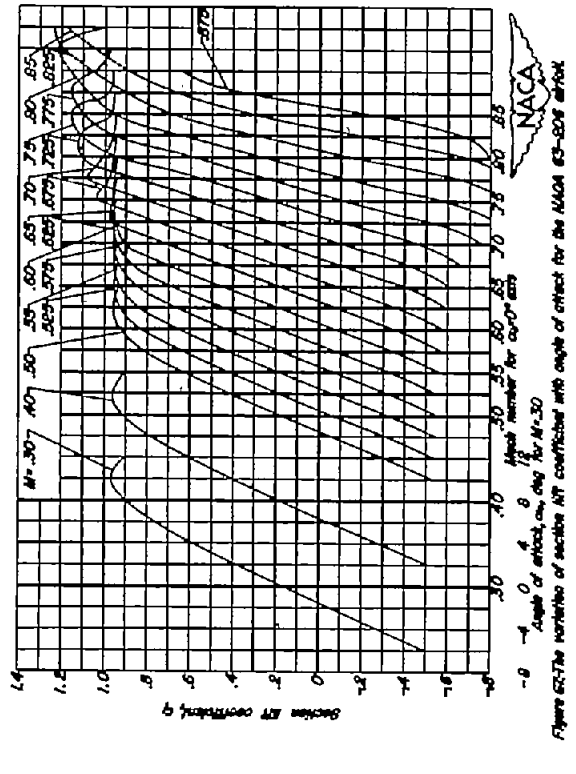

Figure 69.-The variation of section lift coefficient with angle of attack for the NACA 63-610 airfoil.

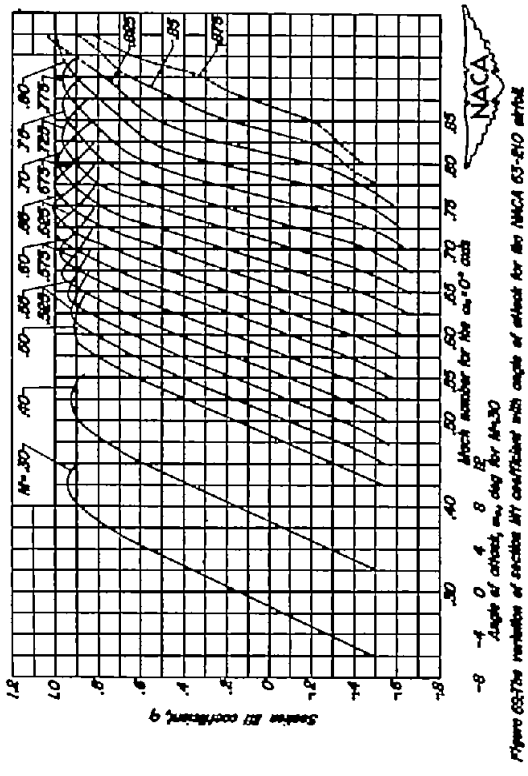

Figure 69.-The variation of section lift coefficient with angle of attack for the NACA 63-612 airfoil.

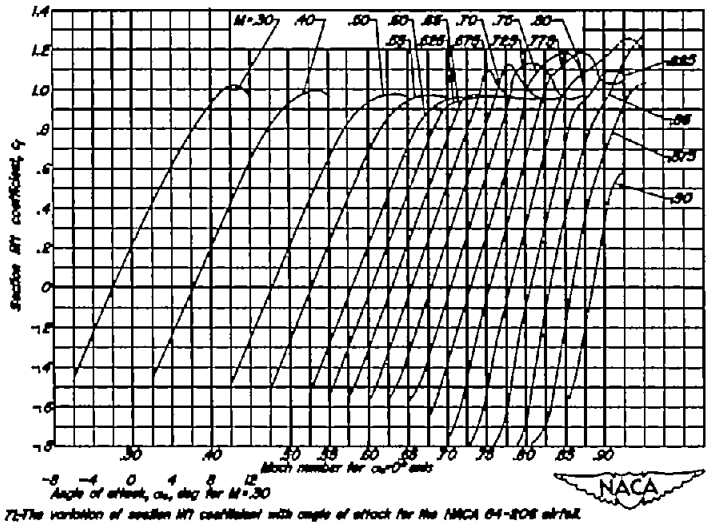

Figure 71.-The variation of section lift coefficient with angle of attack for the NACA 64-206 airfoil.

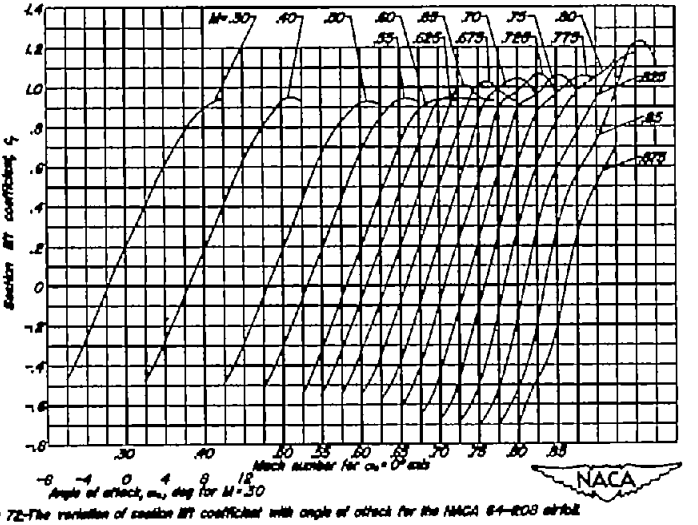

Figure 72.-The variation of section lift coefficient with angle of attack for the NACA 64-208 airfoil.

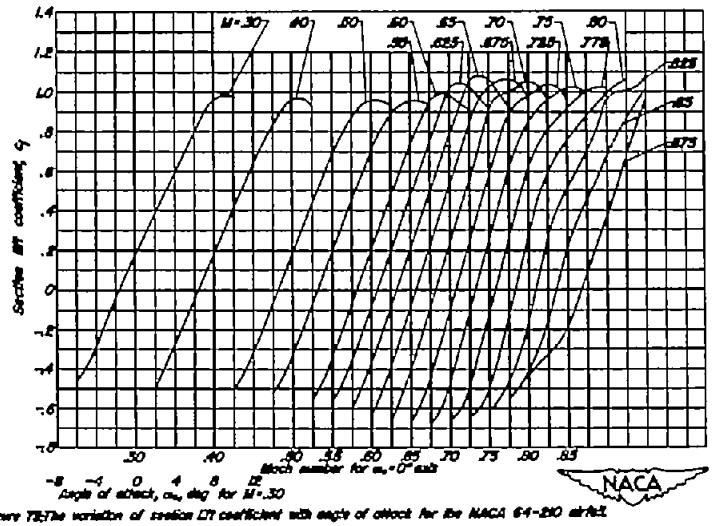

Figure 73.-The variation of section lift coefficient with angle of attack for the NACA 64-210 airfoil.

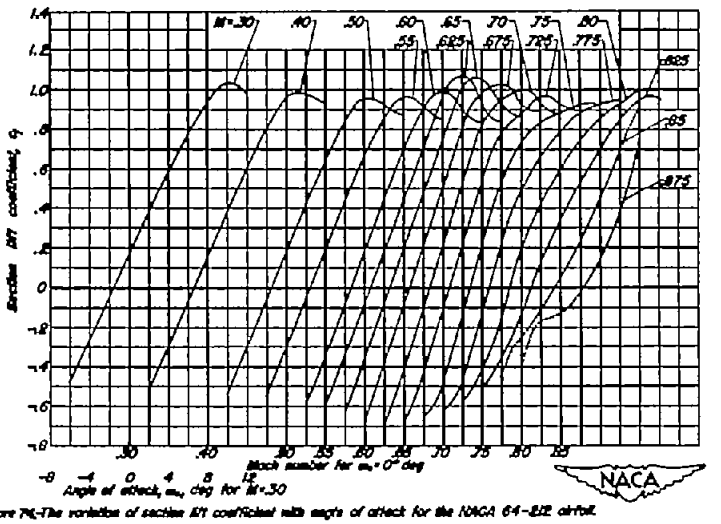

Figure 74.-The variation of section lift coefficient with angle of attack for the NACA 64-212 airfoil.

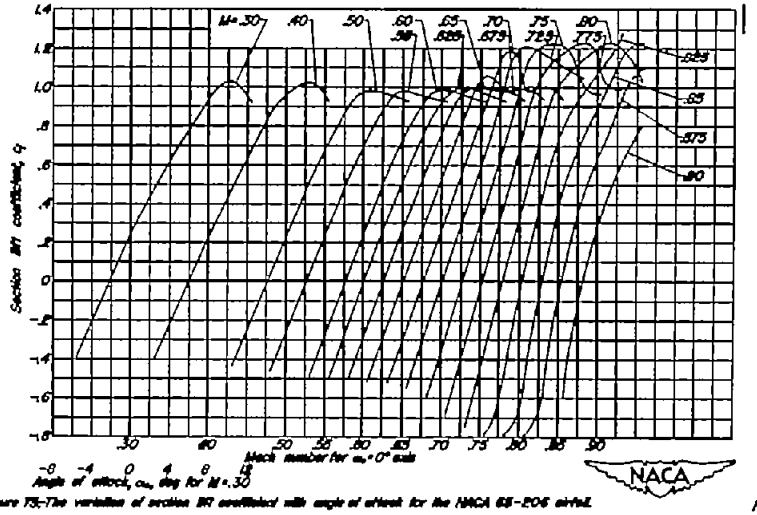

Figure 75.-The variation of section lift coefficient with angle of attack for the NACA 65-206 airfoil.

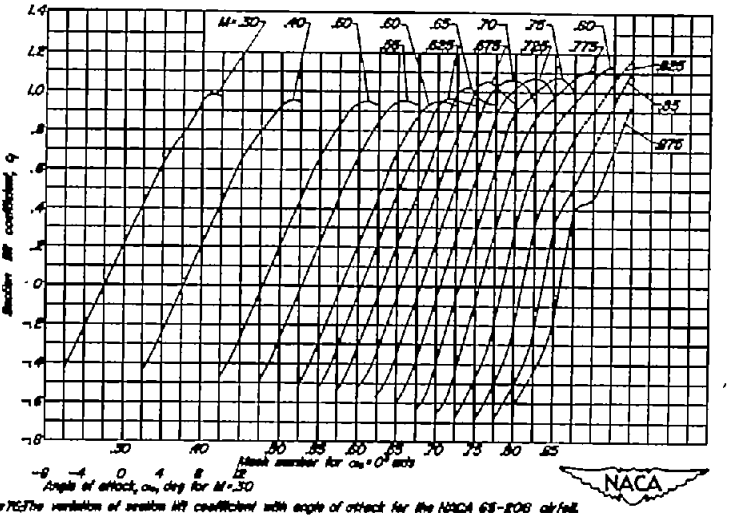

Figure 76.-The variation of section lift coefficient with angle of attack for the NACA 65-208 airfoil.

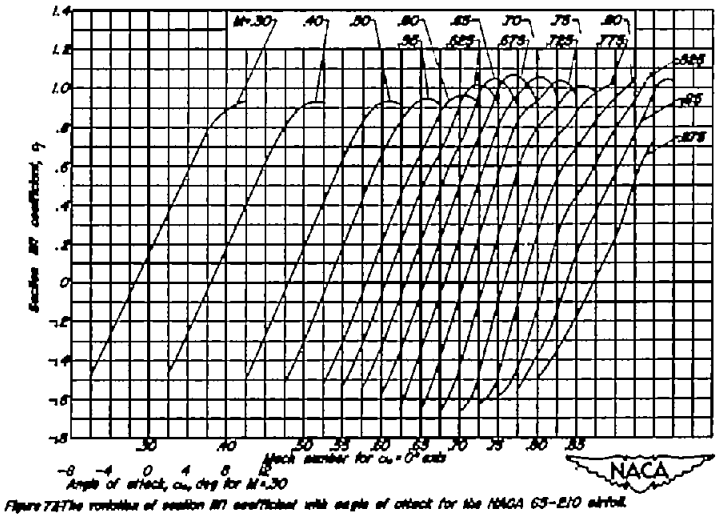

Figure 77.-The variation of section lift coefficient with angle of attack for the NACA 65-210 airfoil.

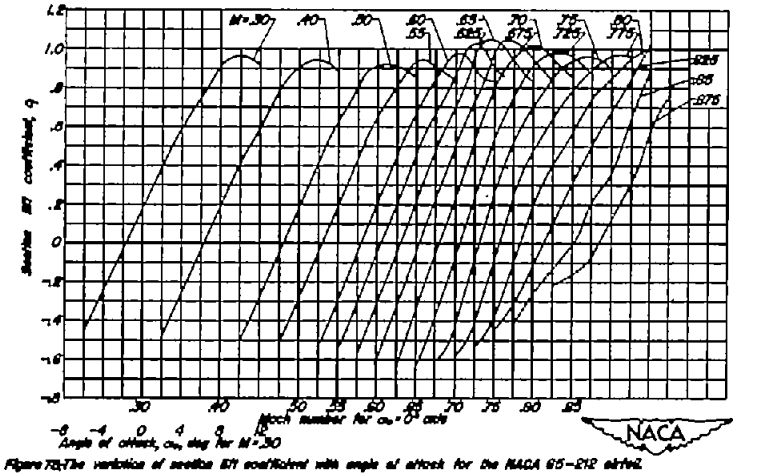

Figure 78.-The variation of section lift coefficient with angle of attack for the NACA 65-212 airfoil.

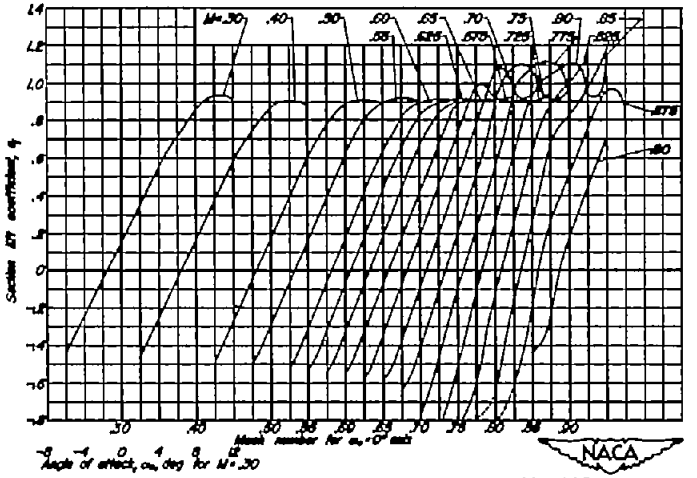

Figure 73.-The variation of section lift coefficient with angle of attack for the NACA 66-206 airfoil.

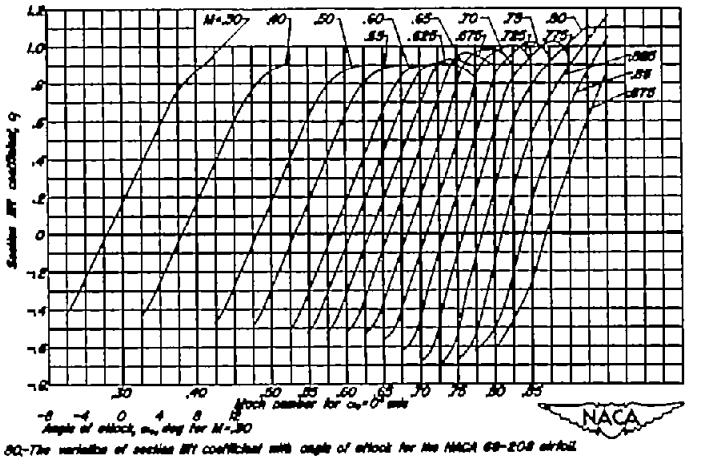

Figure 80.-The variation of section lift coefficient with angle of attack for the NACA 66-208 airfoil.

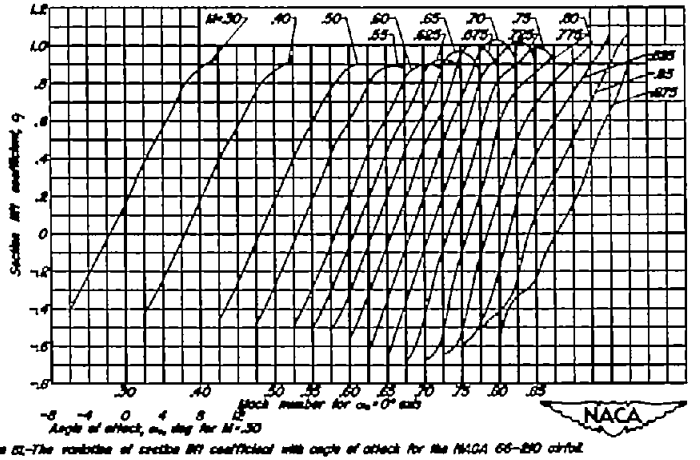

Figure 81.-The variation of section lift coefficient with angle of attack for the NACA 66-210 airfoil.

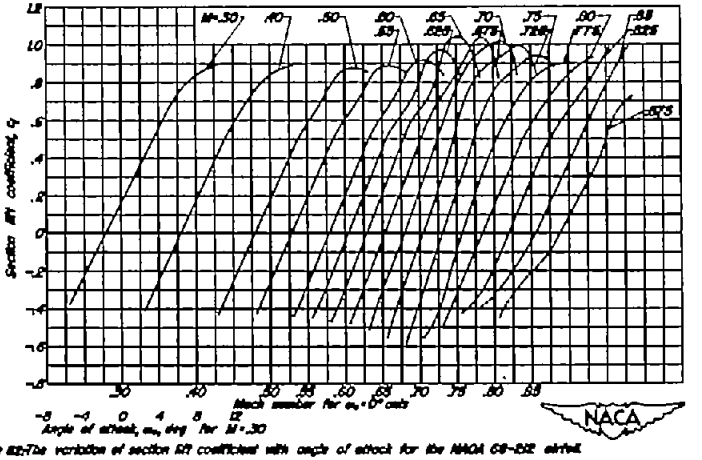

Figure 82.-The variation of section lift coefficient with angle of attack for the NACA 66-212 airfoil.

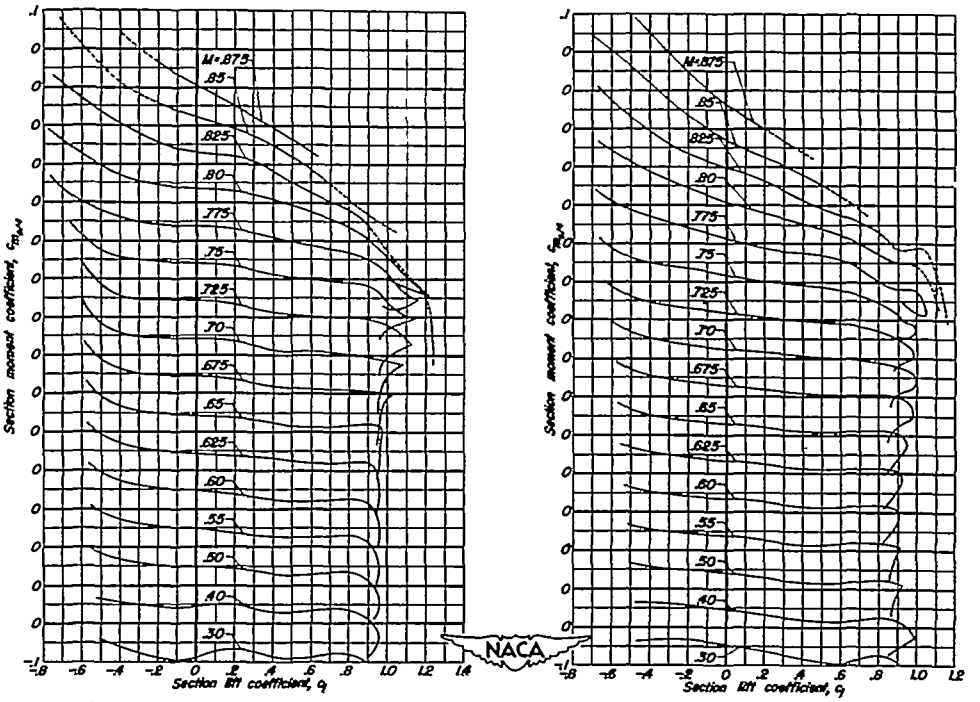

Figure 83.-The variation of section moment coefficient with section lift coefficient for the NACA 63-206 airfoil.

Figure 84.-The variation of section moment coefficient with section lift coefficient for the NACA 63-208 airfoil.

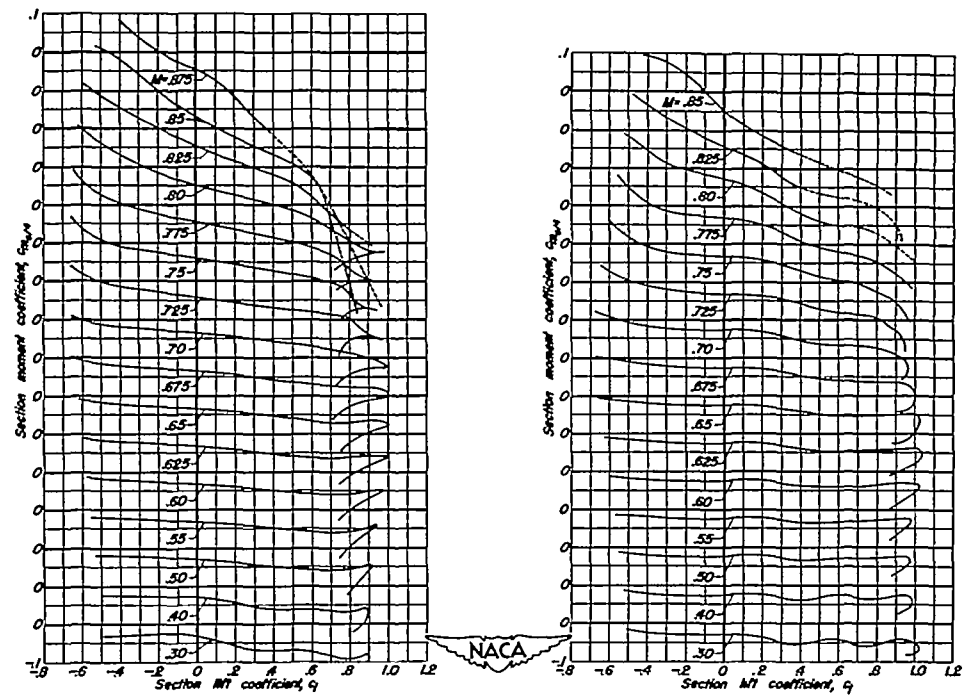

Figure 85.-The variation of section moment coefficient with section lift coefficient for the NACA 63-210 airfoil.

Figure 86.-The variation of section moment coefficient with section lift coefficient for the NACA 63-212 airfoil.

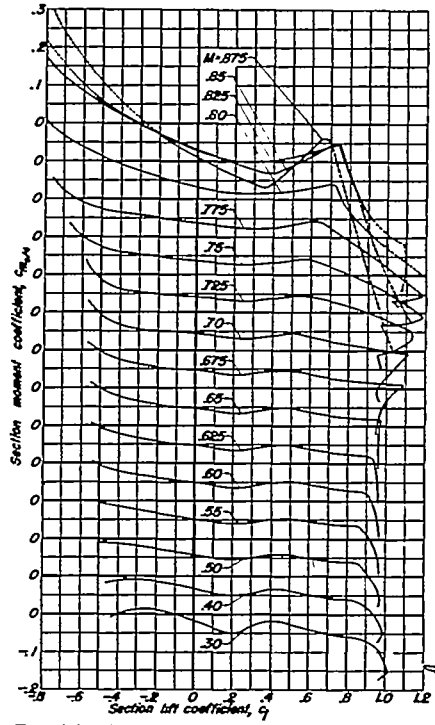

Figure 82.-The variation of section moment coefficient with section lift coefficient for the NACA 64-206 airfoil.

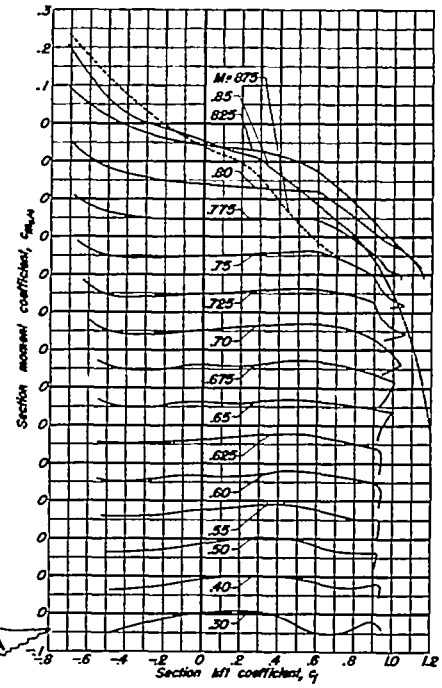

Figure 83.-The variation of section moment coefficient with section lift coefficient for the NACA 64-208 airfoil.

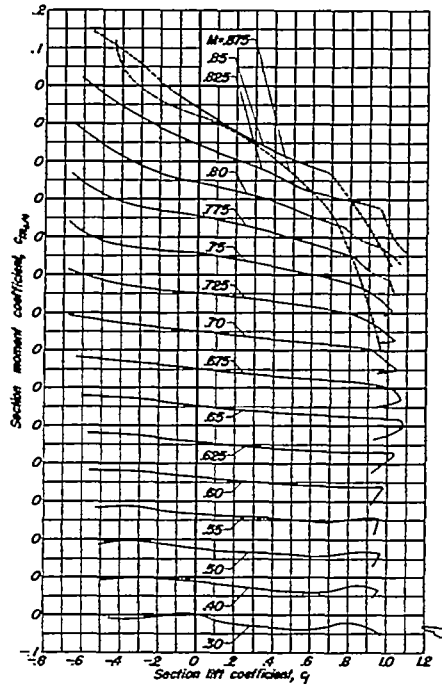

Figure 89.-The variation of section moment coefficient with section lift coefficient for the NACA 64-210 airfoil.

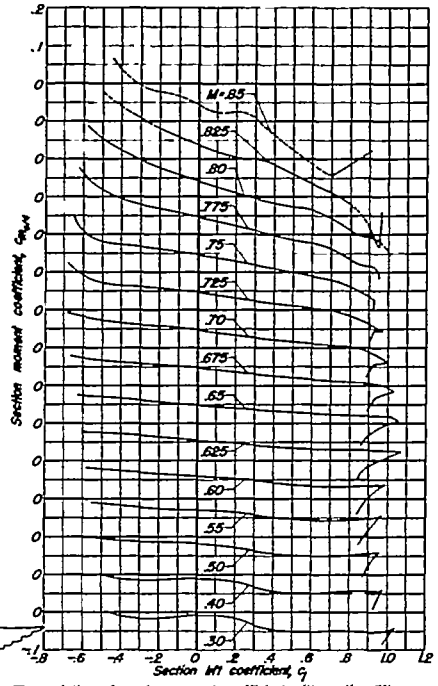

Figure 90.-The variation of section moment coefficient with section lift coefficient for the NACA 64-212 airfoil.

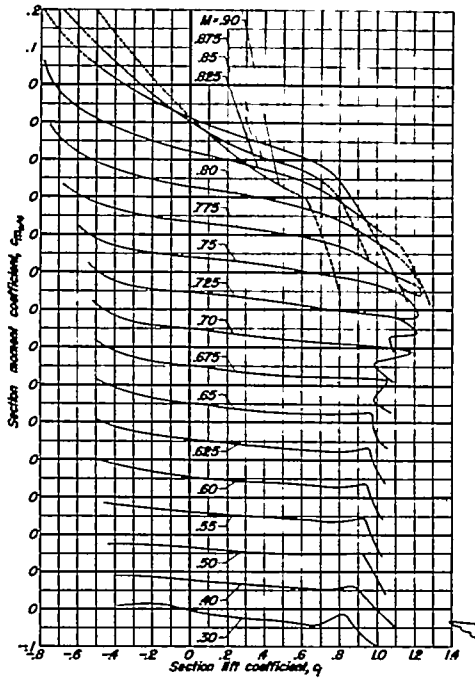

Figure 91.–The variation of section moment coefficient with section lift coefficient for the NACA 65-208 airfoil.

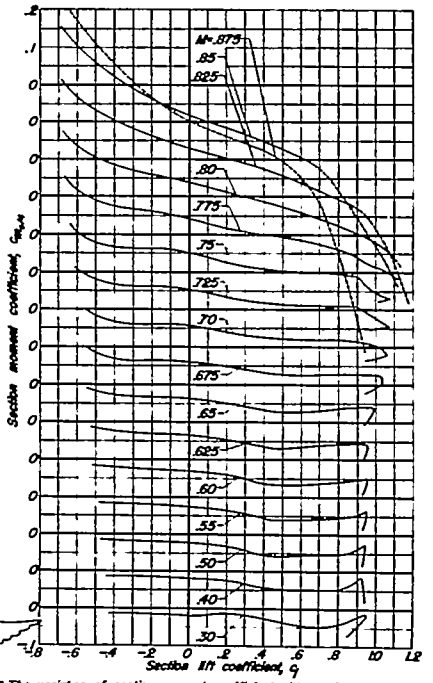

Figure 92.–The variation of section moment coefficient with section lift coefficient for the NACA 65-208 airfoil.

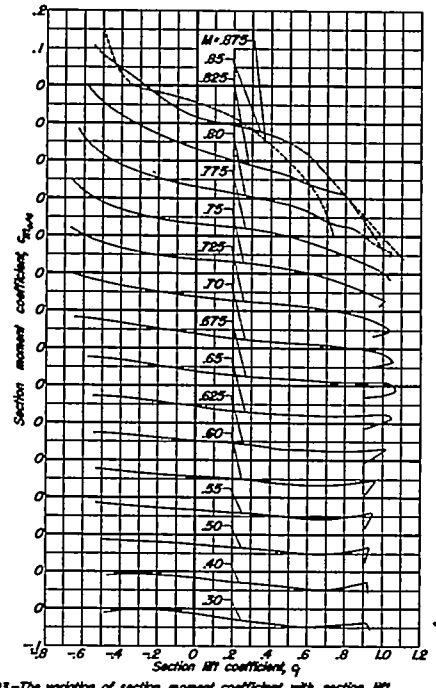

Figure 93.–The variation of section moment coefficient with section lift coefficient for the NACA 65-210 airfoil.

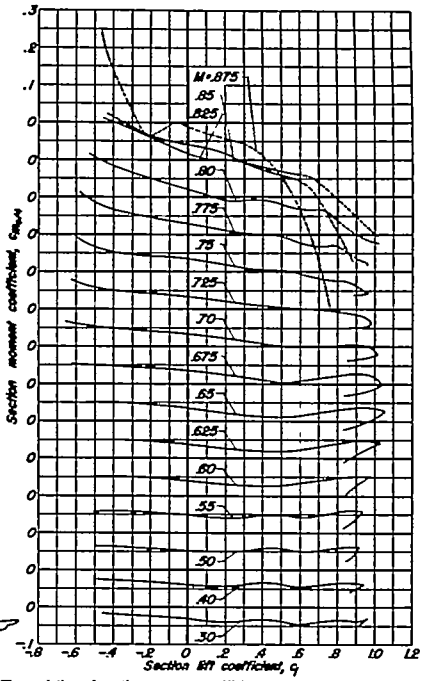

Figure 94.–The variation of section moment coefficient with section lift coefficient for the NACA 65-212 airfoil.

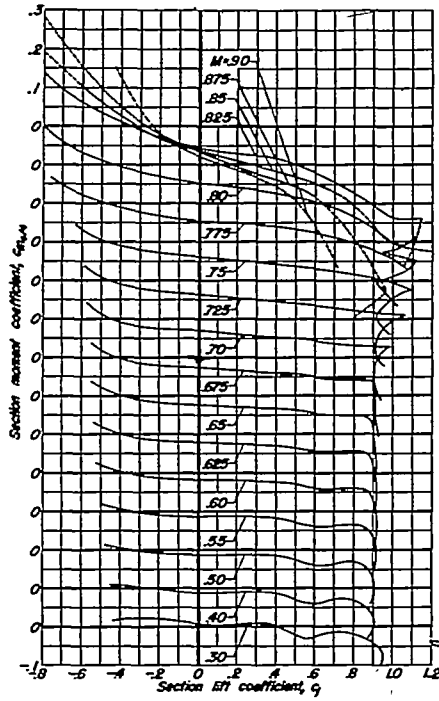

Figure 95.-The variation of section moment coefficient with section lift coefficient for the NACA 66-206 airfoil.

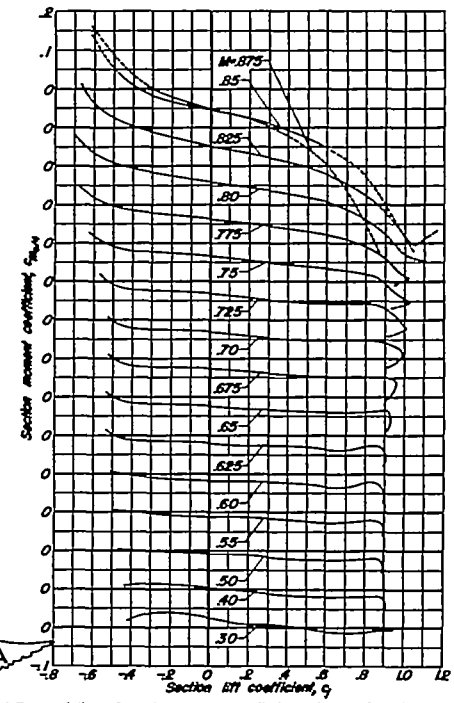

Figure 96.-The variation of section moment coefficient with section lift coefficient for the NACA 66-208 airfoil.

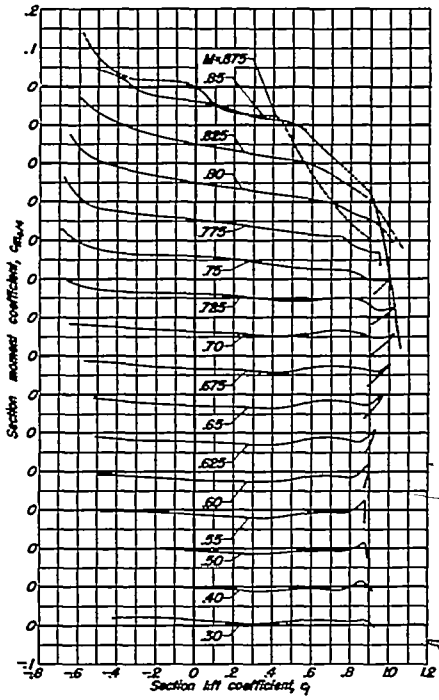

Figure 97.-The variation of section moment coefficient with section lift coefficient for the NACA 66-210 airfoil.

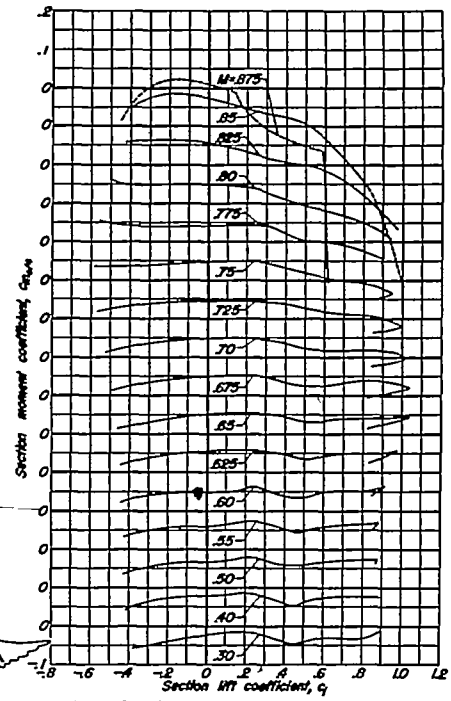

Figure 98.-The variation of section moment coefficient with section lift coefficient for the NACA 66-212 airfoil.

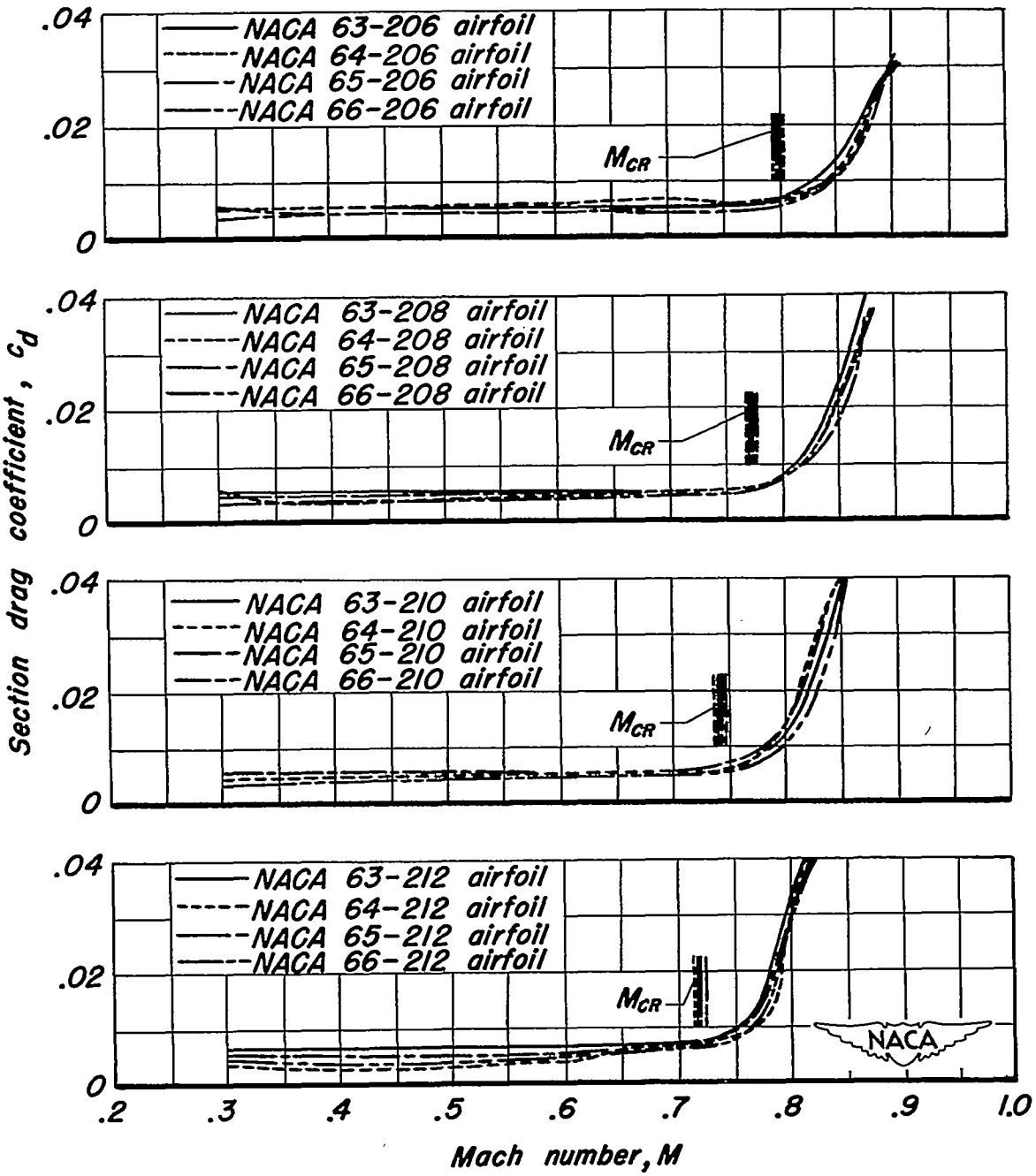

Figure 99.- Variation of section drag coefficient with Mach number at the design lift.

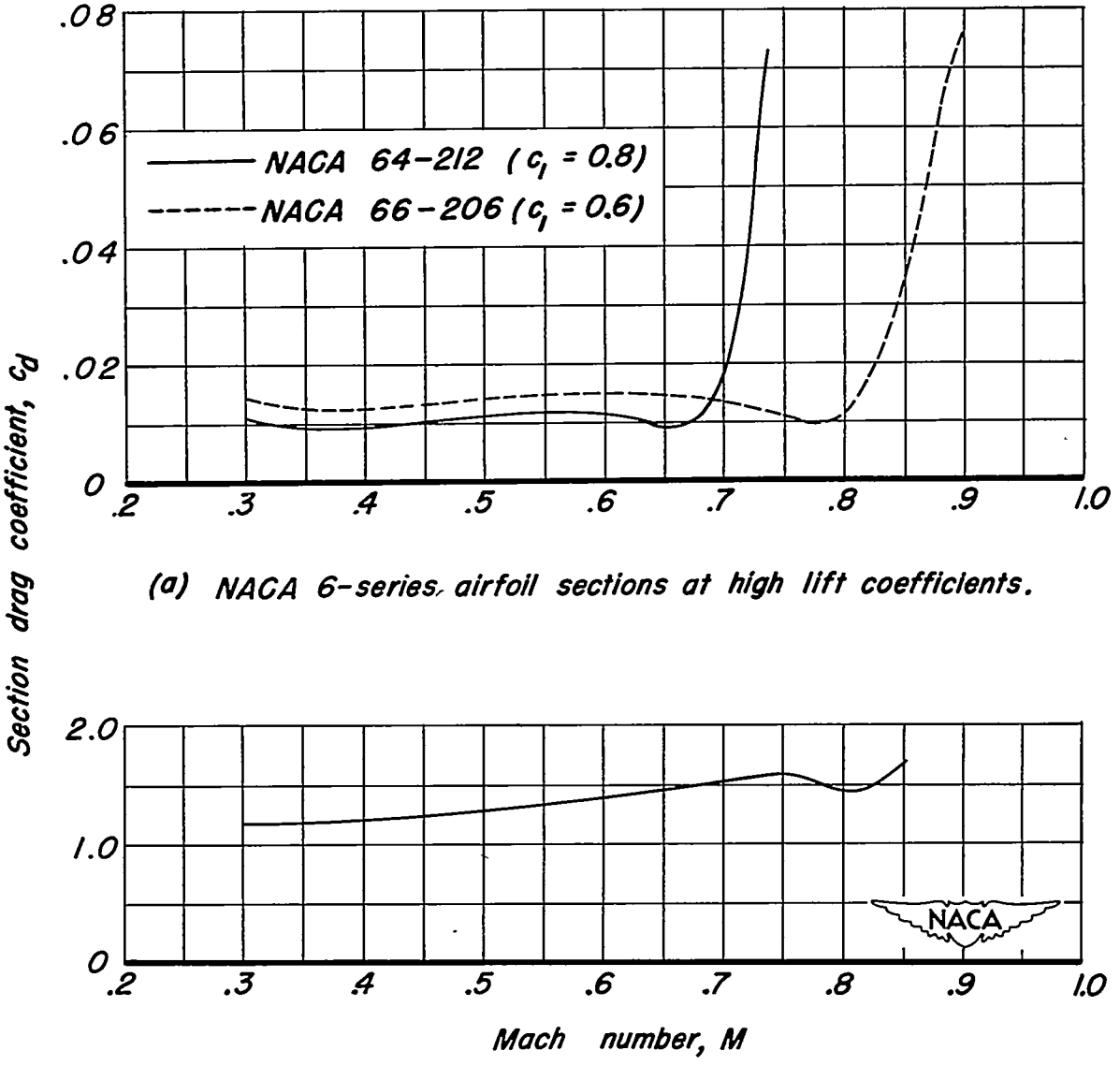

(a) NACA 6-series airfoil sections at high lift coefficients.

(b) Circular cylinder (reference 7).

Figure 100.-Variation of section drag coefficient with Mach number.

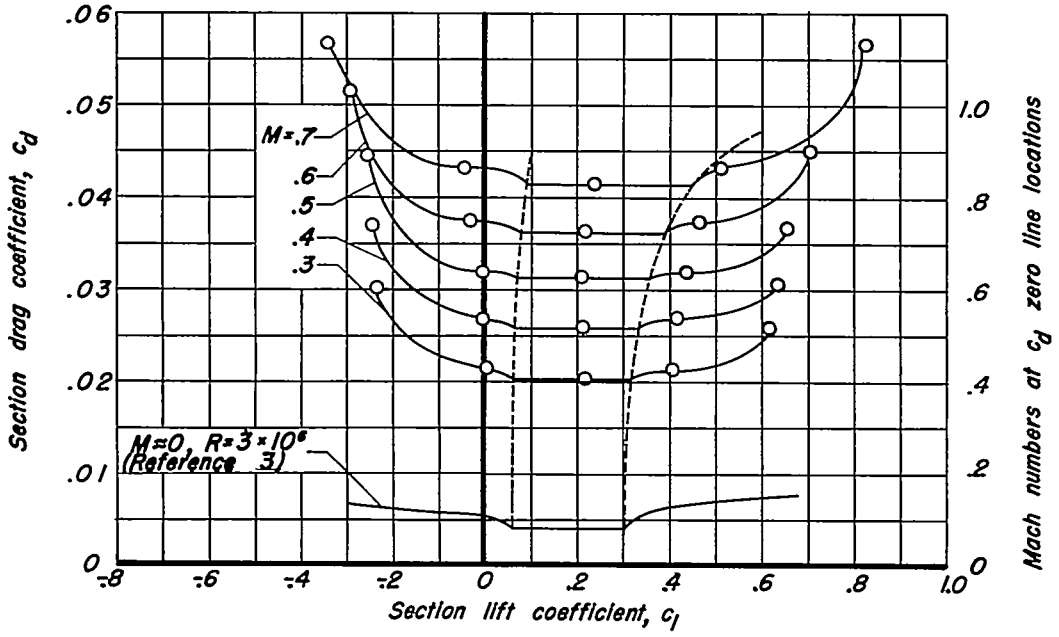

(a) NACA 64-206 airfoil.

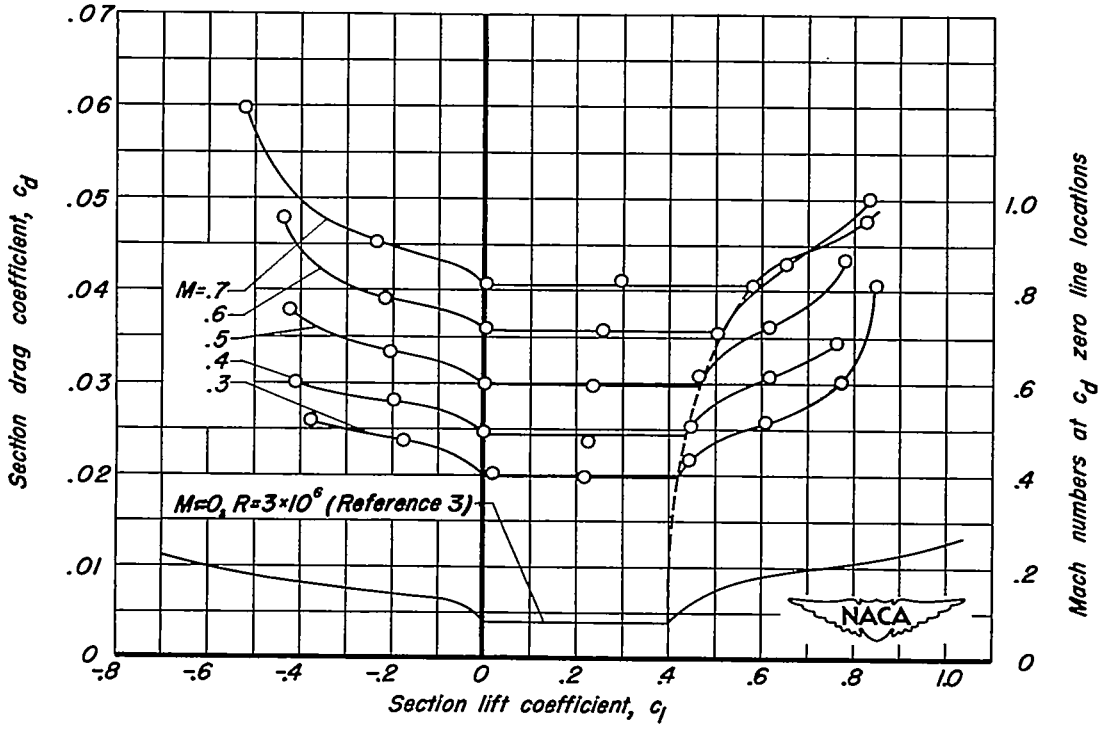

(b) NACA 66-212 airfoil.

Figure 101.–Variation of low drag range with Mach number.

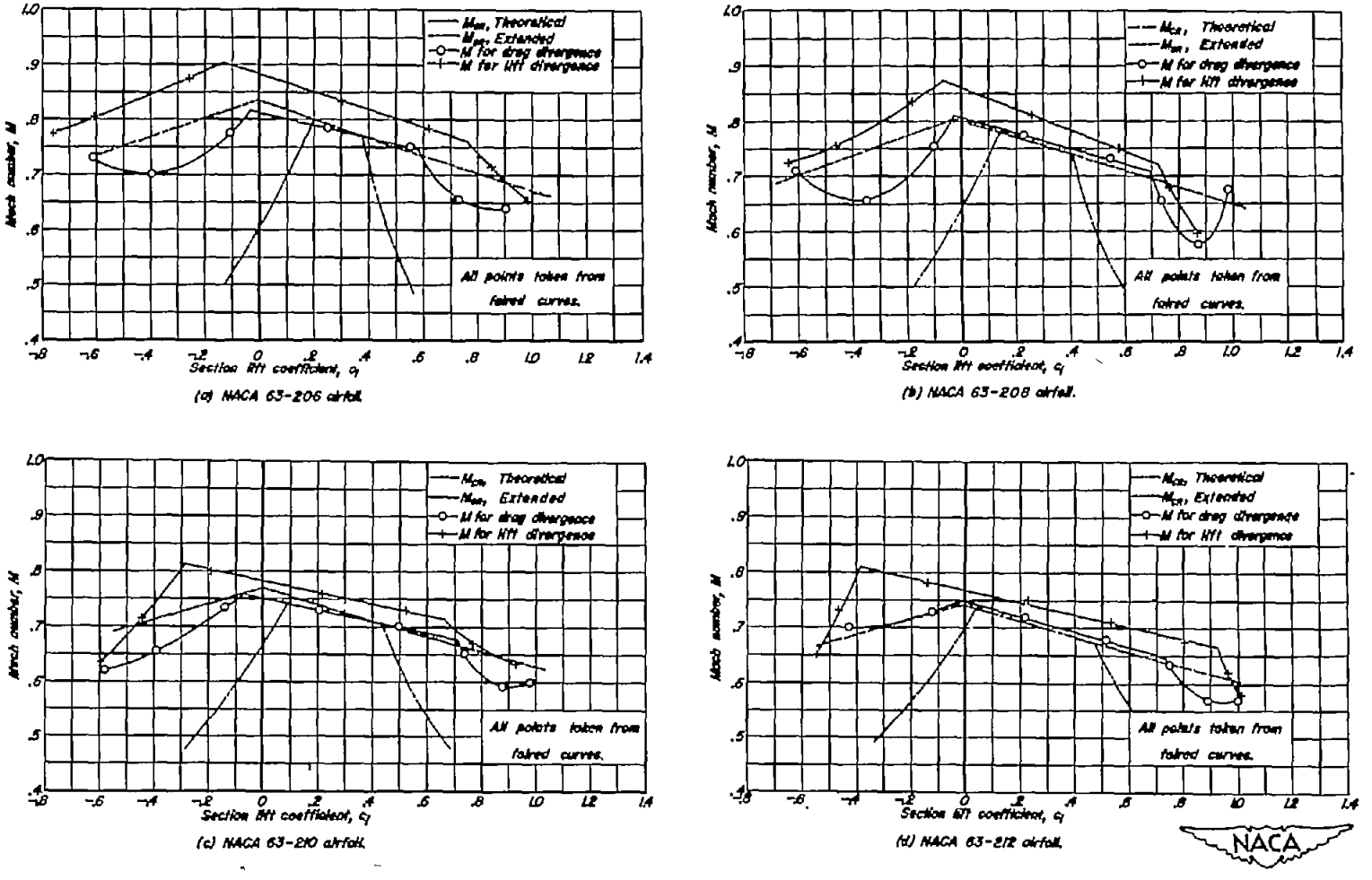

Figure 102.—The variation of lift- and drag-divergence Mach numbers with section lift coefficient.

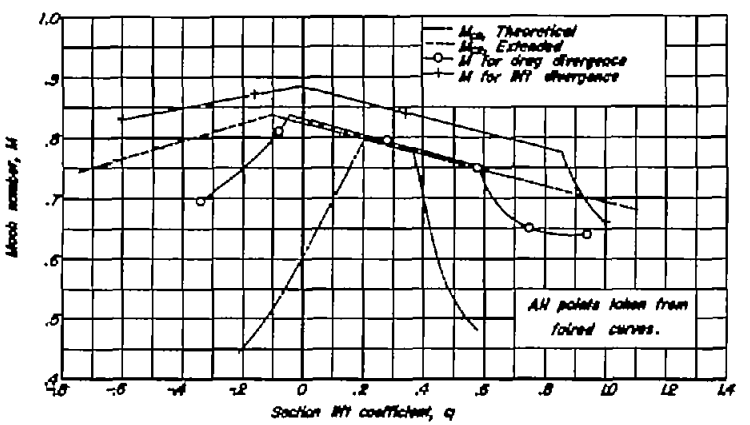

(e) NACA 64-206 airfoil.

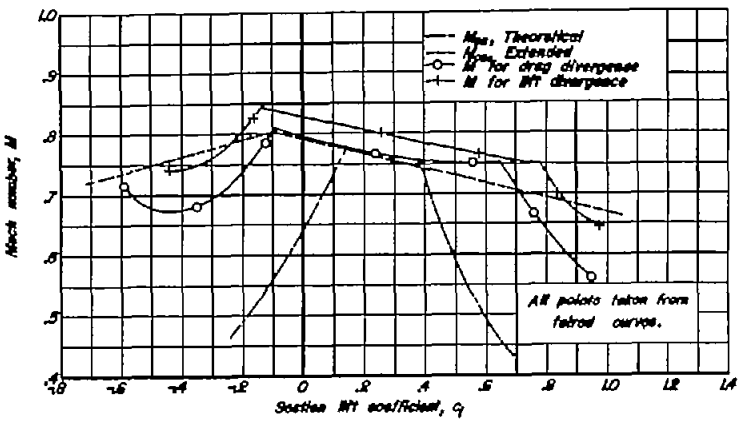

(f) NACA 64-208 airfoil.

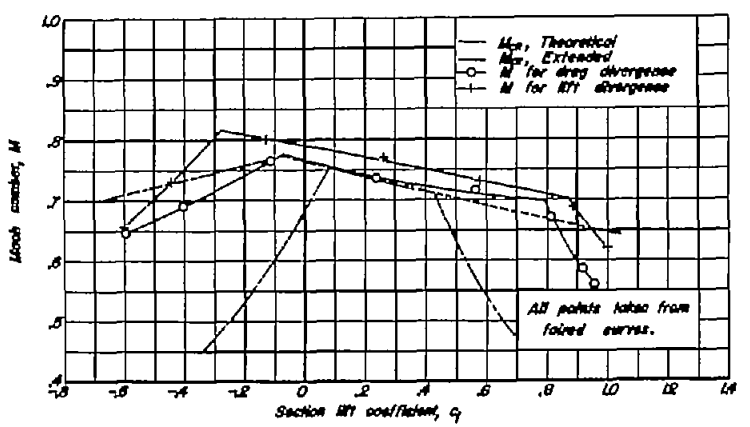

(g) NACA 64-210 airfoil.

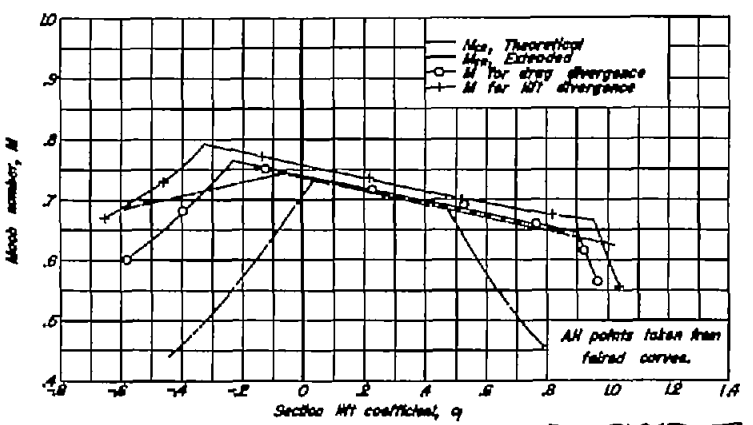

(h) NACA 64-212 airfoil.

Figure 10(b)-Continued.

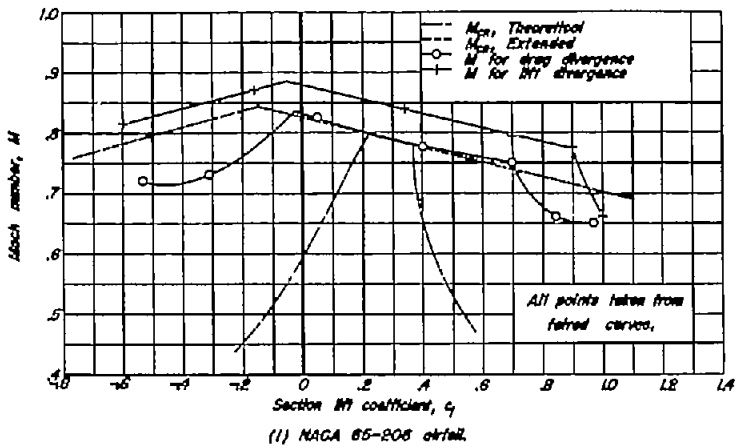

(l) NACA 65-208 airfoil.

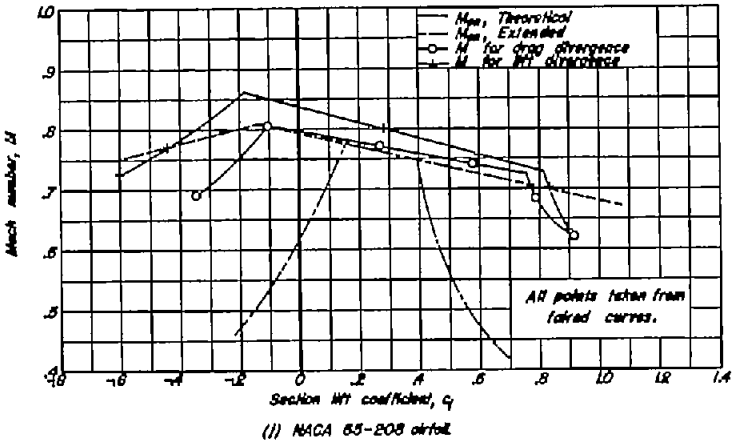

(l) NACA 65-208 airfoil.

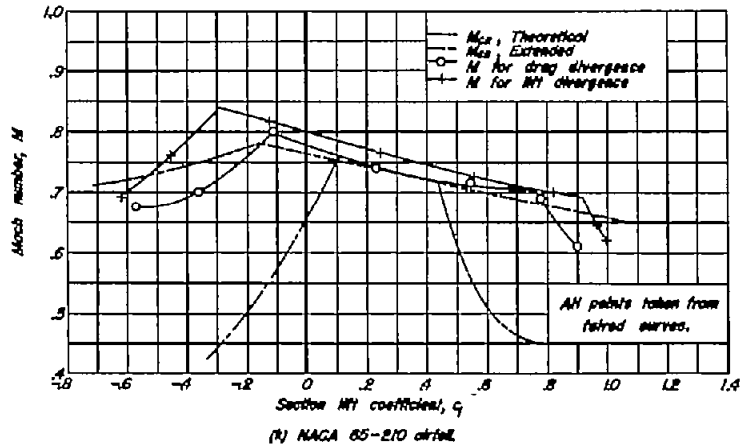

(k) NACA 65-210 airfoil.

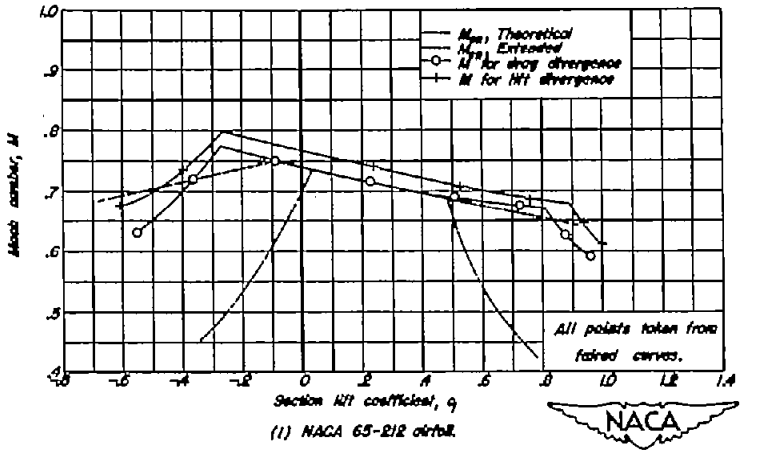

(l) NACA 65-212 airfoil.

Figure 102.-Continued.

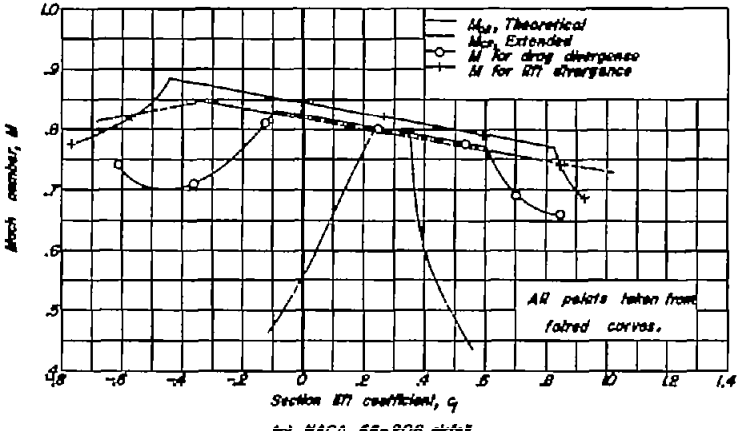

(m) NACA 66-206 airfoil.

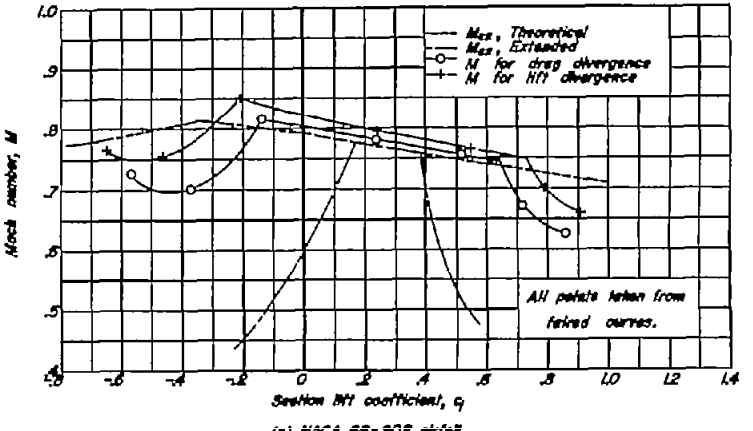

(n) NACA 66-206 airfoil.

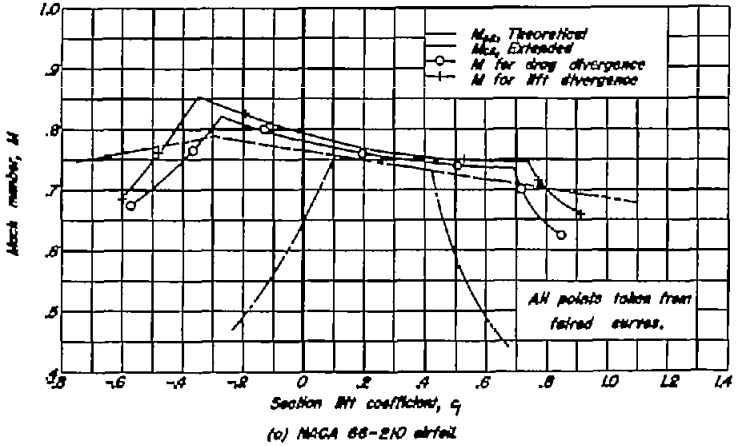

(o) NACA 66-210 airfoil.

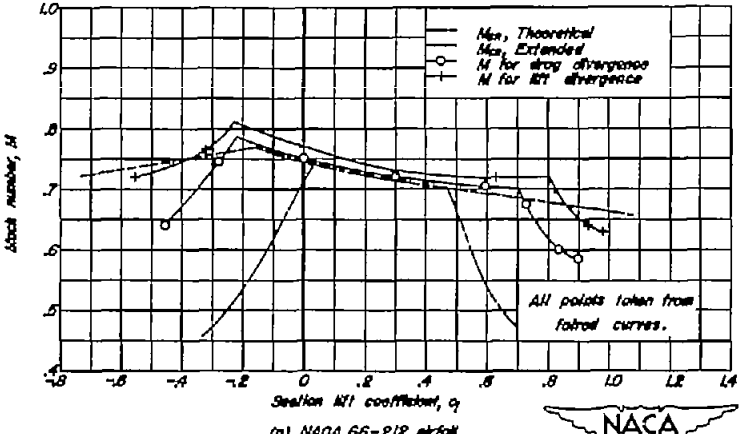

(p) NACA 66-212 airfoil.

NACA

Figure 102.-Concluded.

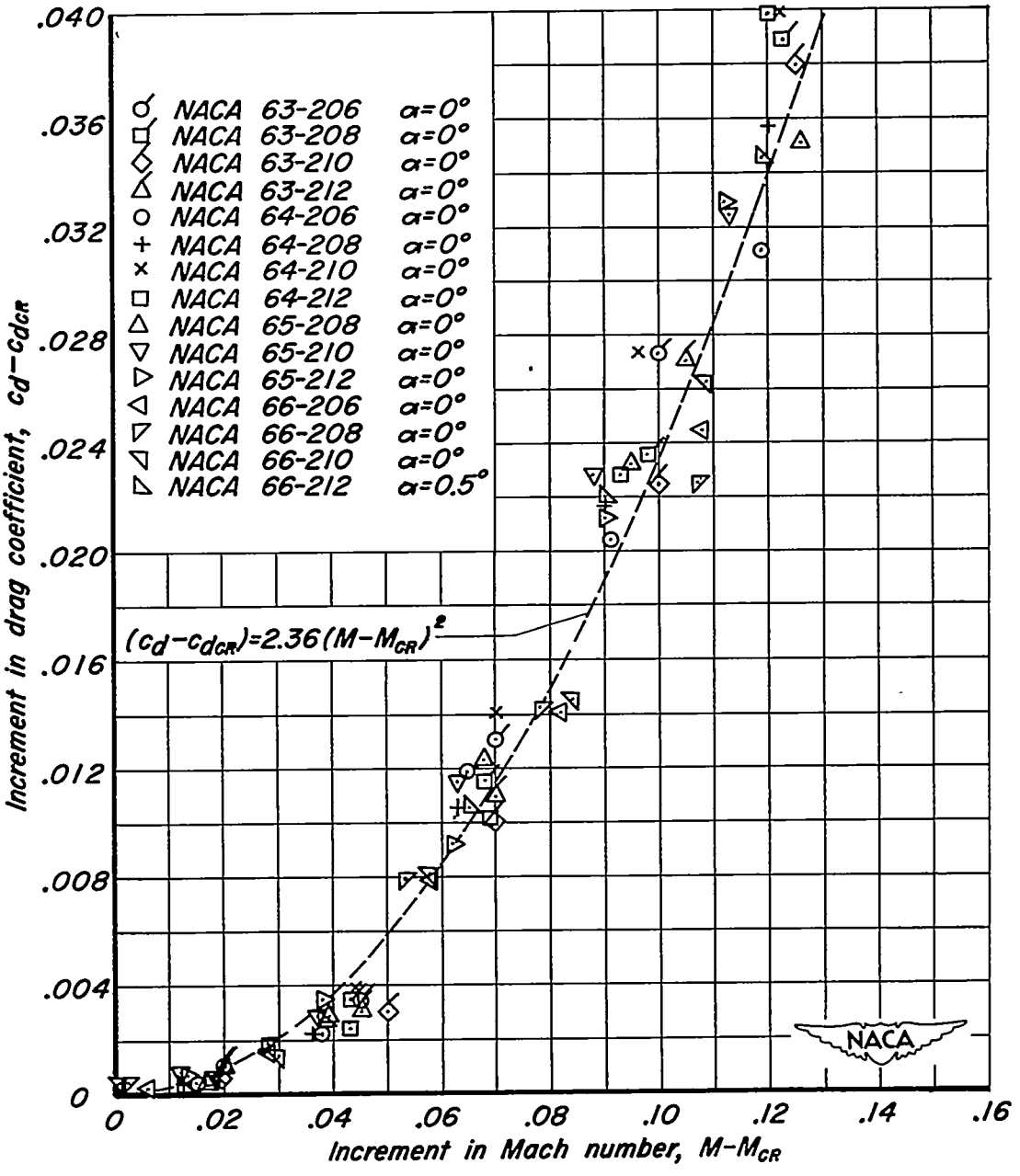

Figure 103.-Increase of section drag coefficient beyond theoretical critical Mach number.

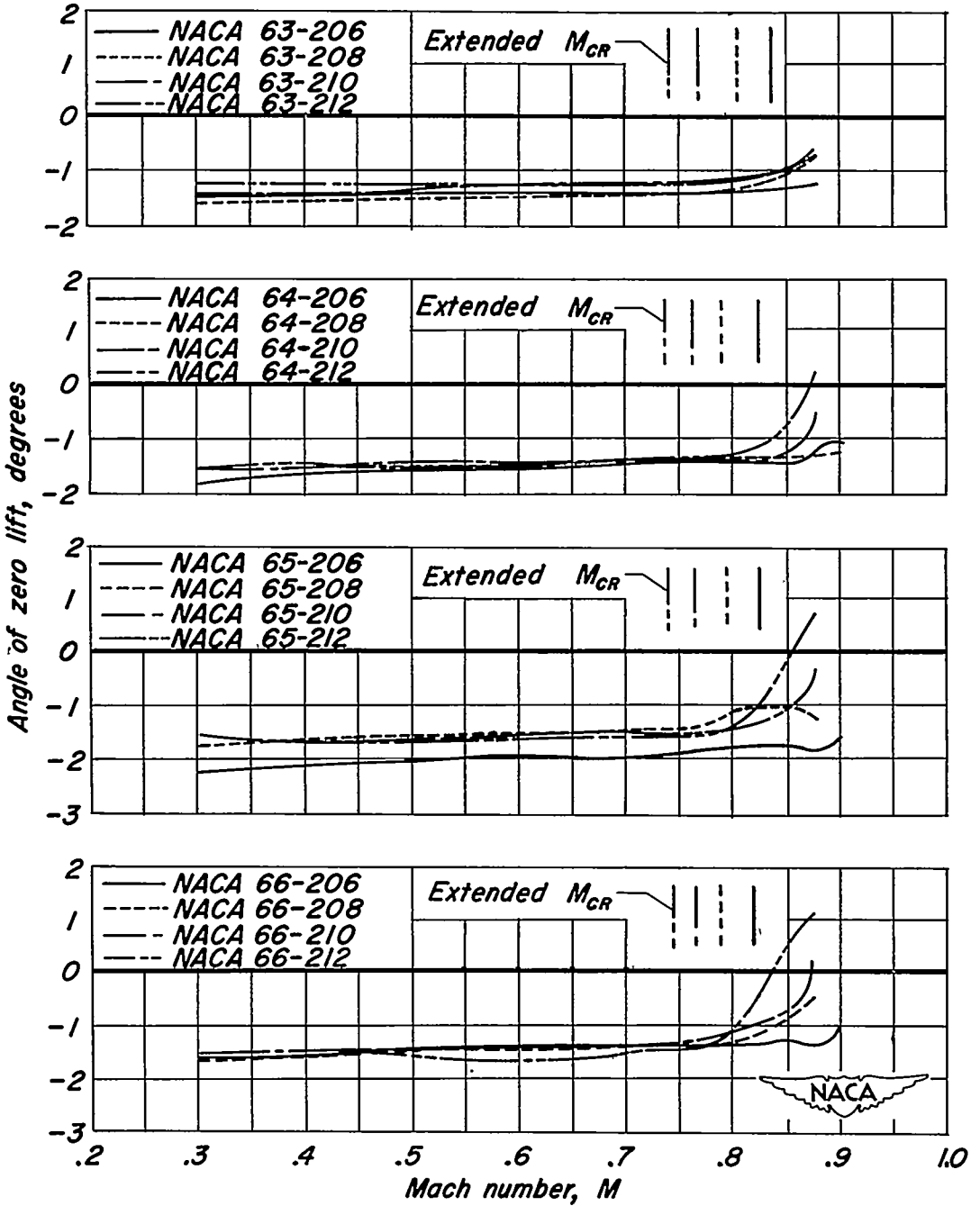

(a) Effect of thickness.

Figure 104.-The variation of angle of zero lift with Mach number for the NACA 6-series airfoils.

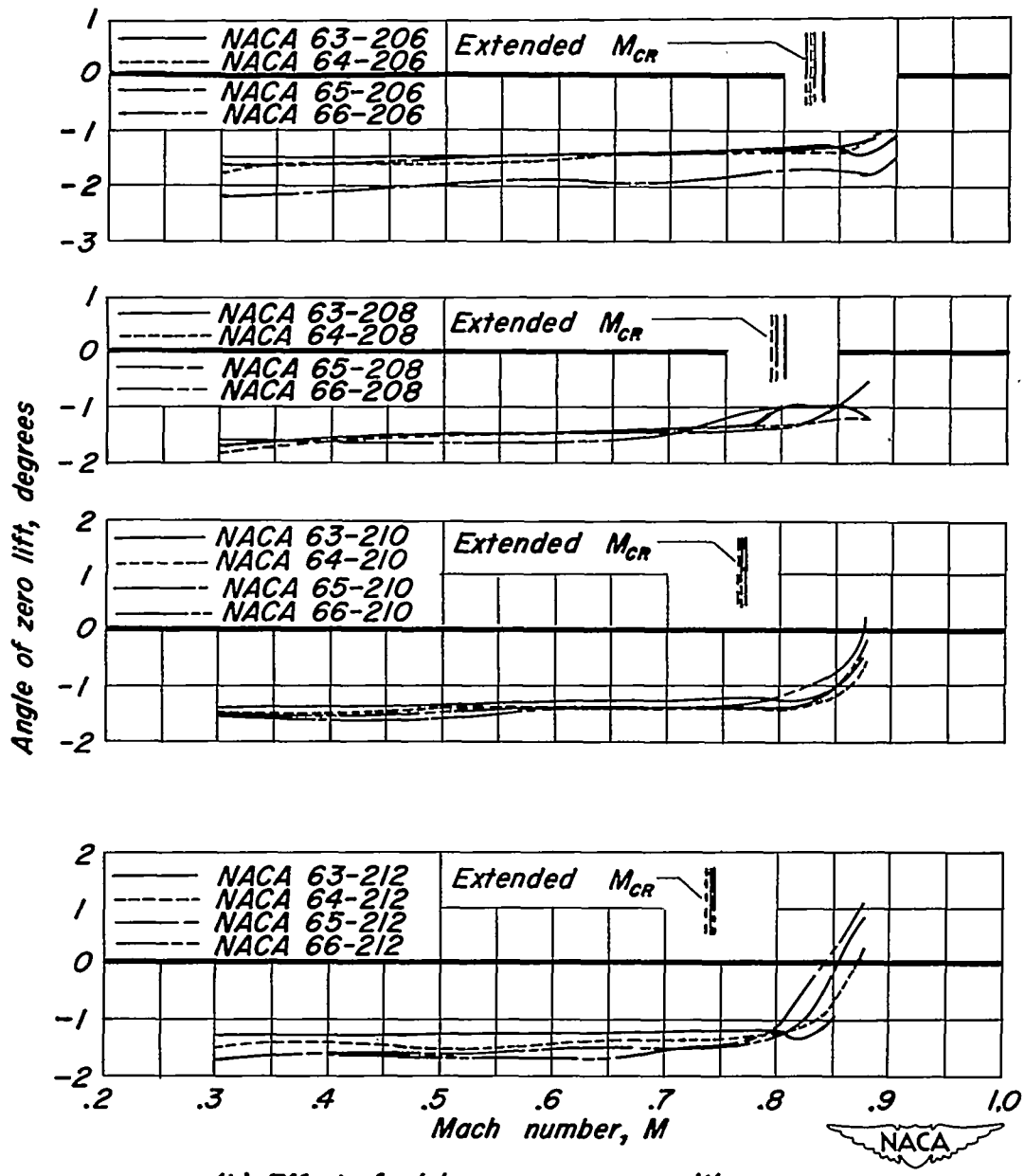

(b) Effect of minimum pressure position.

Figure 104.- Concluded.

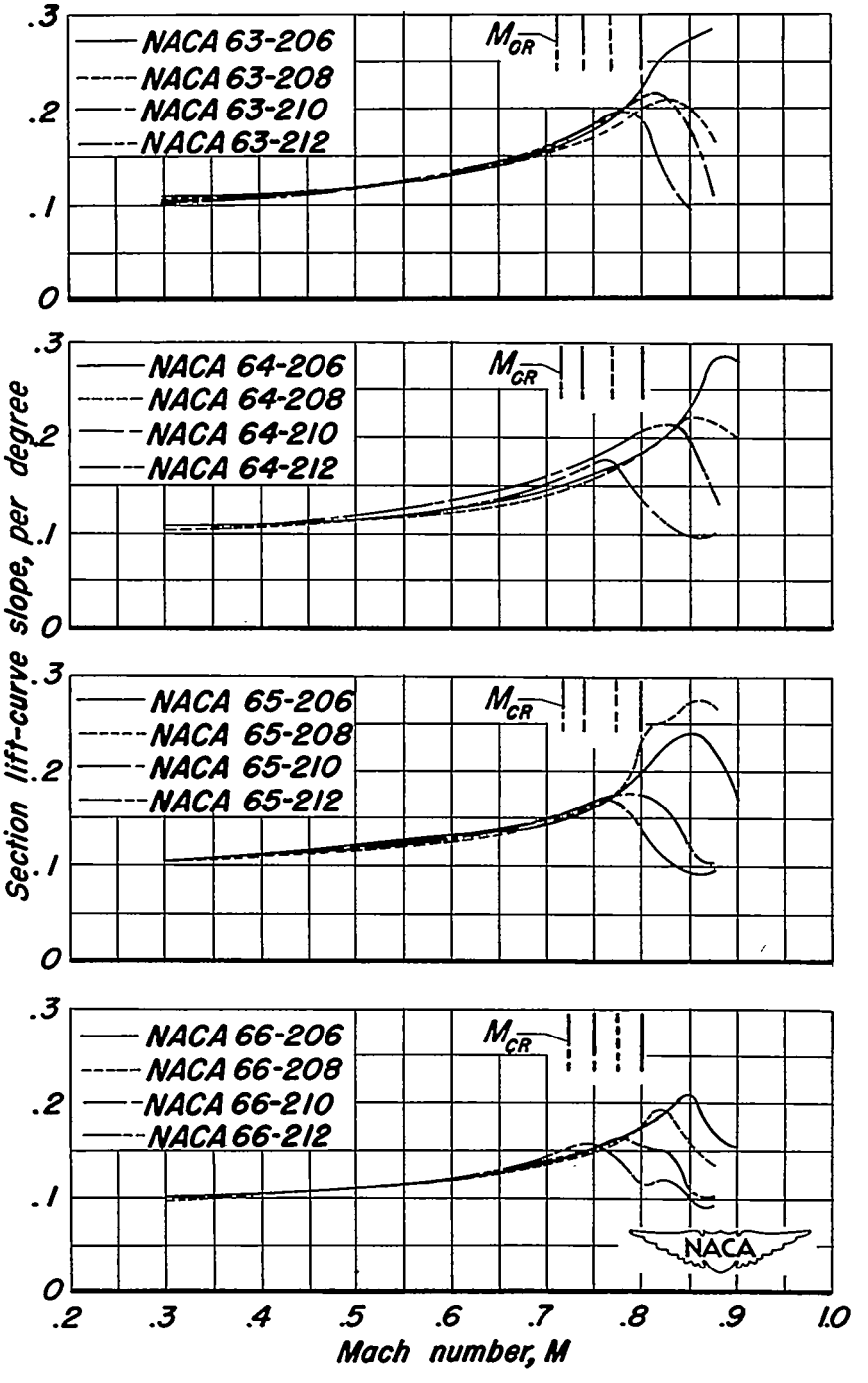

(a) Effect of thickness.

Figure 105.- The variation of section lift-curve slope with Mach number at the design lift coefficient for the NACA 6-series airfoils.

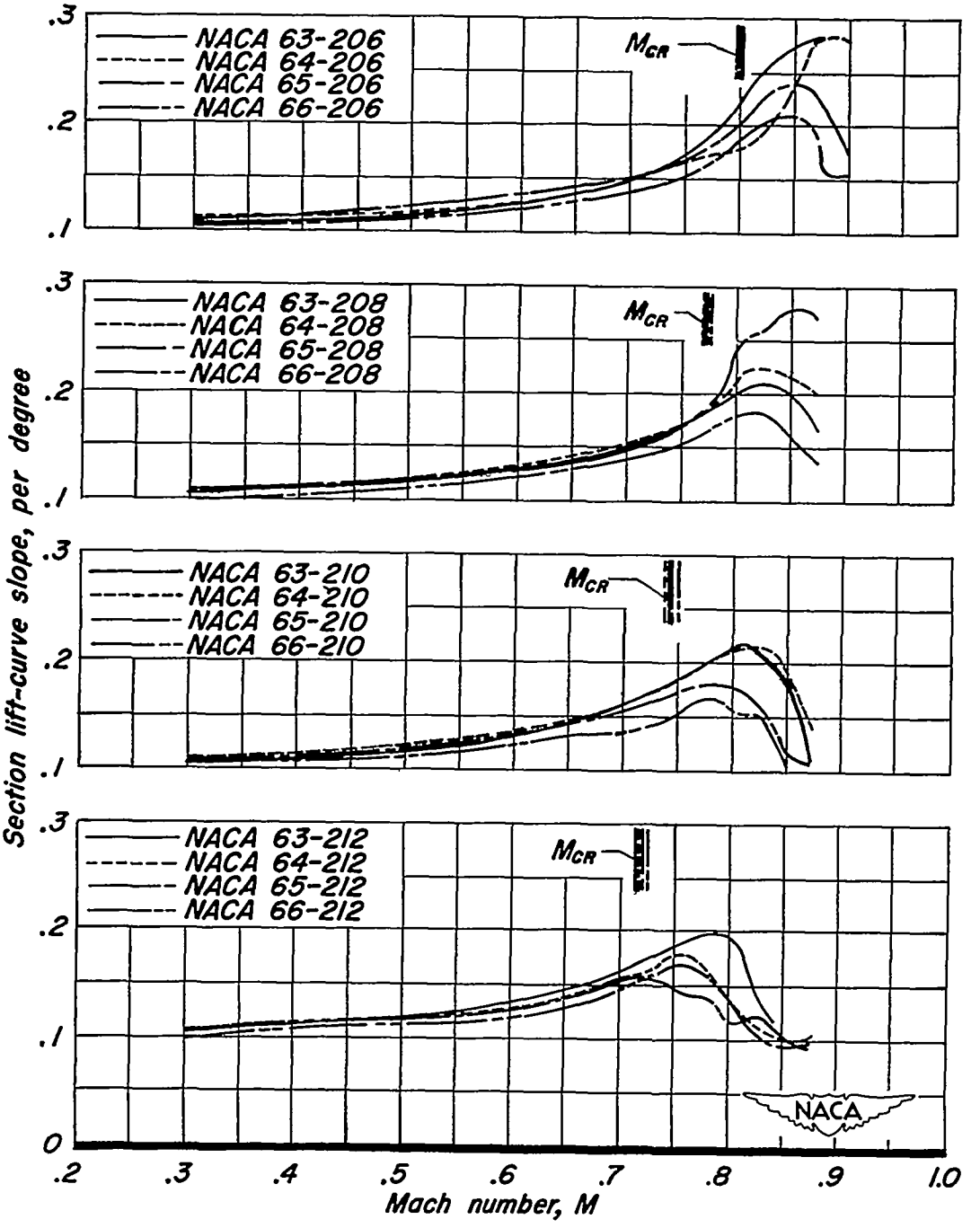

(b) Effect of minimum pressure position.

Figure 105.– Concluded.

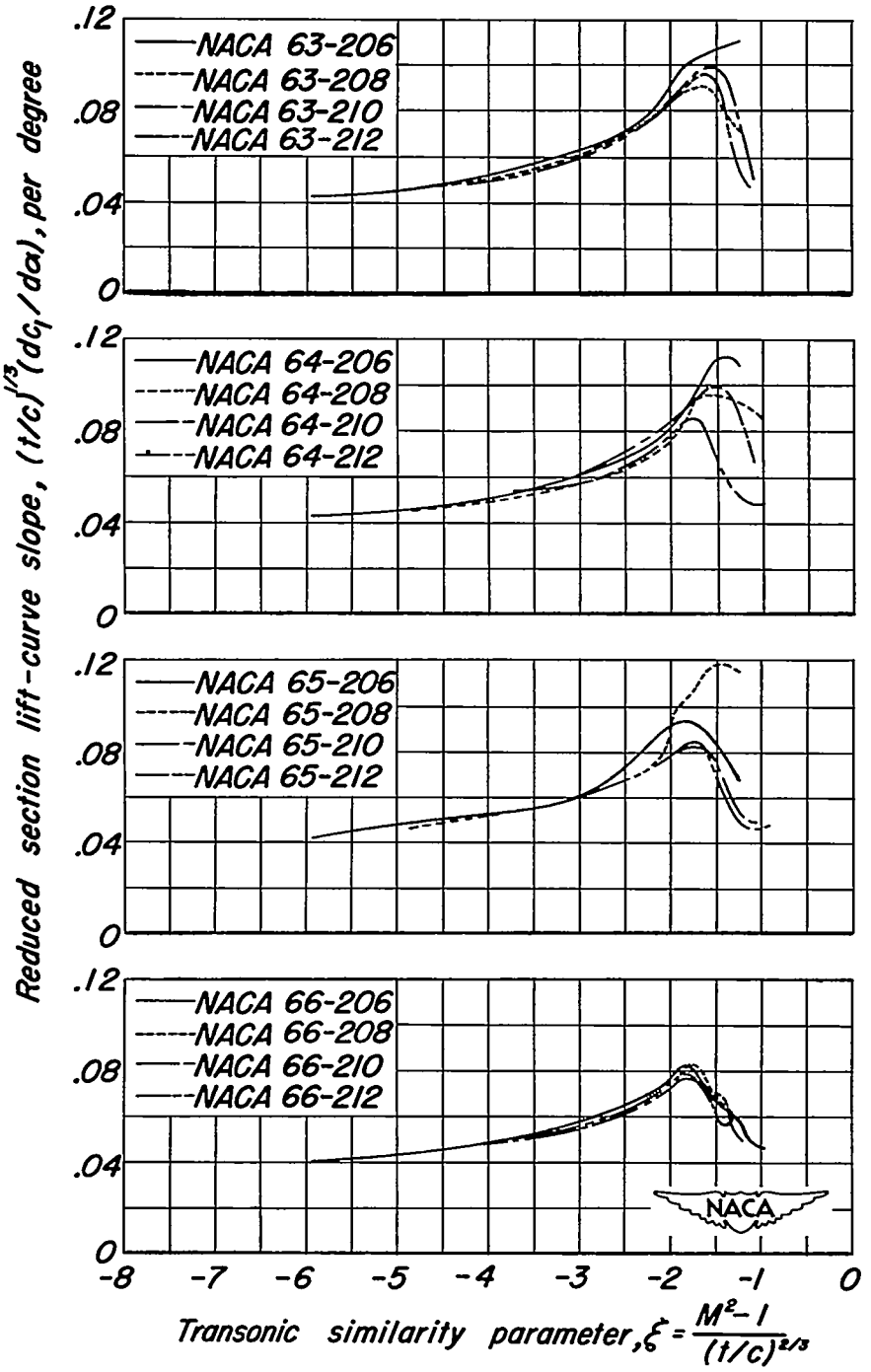

Figure 106.– Correlation of section lift-curve slope according to the transonic similarity rule.

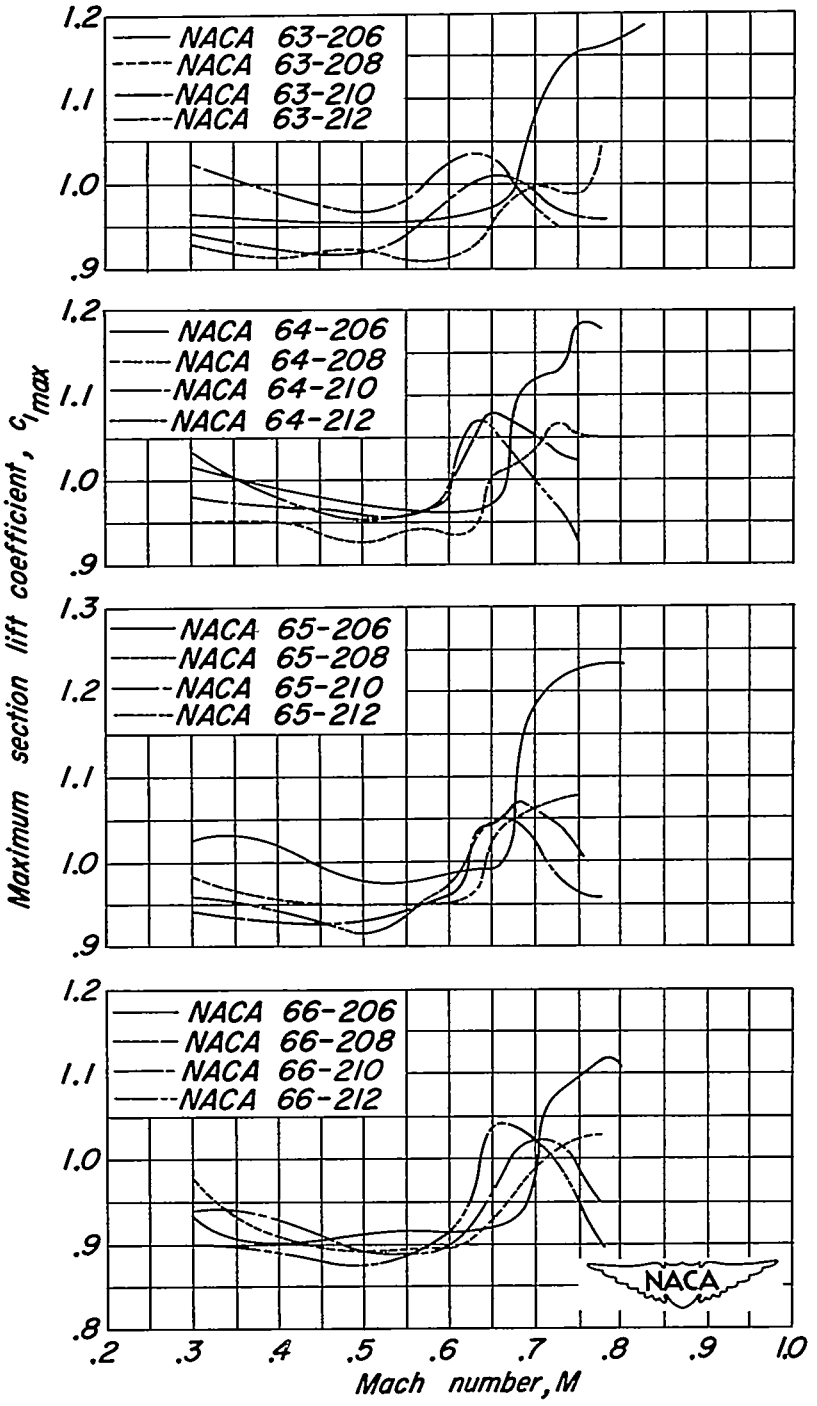

(a) Effect of thickness.

Figure 107.- The variation of maximum section lift coefficient with Mach number for the NACA 6-series airfoils.

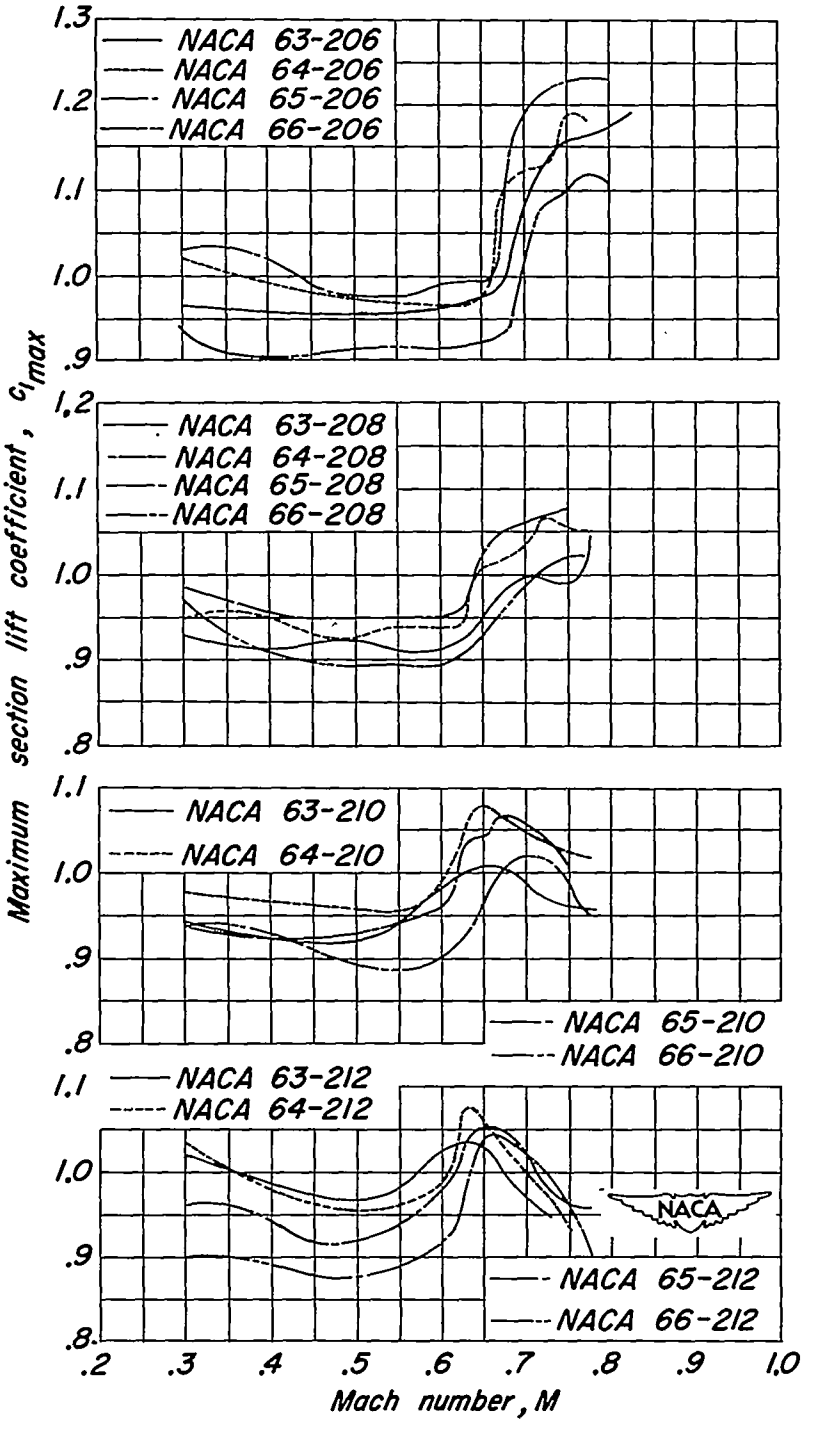

(b) Effect of minimum pressure position.

Figure 107.- Concluded.

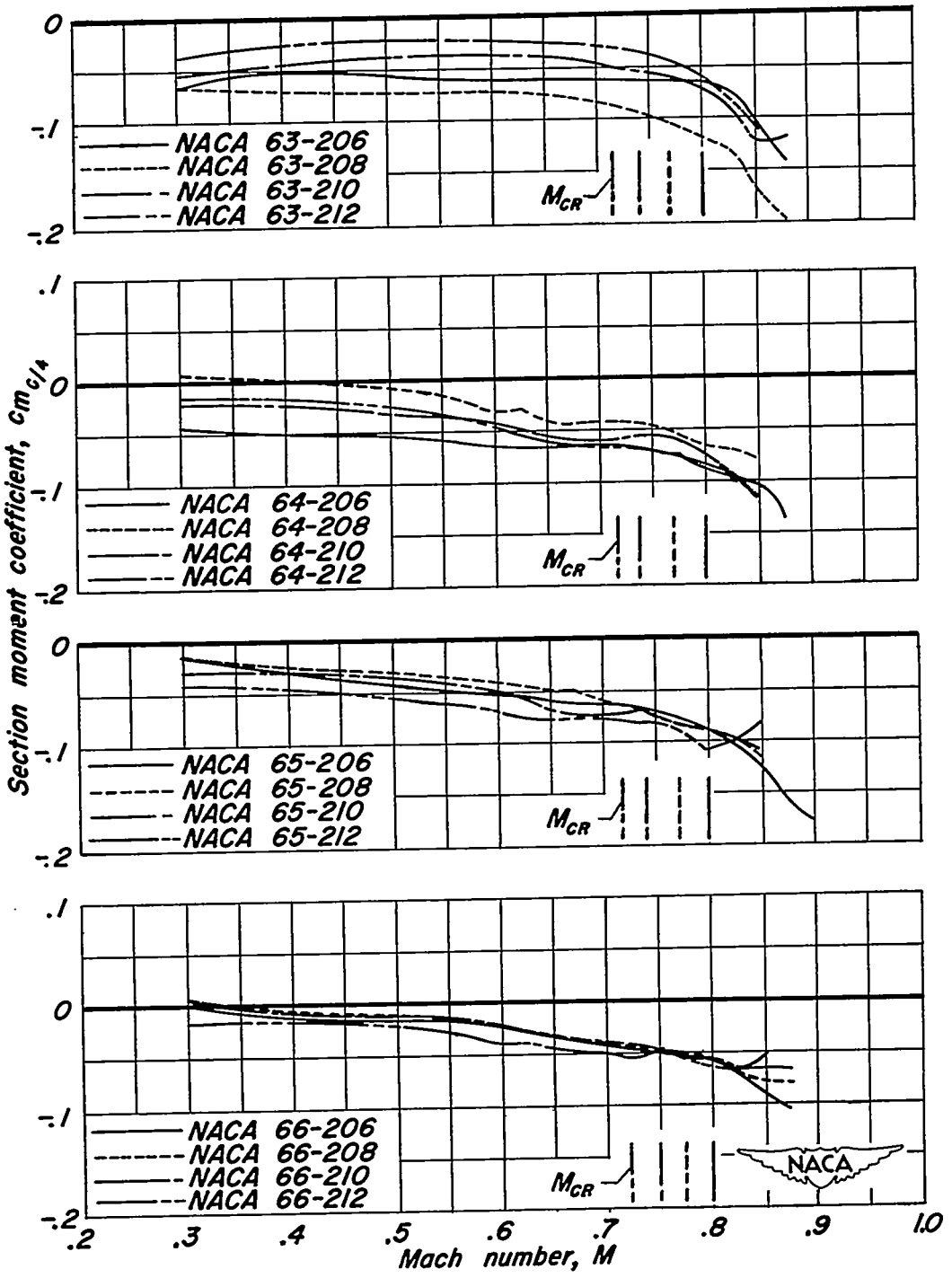

(a) Effect of thickness.

Figure 108-The variation of section moment coefficient with Mach number at the design lift coefficient for the NACA 6-series airfoils.

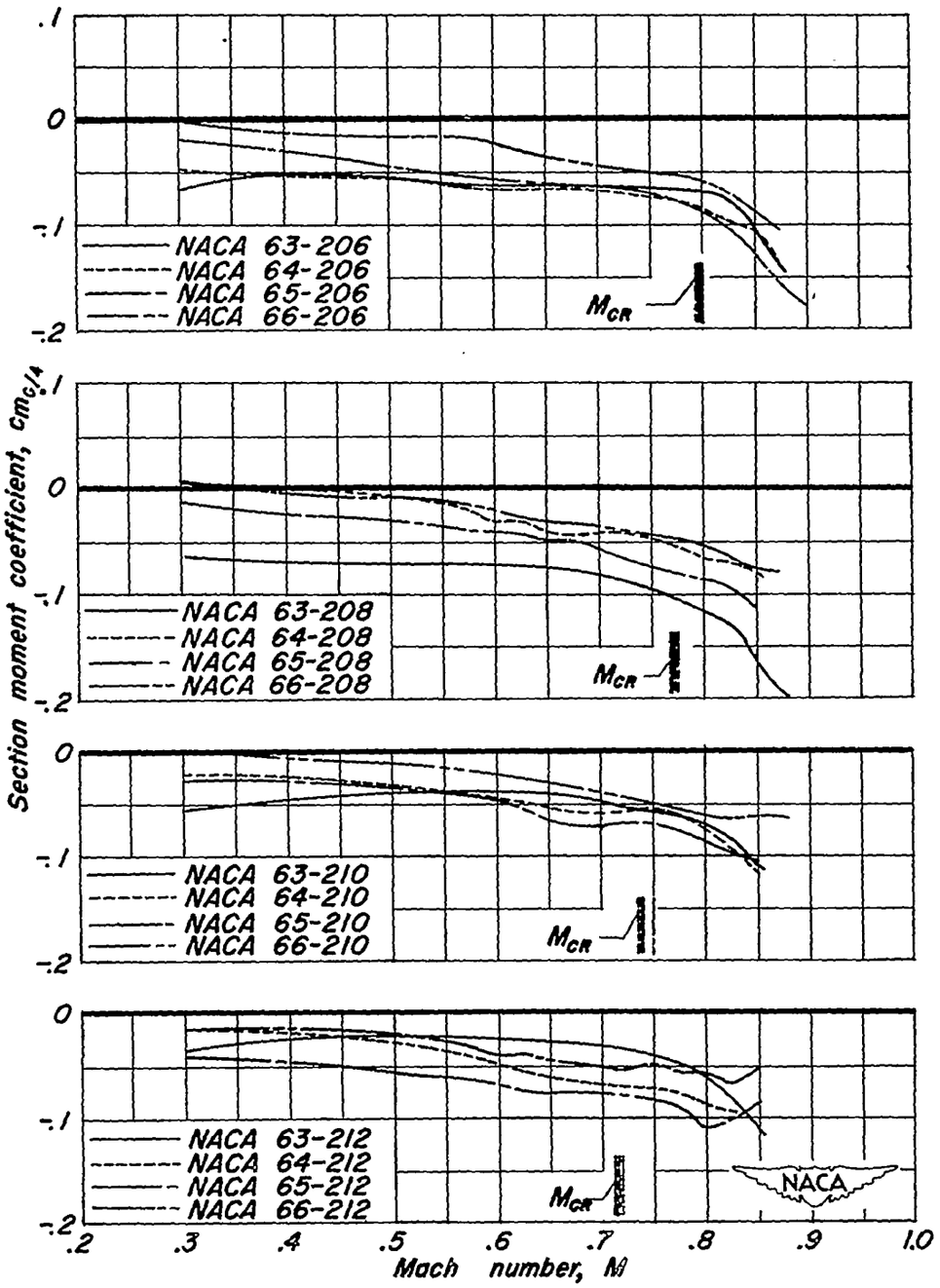

(b) Effect of minimum pressure position.

Figure 108.- Concluded.

NACA-Langley - 5-3-55 - 100